THE USE OF SUPERCRITICAL CARBON DIOXIDE IN THE PROCESSING OF THERMOPLASTIC ELASTOMER NANOCOMPOSITES

THE USE OF SUPERCRITICAL CARBON DIOXIDE IN THE PROCESSING OF THERMOPLASTIC ELASTOMER NANOCOMPOSITES

By

JINLING LIU, B. Eng., M. A.Sc.

A Thesis

Submitted to the School of Graduate Studies

in Partial Fulfillment of the Requirements

For the Degree

Doctor of Philosophy

McMaster University

DOCTOR OF PHILOSOPHY (2011) McMaster University

(Chemical Engineering) Hamilton, Ontario, Canada

TITLE: The Use of Supercritical CO_2 in the Processing of Thermoplastic Elastomer Nanocomposites

AUTHOR: Jinling Liu

SUPERVISOR: Dr. Michael R. Thompson

NUMBER OF PAGES: xvii, 239

ABSTRACT

This research studied the use of supercritical CO_2 ($scCO_2$) in the processing of layered silicate thermoplastic olefinic polymer (TPO) nanocomposites. Focus of the work was to understand how CO_2 interacts with the nanofiller in a manner that may lead to increased interlayer spacing of the clay platelets during processing, and if that interaction can be exploited as a mechanism for creating a fully exfoliated structure. After a series of studies, it is understood that $scCO_2$ indirectly improves the level of exfoliation and dispersion for a TPO/clay nanocomposite by plasticizing the maleated polypropylene (compatibilizer species used for preparing TPO nanocomposites) and the surfactant of an organoclay filler. The effect of plasticization aided intercalation of the compatibilizer into the interlayer areas of the clay. For intercalation, concentrating $scCO_2$ at the compatibilizer/clay interface was found to be more effective than when the clay was annealed alone under the gas before mixing or when all components of the nanocomposite formulation were heated together in the presence of the gas. In the latter case, the effectiveness of $scCO_2$ to plasticize the compatibilizer/clay association was diminished by inclusion of the TPO matrix which similarly sought to absorb the gas. In the case of the clay alone in the presence of $scCO_2$, surfactant rearrangement was noted to occur increasing its surface coverage over the oxygen plane. This in turn, was hypothesized to reduce the available sites for the compatibilizer to form associations within the galleries as opposed to the broken edges of the clay particles, thereby lowering the driving force for interlayer intercalation.

The aiding effect of $scCO_2$ on the interlayer intercalation was found dependent on the organoclay species, i.e. chemical structure of its surfactant and the manner which that surfactant was arranged within the galleries of the silicate. For a surfactant with two alkyl chains and paraffinic arrangement, $scCO_2$ significantly aided the interlayer intercalation. However, this surfactant appeared fairly unique with other examined organoclays not displaying $scCO_2$ influence, namely an organoclay with surfactant having three alkyl chains and paraffinic arrangement, or one with surfactant possessing either monoalkyl or dialkyl chains and a lateral bilayer arrangement. Surfactant rearrangement occurring due to the presence of $scCO_2$ was ascribed to the different response of the organnoclay to the intercalation. As observed by X-ray diffraction and differential thermogravimetric analysis, for the organoclay with two alkyl chains and paraffin-type arrangement the presence of $scCO_2$ resulted in increased interlayer distance and decreased surfactant packing at the edge area of silicate platelets, both of which were favourable factors to the interlayer intercalation.

Finally, adding a cosolvent of either water or ethanol with $scCO_2$ was observed by infrared analysis to significantly promote chemical associations between the compatibilizer and clay during melt processing. Water enhanced the compatibilizer/clay carboxylation whereas ethanol reacted with the compatibilizer generating ester bonds. The increased chemical affinity was believed to be responsible for the significantly improved compatibilizer/clay intercalation, and resulting exfoliation and dispersion of the TPO nanocomposite revealed by XRD, TEM and rheology analysis.

ACKNOWLEDGEMENT

I am very glad that I have the opportunity to use this page to profoundly thank the people who helped and supported me to pursue my PhD study at McMaster University:

My supervisor Dr. Michael Thompson for his invaluable role in guiding, inspiring and encouraging me during these years, I learned from him not only a lot of scientific and engineering knowledge but also the beauty of ethics, integrity and dedication in the academic environment.

The Natural Science and Engineering Research Council (NSERC) of Canada, General Motors of Canada Limited (GMCL), and the Ontario's Initiative for Automotive Manufacturing Innovation (IAMI) for their funding that made my studies and researches possible.

Dr. Shiping Zhu and Dr. Harald Stover as members of my supervisory committee for valuable guidance, remarks and advice and Dr. John Vlachopoulos as the chair of my comprehensive examining committee for his time, patience and guidance.

Dr. William Rodgers, Paula Fasulo, and Ting Cao from General Motors for their helpful advice, analysis and assistance during the research, Dr. Douglas Hunter from Southern Clay Products for his assistance in the preparation of the organoclays as well for his technical advice, Dr. L. Simon at Waterloo University for his mini-extruder in the

preparation of the TPO nanocomposites, and Ingenia Polymers for the cryogenic grinding of the compatibilizer and LyondellBasell for providing TPO materials.

Mr. Paul Gatt for his exceptional and unique role and technical support in making high pressure batch vessel, extensional flow mixer and many other valuable technical needs and Dr. Elizabeth Takacs as CAPPA-D lab manager for the trainings on instrument and equipment operations.

Dr. James Britten (X-ray facility manager), Marcia Reid (research assistant), Dr. Bob Berno (NMR lab manager), Dr. Steven Kornic (general instrument specialist), Graham Pearson (lab technician) and Frank Gibbs (research analyst) for their instructions and valuable help in conducting my experiments and analysis.

Kathy Goodram, Lynn Falkiner and Nanci Cole, secretaries at our department, for their unseen but vital responsibilities.

My colleagues and friends in the department: Lina Liu, Tayyeb Hamid, Zijin Zhuang, Maryam Emami, Dr. Mary Jin, Arvin M. Malayery, and David Lawton, for their friendship, constructive discussions and support.

And my husband Sichuan Xu and my daughter Jing Xu for their love, encouragement and support.

TABLE OF CONTENTS

LIST OF FIGURES

LIST OF TABLES

Chapter 1

Introduction

1.1 RESEARCH BACKGROUND

Polymer-layered silicate (PLS) nanocomposites have great potential within the modern automotive industry (Paul and Robeson, 2008; Pavlidou and Papaspyrides, 2008). However, current industrial applications are extremely limited. The reasons may be related to multiple aspects, but the key factor goes to the high cost/performance ratio of the nanomaterials created using available nanoparticle dispersion technologies, i.e. melt intercalation using industrially available mixing devices like twin screw or single screw extruders. The organic modification of an organoclay and the necessary inclusion of a functionalized compatibilizer for olefinic polymer matrices increase the cost of the nanocomposite materials. Even with the organic modification and compatibilizer inclusion, there are still challenges to manufacturing polyolefinic nanomaterials because the available processing methods are reliant on a strongly thermodynamic dependent mechanism, i.e. intercalation process. Processing time and level of exfoliation have to be

balanced. In order to reduce processing time, level of exfoliation has to be sacrificed, which diminishes advantages related to nanocomposite materials; or in order to get a fully exfoliated morphology, the processing time has to be very long, which is not acceptable to industrial manufacturers.

Aiming at the time-dependent intercalation mechanism, several disruptive technologies have been proposed to advance the intercalation rate, level of exfoliation, and uniform dispersion. These technologies include high energy ultrasonification (Lim et al., 2003), electrical fields (Lu et al., 2006), magnetic fields (Koerner et al., 2005), and the use of supercritical fluids (Horsch et al. 2006; Nguyen and Baird, 2007; Treece and Oberhauser, 2007; Zhao and Huang, 2008). Among them, the use of supercritical fluids can be seen as the most applicable to current industrial processing practices, and the least damaging to equipment and the polymer structure. The usefulness of supercritical CO_2 for improving clay exfoliation was originally noted by Manke et al. (2002) in preparation of microcellular foams but its effect was not investigated at that time. Since that discovery many research groups have put forth technologies showing improved clay dispersion for a polyolefin nanocomposite but none have investigated the underlying mechanism. By understanding the mechanism it is hoped the technology can be optimized to realize a fully exfoliated nanocomposite material.

In the literature, studies on the use of $scCO_2$ in the processing of polymer layered silicate nanocomposites are basically based on one of two proposed mechanisms. The first one is the plasticization mechanism which states that $scCO_2$ dissolved in polymer melt can increase mobility of the polymer chains and therefore increase their intercalating

ability. The direct gas injection technology was developed based on this assumption (Treece and Oberhauser, 2007; Ma et al., 2007; Zhao and Huang, 2008). The other one is the fracturing mechanism. It is believed that clays can be expanded or even exfoliated when the highly pressurized gas saturated in the interlayer area is rapidly released and thus the ordered or randomly exfoliated clay is readily mixed into matrix materials without energy-intensive delamination requirements. Several reports are based on this assumption (Manke et al., 2002; Horsch et al., 2006; Nguyen and Baird, 2007).

1.2 RESEARCH OBJECTIVES

The work of this thesis was to better understand the nature of the intercalation/exfoliation aiding mechanism of $scCO_2$ and based on that understanding to propose a means of aiding the production of a polymer (specifically in the case of this study, a thermoplastic polyolefin elastomer, TPO) nanocomposite with a higher degree of exfoliation than melt-intercalation could achieve. To reach this goal, the above two methods had to be studied. Considering previous studies by this researcher (Thompson et al., 2008, 2009) and the well-recognized diffusion-controlled intercalation-exfoliation mechanism for development of a PLS nanocomposite (Vaia et al., 1995, 1996, 1997; Hasegawa et al., 2000; Schmidt et al., 2002), it was the hypothesis of this work that the plasticization mechanism was dominant for melt preparation of a TPO nanocomposite. To test the hypothesis the following three objectives were undertaken:

1) Step-wise examination on how $scCO_2$ interacted with the components of the nanocomposite material. Prior work in my Masters had already established the

interactions specifically for a selection of organically modified clays. The work in this thesis continued to study $scCO_2$ interactions now with compatibilizer in intimate contact with an organoclay, and subsequently when all the three components, matrix, compatibilizer and organoclay, were mixed together in the presence of the gas.

2) Investigation of how the mixing order of the three components influenced the final exfoliated structure of the clay after processing in the presence of $scCO_2$. In collaboration with the findings of the previous objective, we infer by undertaking this second objective that the gas may only be needed at certain points in the preparation of the nanocomposite and not required throughout the whole process.

3) Further studies on effect of $scCO_2$ on the interactions between compatibilizer and organoclay and on exfoliation and dispersion of the TPO nanocomposite by adding small amount of polar solvent to the supercritical gas. By altering the polarity of the supercritical solvent it was believed the interactions of $scCO_2$ with the clay could be better understood, and hopefully a better method of intercalation/exfoliation could be identified.

1.3 THESIS OUTLINE

The thesis contains the following chapters.

Chapter 1 is this introduction and stated objectives of the research.

Chapter 2 is a literature review on the relevant aspects of this research field. It reviews the field of PLS nanocomposites for the aspects of structures and mechanical properties, reinforcement mechanism and intercalation/exfoliation process. It also introduces the research work by other researchers concerning $scCO_2$ in the fields of polymer processing, clay minerals and specifically processing of a PLS nanocomposite.

Chapter 3 looks at the influence of $scCO_2$ on the diffusion-controlled interactions between organoclay and maleated polypropylene (MA-PP). The work attempted to validate or dismiss the hypothesis that plasticization of the MA-PP melt by the supercritical fluid would allow for the polymer chains to more readily diffuse into the gallery spaces of an organoclay. In this work, one organoclay was specified and several MA-PP were tested to vary properties. The evaluation focused on how properties of the compatibilizer affect the $scCO_2$-aided intercalation. The paper forming this chapter has been accepted by *Journal of Applied Polymer Science* in July 2010.

Chapter 4, similar to the last chapter, is to understand the intercalation mechanism for our compatibilizer/organoclay annealing system and repercussions of intercalation on the final TPO nanocomposite. Focus of this work is on how chemical structure of a surfactant and its arrangement in the silicate interlayer region affected the $scCO_2$ aided compatibilizer/organoclay intercalation and dispersion of the TPO nanocomposite. Five organoclays were selected to make masterbatch mixtures with an MA-PP, with TPO nanocomposites being made from these masterbatches. The paper constituting this chapter is intended to submit to *Applied Clay Science* in December 2010 and is under review by GM currently.

Chapter 5 further explores the intercalation mechanism and examines the role of $scCO_2$ in the processing of a TPO nanocomposite. This work tested two assumptions: i) $scCO_2$ present at different interfaces of the three components during preparation may have different effect on exfoliation and dispersion of an organoclay in the TPO nanocomposite and ii) pre-swollen or exfoliated organoclay generated using $scCO_2$ may better favour exfoliation and clay dispersion in our TPO. Different mixing orders of the three components for a nanocomposite, nanofiller, compatibilizer and matrix polymer, were evaluated. Part work of this chapter was presented in *the 26th Annual Meeting of Polymer Processing Society*, Banff, Alberta, Canada, July 4th – 8th, 2010 and the paper is intended to be submitted to a relevant technical journal.

Chapter 6 further studies the $scCO_2$-aided compatibilizer/organoclay intercalation mechanism by adding water or ethanol as a cosolvent and evaluating the relevance of these cosolvents on the TPO nanocomposite. The original hypothesis of this work considered that water or ethanol has good affinity with silicate surface, MA-PP and CO_2 and that their addition to the $scCO_2$ aided mixing system may increase the compatibilizer/organoclay intercalation. The paper for this chapter will be submitted to a relevant technical journal.

Chapter 7 summarizes the data of the previous chapters and through that consolidation proposes a mechanism for how $scCO_2$ aids the intercalation, exfoliation and dispersion of the silicate nanofiller in a TPO nanocomposite.

Chapter 8 will address major conclusions from the research, the author's contributions to scientific knowledge and recommendations for the future work.

References

Koerner H., Hampton E., Dean D., Turgut Z., Drummy L., Mirau P., Vaia, R. Generating Triaxial Reinforced Epoxy/Montmorillonite Nanocomposites with Uniaxial Magnetic Fields, *Chem. Mater.* 17 (2005), 1990

Hasegawa N., Okamoto H., Kawasumi M., Kato M., Tsukigase A., Usuki A., *Macromol. Mater. Eng.* 280/281 (2000), 76

Horsch S., Serhatkulu G., Gulari E., Kannan R.M. Supercritical CO2 dispersion of nano-clays and clay/polymer nanocomposites, *Polymer* 47 (2006), 7485

Lim S.T., Choi H.J., Jhon M.S. Dispersion quality and rheological property of polymer/clay nanocomposites: Ultrasonification effect, *J. Ind. Eng. Chem.* 2003, 9:51-57

Lu W., Loerner H., Vaia R. Effect of electric field on exfoliation of nanoplates, *Appl. Phys. Lett.* 2006, 89: Art. No. 223118

Ma J., Bilotti E., Peijs T., Darr J.A., Preparation of polypropylene/sepiolite nanocomposites using supercritical CO_2 assisted mixing, *European Polymer Journal* 43 (2007), 4931-4939

Manke, C. W.; Gulari, E.; Mielewski, D. F.; Lee, E. C. (Ford Global Technologies, Inc.; Wayne State University). US Patent 6,468,073, October 22, 2002

Nguyen Q.T., Baird D.G. An improved technique for exfoliating and dispersing annoclay particles into polymer matrices using supercritical carbon dioxide, *Polymer* 48 (2007), 6923

Paul D.R., Robeson L.M. Polymer nanotechnology: Nanocomposites, *Polymer* 49 (2008), 3187

Pavlidou S., Papaspyrides C.D. A review on polymer layered silicate nanocomposites, *Prog. Polym. Sci.* 33 (2008), 1119

Schmidt D. et al., *Current Opinion in Solid State and Mater. Sci.*, 6 (2002), 205

Thompson M.R., Liu J., Krump H., Kostanski L.K., Fasulo P.D., Rodgers W.R., *J. Colloid Interf. Sci.* 2008, 324, 177-184

Thompson M.R., Balogh M.P., Speer R.L. Jr., Fasulo P.D., Rodgers W.R., *J. Chem. Phys* 2009, 130 (044705), 1-8

Treece M.A., Oberhauser J.P. Processing of Polypropylene-clay nanocomposites: single-screw extrusion with in-line supercritical carbon dioxide feed versus twin-screw extrution, *J. Appli. Polym. Sci.* 103 (2007), 884

Vaia R.A., Jandt K.D., Kramer E.J., Giannelis E.P., Kinetics of Polymer Melt Intercalation, *Macromolecules*, 28 (1995), 8080

Vaia R.A., Jandt K.D., Kramer E.J., Giannelis E.P., Microstructural Evolution of Melt Intercalated Polymer--Organically Modified Layered Silicates Nanocomposites, *Chem. Mater.* 8 (1996), 2628

Vaia R.A., Giannelis E.P., Lattice Model of Polymer Melt Intercalation in Organically-Modified Layered Silicates, *Macromolecules* 30 (1997), 7990

Zhao Y,, Huang H,-X. Dynamic rheology and microstructure of polypropylene/clay nanocomposites prepared under sc-CO_2 by melt compounding, Polymer Testing 27 (2008), 129-134

Chapter 2

Literature Review

2.1 INTRODUCTION

Though successful reinforcement of polymers with nanoparticles started in the early 1900's (Baekeland, 1909), the broad scientific community was not aroused by nanocomposites until the early 1990's when the Toyota research group reported that a multiple-fold increase in mechanical properties of nylon 6 was achieved by adding small amounts of nano-scale layered silicates (Usuki et al., 1993; Kojm et al., 1993). Subsequent interest surged in not only layered silicate platelets but also many other nanoparticles, such as carbon nanotubes, bionanoparticles, etc. For polymer-layered silicate nanocomposites (PLS), nearly two decades of studies have made the technology and the materials available for commercial applications. However, industrialization of nanotechnologies is still limited. Further efforts in this field are being made by numerous scientists and engineers.

2.2 STRUCTURES OF PLS NANOCOMPOSITES

No mater what processing method is used, structural morphologies of clay (modified and unmodified) mixed in a polymer matrix can be summarized in three categories: phase separated (or immiscible), intercalated and exfoliated, as illustrated in Figure 2.1. In regards to this thesis, a clay particle is considered to be an aggregate of tactoids, which in turn are composed of stacked thin disc-like sheets referred to as platelets. The platelet is the primary component sought by nanocomposite manufacturing but more often the multi-layered tactoid is the limiting cases based on chemistry or poor interfacial stress transfer. For the case of the phase separated morphology, no platelets separate from tactoids (stacks of platelets) during processing and possibly the tactoids never separate from the macro-scale aggregate, so a conventional composite is generated. In the intercalated morphology, a single polymer chain or more penetrates the galleries (interlayer space) within the tactoids, interlayer distance is increased, but the platelets still maintain a stack order. For the exfoliated structure, the silicate layers are completely separated and may be uniformly dispersed in a continuous polymer matrix. Composites with one of the latter two structures are considered as nanomaterials. For most purposes, however, only the exfoliated morphology is desired because this structure is believed to be able to maximize enhancement of properties. Unfortunately, this ideal structure is not readily achieved; in fact, by using the melt compounding method a truly complete exfoliation is unlikely to be obtained even for the cases where affinity between the filler and matrix is best tuned and processing parameters are optimized (Paul and Robeson

2008). A practical situation is that structure of a PLS nanocomposite is often mixed intercalated and exfoliated.

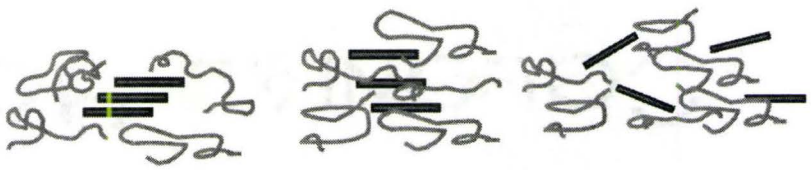

Immiscible Intercalated Exfoliated

Figure 2.1 Illustration of different states of dispersion of layered silicate in polymers. Reproduced from Reference (Paul and Robeson, 2008)

2.3 MECHANICAL PROPERTIES OF PLS NANOCOMPOSITES

A common reason for adding fillers into polymers is to increase their stiffness. Properly dispersed and aligned silicate platelets have proven to be very effective for increasing stiffness. Figure 2.2 gives an example of high reinforcement efficiency seen by a layered silicate filler (Lee et al., 2005). The relative tensile modulus, i.e. modulus ratio of a composite to its corresponding neat polymer, for a polypropylene /ethylene-based elastomer blend (TPO) that was reinforced by montmorillonite (MMT) is shown to be much higher than that by talc; talac being similarly composed of silicate sheets but in this case unable to separate like MMT. To double the tensile modulus of the matrix material, four times more talc than MMT is needed, which signifies both weight and fuel savings for an automotive part made with such a material. Therefore, polymer/MMT

nanocomposites are, in some cases, replacing the talc species (Paul and Robeson, 2008). Similar reinforcement is found for other polymer matrices, such as polyamides (Fornes and Paul, 2003; Liu and Wu, 2002), polystyrene (Vaia et al., 1993), polyethylene (Goettler, 2005), and polyurethane (Finnigan et al., 2004).

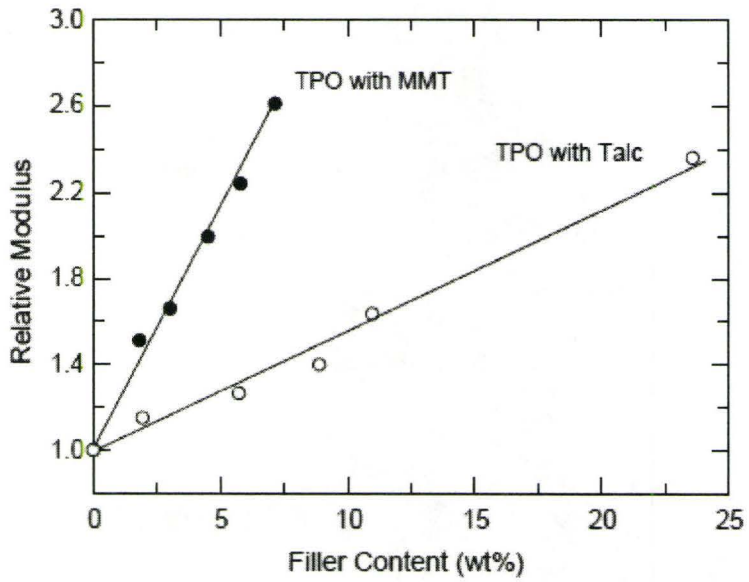

Figure 2.2 Stiffness of PLS nanocomposites: comparison of relative tensile modulus for TPO composites based on MMT vs. talc (Lee et al., 2005)

Similarly, the storage modulus of PLS nanocomposites is also improved in comparison with the neat polymers with introduction of MMT. Figure 2.3 gives an example of the improvement of this property where storage modulus of polyamide 6 nanocomposite significantly increases with increased MMT contents (Fornes and Paul,

2003). At a specific temperature, especially above the glass transition temperature, the storage modulus of a nanocomposite can be much higher than that of the neat polymer. In this figure, the intersection of these curves with the horizontal line at E' = 1.82 MPa is a good approximation to the heat distortion temperature of these materials and we can see that this temperature can be increased by approximately 100°C when added about 7 wt% of MMT.

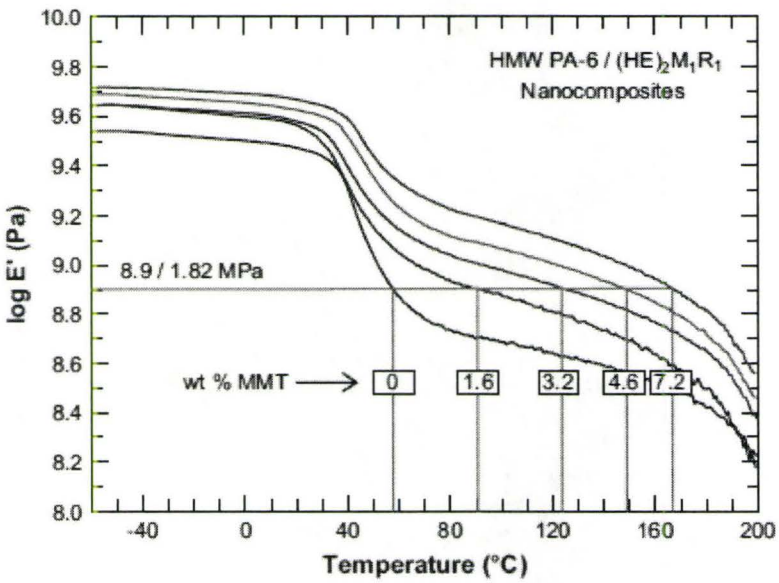

Figure 2.3 Storage moduli for nylon 6 nanocomposites with different MMT content (Fornes and Paul, 2003)

Similarly, the strength of PLS nanocomposites is usually increased compared to neat polymers. For example, Shelley et al. (2001) reported a 175% improvement in yield stress for a nylon 6 nanocomposite containing 5 wt% of MMT. However, the opposite

may also occur. For example, the tensile strength of poly(styrene-co-acrylonitrile)/MMT nanocomposite was found to decrease as clay loading increased (Stretz et al., 2005). Paul and Robeson (2008) argued that strength of a nanocomposite is mainly dependent on the level of adhesion of the filler to the matrix (an important point for discussion later in this thesis) and that the addition of organoclays to ductile polymers increases the yield strength; however, for brittle matrices failure typically occurs at lower strain.

Conversely, addition of fillers generally decreases the ductility of polymers, e.g., elongation at break. A recent review lists tensile properties of varied PLS nanocomposites (Pavlidou and Papaspyrides, 2008). Reduced elongation means a reduction in impact strength because less energy is needed to break; however, for PLS nanocomposites, this is not always the case because the reduced elongation may be compensated by reinforced strength. The fracture energy of poly(ethylene-co-methacrylic acid)/MMT nanocomposites was found increased with organoclay addition at low concentrations (less than 3 wt% MMT) but decreased with further increases in the organoclay concentration (Yoo et al., 2007). The initial increase in fracture energy was attributed to a result of the higher forces during loading caused by the increased modulus and increased yield stress upon addition of organoclay. The decrease in fracture energy with further addition of the clay was owing to the continuous decrease in ductility.

2.4 REINFORCEMENT MECHANISM OF PLS NANOCOMPOSITES

To design and create better performing PLS nanocomposites, theoretically understanding how greater reinforcement by the silicate sheets develops is important.

Some researchers attribute the high reinforcement efficiency of MMT to "nano-effects", i.e. geometric confinement produced by the platelets on macromolecules (Anastasiadis et al., 2000; Zax, et al., 2000; Crosby and Lee, 2007) while others think that there is no such "nano-effects" and that common composite theories are sufficient to depict the MMT reinforcement (Paul and Robeson, 2008; Fornes and Paul, 2003).

The geometric confinement theory states that the dramatic improvement in modulus for a clay concentration as low as 2–5 wt % cannot be attributed simply to the introduction of the higher modulus inorganic platelets (a reasonable in-plane modulus of a MMT platelet is about 178 GPa (Fornes and Paul, 2003), much higher than that of a virgin polymer). It infers that the silicate surface has a confinement effect on the polymer melt at the nanometer scale. Fluids, due to the nanoscopic confinements, possess a variety of unusual properties and, in particular, remarkable dynamic heterogeneities which vary on length scales as short as a fraction of a nanoscale filler surface. A polymer in the center of these nanopores is more mobile than the bulk while chain segments which interact with the silicate surface are dynamically inhibited. A polymer layer formed and physically adsorbed on the silicate surface possesses much higher modulus than the bulk. Due to high aspect ratio of the silicate sheets, the surface area exposed to the polymer melt is huge and numerous such stiffer polymer layers are generated, and therefore the modulus of the composites increases significantly even with very low filler content.

However, Fornes and Paul (2003) successfully predicted the modulus of nylon-6 nanocomposites simply based on the Halpin-Tsai and Mori-Tanaka equations, two traditional micromechanics theories. A basic premise of these theories is that the matrix

and filler have the same properties as when the other component is not there, i.e. without allowing for any "nano-effect" mentioned in the geometric confinement mechanism. These theories consider only the aspect ratio, orientation and volume fraction of a filler in a matrix. As shown in Figure 2.4, for the reinforcement of nylon 6 with unmodified MMT, the Halpin-Tsai equation predicts higher values than the Mori-Tanaka theory, but the experimental data is bracketed by the two predictions. Thus, they concluded that simple reinforcement considerations adequately explain the observations, i.e. the superior reinforcement of nylon 6/MMT nanocomposites arises primarily from the combination of high modulus and aspect ratio of MMT platelets, rather than from phase changes in the polymer matrix caused by the clay. Their analyses also showed that that incomplete exfoliation of the clay stacks caused a dramatic decrease in reinforcement efficiency which was a result of a reduction in both the aspect ratio and effective modulus of the clay stacks. The largest decrease in reinforcing efficiency was observed when going from one to two platelets per stack.

No matter which reinforcement mechanism is applicable, the key factor for mechanical properties of PLS nanocomposites is the aspect ratio of the nanofiller. The higher aspect ratio obtains the more intense improvement in mechanical properties. It is this reason that all reinforcement studies with PLS nanocomposites have a common goal: pursuing complete exfoliation.

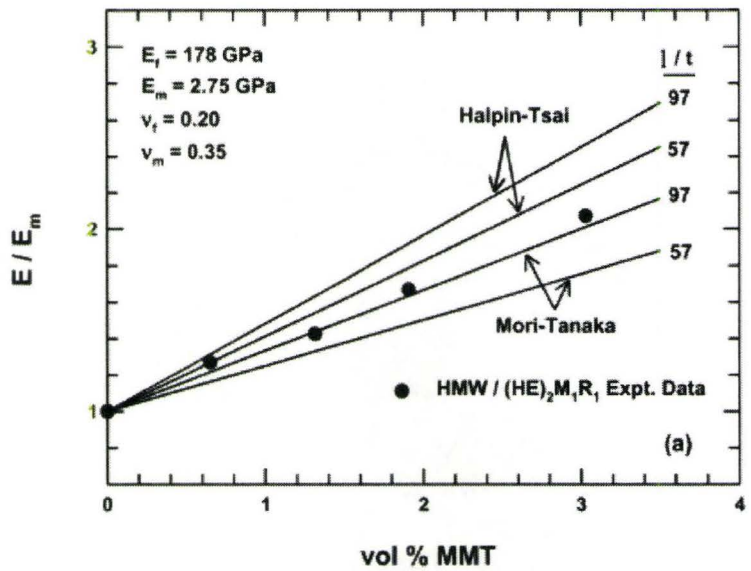

Figure 2.4 Experimental and theoretical stiffness data for nylon 6 nanocomposites: model predictions are based on unidirectional reinforcement of pure MMT having a filler modulus of 178 GPa and aspect ratio of 57, experimentally determined number average value, and 97, corresponding to complete exfoliation. (Fornes and Paul, 2003)

2.5 EXFOLIATION PROCESS OF PLS NANOCOMPOSITES

Knowing how exfoliation develops during melt compounding is the key to obtaining the ideal structure through this method. In literature, basically there are two typical mechanics for formation of a PLS nanocomposite: one is the diffusion-controlled process established by Giannelis' group as well as by the Toyota research team (Vaia et al., 1995, 1996, 1997; Hasegawa et al., 2000; Schmidt et al., 2002) and the other is the "peeling" hypothesis proposed by Paul and co-workers (Paul and Robeson, 2008; Fornes and Paul, 2003; Cho and Paul, 2001; Fornes et al., 2001). Figure 2.5 depicts the former

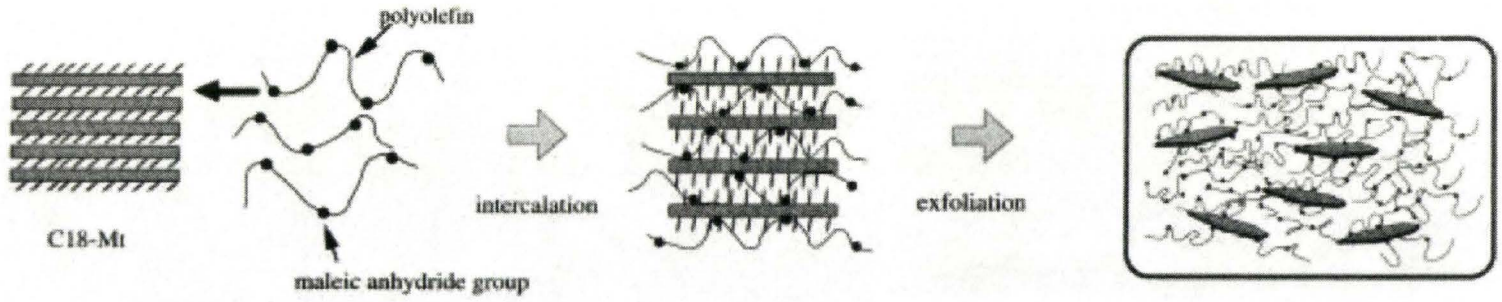

Figure 2.5 Schematic representation of clay dispersion process. Reproduced from reference [Hasegawa 2000]

mechanics where polymer chains first diffuse into galleries of an organoclay. During this stage, the pathway does not require high shear, and the major driving force is either physical or chemical affinity of the polymer to the organoclay surface which overcomes the strong attractive van der Waals forces between two silicate platelets. In this process, if enough time is given, the platelets will be pushed apart further and further until an exfoliated state is reached. Following this stage, the platelets delaminate from the swelled stacks. During the delamination stage, shear is the major driving force, and therefore, high shear intensity will facilitate exfoliation. It is the intercalation stage that controls the whole processing because the diffusion is a time-dependent process.

Paul and coworkers considered polymer systems which did not readily demonstrate the intercalation-controlled process. This is particularly true of olefinic polymers where no favourable bond associations are conceivable with the clay mineral. They considered that shear was the primary driving force in such systems for exfoliation to occur. In Figure 2.6, initially the stresses imposed during melt compounding break up aggregates of tactoids or organoclay particles into individual tactoids and can shear the individual tactoids into smaller ones. Then, diffusion driven by affinity between the filler and matrix plays a major role. The affinity allows polymer chains to access and enter the edge area of a clay tactoid pushing the ends of platelets apart. With the synergistic effect of the affinity and shear force, the outside platelet initially bends from others in the tactoid at the edge and then peels off from the tactoid. With peeling one by one, platelets exfoliate and disperse in the polymer matrix.

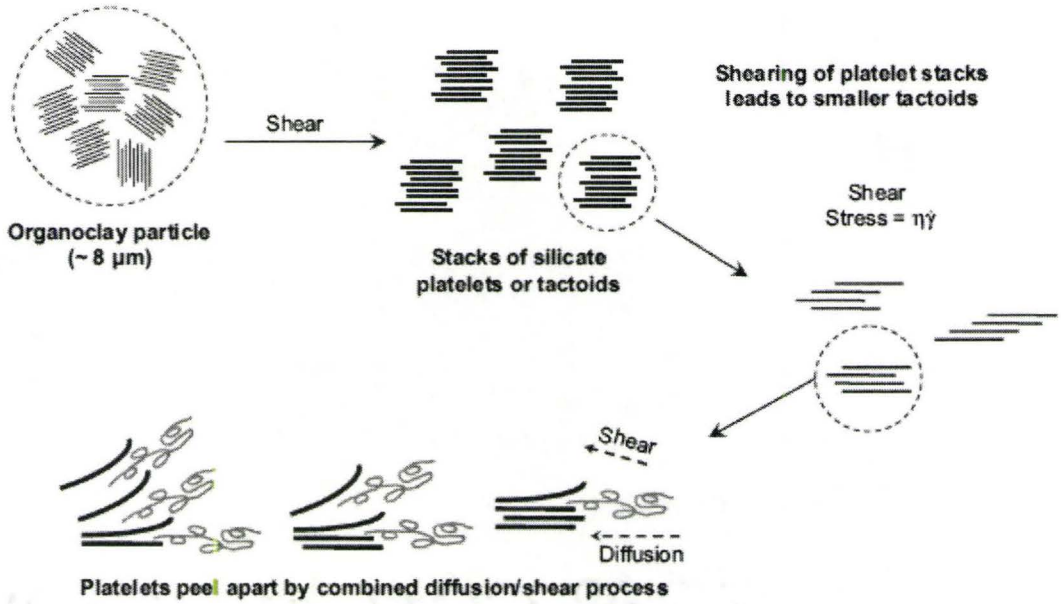

Figure 2.6 Mechanism of organoclay dispersion and exfoliation during melt processing (Paul and Robeson, 2008)

Despite significant differences between the two proposed mechanisms in regard to exfoliating process, both of them emphasize roles of affinity between the nanofiller and the polymer chains and the importance of shear stress during the melt compounding. Both also recognize that it is the affinity that finally determines whether or not an exfoliated morphology is developed. The intercalation-controlled mechanism was proposed several years earlier than the peeling hypothesis and therefore it has been more widely accepted. In literature, huge amount of research work quote the diffusion-controlled intercalation mechanic when explaining their results. Nevertheless, a recent theoretical study by Borse and Kamal (2009) suggests that surface peeling appears to be a more likely mechanism for size reduction or exfoliation of the clay particles via melt processing.

2.6 INTERCALATION BARRIERS AND DRIVIVING FORCES

The occurrence of intercalation and exfoliation during melt compounding is difficult because in most cases diffusion of a polymer chain into the interlayer region of a silicate nanofiller is not thermodynamically favoured. Even for organically modified MMT, the gallery spacing is on the order of 1 nm, much smaller than the radius of gyration of typical macromolecules (Flory, 1992). Thus, a large entropic penalty exists due to the interlayer confinement, which inhibits the polymer chains from diffusing or penetrating the gaps of the layered tactoids. On the other hand, silicate sheets tightly hold together due to van der Waals attractive forces in between them. The cohesion is another major barrier for the intercalation. If intercalation occurs, the affinity between filler and matrix has to be strong enough to overcome the interlayer cohesion and the entropic penalty for polymer chains.

For an orgnoclay/polymer system there are two major interactions which are involved in intercalation and exfoliation: one is the interaction between surfactant and polymer while the other is the interaction between silicate surface and polymer chains. In order to increase compatibility of the silicate filler with polymer matrix, the silicate sheets (e.g. MMT) are modified using organic surfactant. It is conceivable that more oleophilic nature of a modified MMT would increase the filler/matrix compatibility; at the same time, the intercalated surfactant reduces cohesion between silicate layers and the increased interlayer distance reduces confinement of the polymer chains, all of which are factors that favour the intercalation. Therefore, structure and properties of a surfactant play an important role in the intercalation and exfoliation. Fornes at al. (2002) examined

six pairs of amine surfactants modifying MMT which were used to prepare nylon 6 nanocomposites. Their studies show that in terms of degree of exfoliation a single long alkyl tail gave the best exfoliation, that methyl groups was better than hydroxyl-ethyl groups and that surfactant loading equivalent to the cation exchange capacity of the MMT was better than overloading. These results imply that increase in interaction between surfactant and polymer negatively affects intercalation. They remarked that nylon 6 has good affinity for the silicate surface, probably by hydrogen bonding, and as a result very high levels of exfoliation could be achieved in this matrix provided the processing conditions and melt rheology are properly selected. One alkyl tail is needed to reduce the platelet-platelet cohesion while adding more than one tends to block access of the polyamide chains onto the silicate surface, diminishing the favorable interactions of silicate surface and the polyamide. More than one alkyl tails also increase the very unfavorable alkyl-polyamide interactions. Better effect of methyl groups than hydroxyl-ethyl groups may be understood that favorable enthalpy between polymer and silicate surface is more important than that between surfactants and polymer. Their work indicated that favorable interactions between the silicate surface and the polymer matrix were more important than those between surfactant and polymer.

However, for a non-polar matrix, e.g. polyolefins, the surfactant/polymer interactions are the major favorable enthalpic affinity and the unfavourable silicate-matrix interactions will repel the polymer chains from accessing to organoclay surface. Therefore, in such a polyolefin/organoclay mixing system, the affinity for intercalation is weak. In order to increase attractions between silicate surface and the polymer matrix, the

non-polar matrix material is functionalized. Maleation of polyolefins shown in Figure 2.5 is an example of the functionalization. The grafted polar groups provide favourable enthalpic interactions with silicate surface, and thus driving force for intercalation increases. Apparently, the more functional groups the stronger attractive force between silicate and polymer (Kato et al., 1997). Unfortunately, the functionalization, for instance, maleation of polypropylene, usually results in significant drop in molecular weight (Shi et al., 2001). The more functionalized the lower molecular weight. The reduced molecular weigh diminishes mechanical properties of the nanocomposites. On the other hand, the functionalized polymer is very expensive. Therefore, the functionalized materials are mostly used as a coupling agent, which is usually called compatibilizer. Addition of small amount of compatibilizer into the polyolefin/organoclay system is expected to have two functions. One is to intercalate stacks of an organoclay making the organoclay swell and ready to delaminate in a shear stress field and the other is to provide a bridge between the filler and the apolar matrix increasing thermodynamic stability of the nanocomposite. Experimental studies show that a compatibilizer works well in non-polar PLS nanocomposites (Kato et al., 1997; Kawasumi et al., 1997; Ton-That et al., 2004; Shah and Paul, 2006).

In the literature, there are several theoretic studies on intercalation (Vaia and Giannelis, 1997; Balazs et al., 1998, 1999; Lyatskaya and Balazs, 1998). These studies claim that the entropy gain by configuration changes of surfactant molecules can partially compensate or even balance the entropy loss by polymer intercalation. They go on to infer that the morphology of a PLS composite formed by melt compounding depends on

enthalpic interactions between its components. Favorable energetic interactions between the filler and matrix have to be present to reach a negative total free energy of the mixing system because it is the driving force for intercalation and assurance for the formed nanocomposite being thermodynamically stable.

2.7 APPLICATION OF $scCO_2$ IN THE POLYMER PROCESSING

A supercritical fluid is defined as a substance for which both pressure and temperature are above their critical values and the density of which can be tuned from liquid-like to gas-like simply by changing temperature and/or pressure. The vapor-liquid-coexistence state of a fluid above its critical point makes it an excellent solvent with gas-like viscosity and liquid-like density. Supercritical carbon dioxide has a critical temperature (T_c) of 304.05K and critical pressure (P_c) of 7.40MPa (Kemmere and Meyer, 2005). Compared to other supercritical fluids, carbon dioxide has received much more attention due to its easy accessibility to the supercritical state (particularly for industrial uses), easy removal simply by depressurization, relative benignity to the environment, chemical inertness, low toxicity, low cost, and non-flammability. Its ability to solvate is similar to organic solvents and tunable by simply changing temperature and pressure conditions (Tomasko et al., 2003). For most high molecular weight polymers, $scCO_2$ is not a good solvent, but its solubility in many such polymers is substantial. In such cases, $scCO_2$ acts as plasticizer, suitable for polymer processing and polymer synthesis.

Applications of $scCO_2$ in polymer processing have included polymer modification, blending, foaming, particle formation, etc.

2.8 SUPERCRITICAL CO_2 AND CLAY MINERALS

Supercritical CO_2 is mainly used as a regenerative solvent and an intercalant aid for clay minerals and organoclays. As an extractive or regenerative solvent, $scCO_2$ was reportedly used to clean natural clay soils contaminated with hydrocarbons, especially hydrocarbon polymers, (Reutergardh et al., 1998; Elektorowicz et al., 2007) and regenerate clay minerals (Braida et al., 2007) and organoclays (Mendes and Coelho, 2005) containing adsorbed organic compounds. Supercritical CO_2 has also been used as an aid to exfoliate layered silicate particles (Manke et al., 2002), as a processing medium for intercalating natural clay with sugar acetate and β-D-galactose (Gulay et al., 2006) and with organically modified clay using 4-phenylazoaniline (Ishii et al., 2002). These studies were primarily focused on the extent of desorption achieved for various adsorbed organic species and the morphology of intercalated silicate layer structures. They were not concerned with the interaction of the $scCO_2$ with the organic adsorbents (i.e. surfactants) or the clay surface on a molecular level. Horsch et al. (2006) and the author's group (Thompson et al., 2008, 2009) reported the interactions between $scCO_2$ and surfactant modifier of MMT. In the work by Horssh et al. the $scCO_2$ effect on clay dispersion was attributed to rapid depressurization and proposed that CO_2-philicity to the surfactant of the organoclay might result from the presence of acidic hydrogen atoms on the surfactant. Our studies showed that surfactant rearranged due to presence of $scCO_2$.

2.9 USE OF $scCO_2$ IN THE PROCESSING OF PLS NANOCOMPOSITES

In recent years, $scCO_2$ started to present in studies on PLS nanocomposites made by melt compounding method (Manke et al., 2002; Mielewski et al, 2004; Horsch et al.,

2006; Yang and Ozisik, 2006; Nguyen and Baird, 2007; Treece and Oberhauser, 2007; Ma et al., 2007; Litchfield et al., 2007; Zhao and Huang, 2008; Ottaviani et al. 2008). These studies are generally focused on improving the dispersion of clay into the polymer matrix using a supercritical solvent. Technologies emerging from these patents and published papers can basically be summarized into three categories. The first and most extensively pursued is direct gas injection into a mixing device where all components are melt compounded (Treece and Oberhauser, 2007; Ma et al., 2007; Zhao and Huang, 2008). This approach aims at good solubility of surfactant and polymeric components in the supercritical fluid, expecting improved intercalation and exfoliation occurred during the shear-dominated melt mixing. Another approach focuses on pre-exfoliating the layered silicate filler using the supercritical fluid. Gulari et al. used a technique known as 'particles from gas-saturated solutions/suspensions (PGSS)' in the hopes of fracturing the layered structure of an organoclay before it was added to the compounding process (Manke et al., 2002; Horsch et al., 2006). Baird et al. modified this technology from a batch to a continuous process (Nguyen and Baird, 2007). The third method was recently proposed by Rodgers et al. (Ottaviani et al., 2008) who added the supercritical fluid and organoclay together into a highly pressurized zone of the compounding process which maintains the CO_2 gas in its supercritical state during mixing, at least for the initial stages. This technology can be looked at combination of the last two methods since the fracturing effect in the second approach was expected when the highly pressurized materials eventually reaches a low pressure region. All of the methods refer to improved exfoliation.

REFERENCES

Anastasiadis S.H., et al. Nanoscopic-Confinement Effects on Local Dynamics, *Phys. Rev. Lett.* 84 (2000), 915

Baekeland L.H., *sci. Am.* 68 (Suppl.) (1909), 322

Barry J.J.A., Gidda H.S., Scotchford C.A., Howdle S.M. Porous methacrylated scaffolds: supercritical fluid fabrication and in vitro chondrocyte responses, *Biometerials* 25 (2004), 3559-3568

Balazs A.C., Singh C., Zhulina E., Modeling the Interactions between Polymers and Clay Surfaces through Self-Consistent Field Theory, *Macromolecules* 31 (1998), 8370

Balazs A.C., Singh C., Zhulina E., Lyatskaya Y., Modeling the Phase Behavior of Polymer/Clay Nanocomposites, *Acc. Chem. Res.* 8 (1999), 651

Borse N.K., Kamal M.R., Estimation of stresses required for exfoliation of clay particles in polymer nanocomposites, *Polym. Eng. Sci.* 49(4) (2009), 641-650

Braida I., Mattea M., Cardarelli D. Extraction-adsorption-desorption process under supercritical condition as a method to concentrate antioxidants from natural sources, *J. Supercritical Fluids*, 45(2) 2008, 195-199

Cho J.W., Paul D.R., Nylon 6 nanocomposites by melt compounding, *Polymer* 42 (2001), 1083

Crosby A.J., Lee J.-Y., Polymer Nanocomposites: The "Nano" Effect on Mechanical Properties, *Polym. Rev.* 47 (2007), 217

Dong Z., Liu Z., Han B., Pei X., Liu L., Yang G. Modification of isotactic polypropylene films by grafing of methyl acrylate using supercritical CO_2 as a swelling agent. *J Supercrit Fluids*, 32 (2004) 67-74

Eleektorowicz M., El-Sadi H., Lin J., Ayadat T. Effect of supercritical fluid extraction parameters and clay properties on the efficiency of phenanthrene extraction, *J. Colloid Inerface Sci.* 309 (2007), 445-452

Elkovitch M.D., Lee L.J., Tomasko D.L. Effect of supercritical carbon dioxide on morphology development during blending. *Polym. Eng. Sci.* 40 (2000), 1850-1861

Finnigan B., Martin D., Halley P., Truss R., Campell K., Morphology and properties of thermoplastic polyurethane nanocomposites incorporating hydrophilic layered silicates, *Polymer* 45 (2004), 2249

Flory P.J., Configuration of polymer chains, in Prince of Polymer Chemistry (Chapter X), Cornell University Press, 1992

Fornes T.D., Yoon P.J., Keskkula H., Paul D.R., Nylon 6 nanocomposites: the effect of matrix molecular weight, *Polymer* 42 (2001), 9929

Fornes T.D., Yoon P.J., Hunter D.L., Keskkula H., Paul D.R., Effect of organoclay structure on nylon 6 nanocomposite morphology and properties, *Polymer* 43 (2002), 5915

Fornes T.D., Paul D.R., Modeling properties of nylon 6/clay nanocomposites using composite theories, *Polymer* 44 (2003), 4993

Fujiwara T., Yamaoka, Kimura Y., Wynne K.J. Poly(lactide) swelling and melting behavior in supercritical carbon dioxide and post-venting porous material, *Biomacromolecules*, 6 (2005), 2370-2373

Goettler L.A., *Ann. Tech. Confr. Soc. Plast. Eng.* 2005:1980

Hao J., Whitaker M.J., Serhatkulu G., Shakesheff K.M., Howdle S.M. Supercritical fluid assisted melting of poly(ethylene glycol): a new solvent-free route to micro particles, *J. Mater. Chem.* 15 (2005), 1148-1152

Hasegawa N., Okamoto H., Kawasumi M., Kato M., Tsukigase A., Usuki A., *Macromol. Mater. Eng.* 280/281 (2000), 76

Horsch S., Serhatkulu G., Gulari E., Kannan R.M., Supercritical CO_2 dispersion of nano-clays and clay/polymer nanocomposites, *Polymer* 47 (2006), 7485-7496

Ishii R., Wada H., Ooi K. A comparison of supercritical carbon dioxide and organic solvents for the intercalation of 4-phenylazoaniline into a pillared clay mineral, *J. Colloid Interface Sci.* 254 (2002), 250-256

Kato M., Usuki A., Okada A. Synthesis of polypropylene oligomer—clay intercalation compounds, *J. Appl. Polym. Sci,* 66 (1997), 1781-1785

Kavahara Y., Yoshioka T., Sugiura K., Ogawa S., Kikutani T. Dyeing behavior of high-speed spun poly(ethylene terephthalate) fibers in supercritical carbon dioxide, *J. Macromol. Sci. B: Phys.* 40(2) (2001), 189-197

Kawasumi M., Hasegawa N., Kato M., Usuki A., Okada A., Preparation and Mechanical Properties of Polypropylene–Clay Hybrids, *Macromolecules* 30 (1997), 6333–6338

Kazarian S.G., Brantley N.H., Eckert C.A. Dyeing to be clean: Use supercritical carbon dioxide, *CHEMTECH*, July 1999, 36-41

Kemmere M.F., Meyer T. Supercritical carbon dioxide in polymer reaction engineering, Wiley-Vch Verlag GmbH & Co. kGaA, Winheim, Germany, 2005

Kim S., Kim Y.-S., Lee S.-B. Phase behaviors and fractionation of polymer solutions in supercritical carbon dioxide, *J. Supercrit. Fluids*, 13 (1998), 99-106

Kojima Y., Usuki A., Kawasumi M., Okada A., Fukushima Y., Kurauchi T., Kamigaito O., Mechanical properties of nylon 6-clay hybrid, *J. Mater. Res.* 8 (1993), 1185

Lee H.-S., Fasulo P.D., Rodgers W.R., Paul D.R., TPO based nanocomposites. Part 1. Morphology and mechanical properties, *polymer* 46 (2005), 11673

Li D., Han B., Liu Z. Grafting of 2-hydroxyethyl methacrylate onto isotactic polypropylene using supercritical CO_2 as a solvent and swelling agent, *Macromol. Chem. Phys.* 202 (2001), 2187-2194

Litchfield D., Nguyen Q., Baird D. Super-critical carbon dioxide assisted melt intercalation of polymer layered silicate nanocomposites, *ANTEC* 2007, 72-75

Liu Z., Song L., Dai X., Yang G., Han B., Xu J. Grafting of methylacrylate onto isotactic polypropylene film using supercritical CO_2 as a swelling agent, *Polymer* 43 (2002), 1183-1188

Liu T., Hu G.-H., Tong G.-S., Zhao L., Cao G.-P., Yuan W.-K. Supercritical carbon dioxide assisted solid-state grafting of maleic anhydride onto polypropylene, *Ind. Eng. Chem. Res.* 44 (2005), 4292-4299

Liu X., Wu Q., Polyamide 66/Clay Nanocomposites via Melt Intercalation, *Macromol. Mater. Eng.* 287 (2002), 180

Lyatskaya Y., Balazs A.C., Modeling the Phase Behavior of Polymer–Clay Composites, *Macromolecules* 31 (1998), 6676

Ma J., Bilotti E., Peijs T., Darr J.A., Preparation of polypropylene/sepiolite nanocomposites using supercritical CO_2 assisted mixing, *European Polymer Journal* 43 (2007), 4931-4939

Manke C.W., Gulari E., Mielewski D.F., Lee E.C., System and method of delaminating a layered silicate material by supercritical fluid treatment, *US Patent* 6,469,073 (2002)

McHugh M.A., Krukonis V.J. Supercritical Fluid Extraction, Butterworth-Heinemann, Stoneham, MA, 2nd edition, 1994

Mendes M.F., Coelho G.L.V. Desorption processes: Supercritical fluid regeneration of modified clays, *Adsorption* 11 (2005), 139-146

Mielewski D.F., Lee E.C., Manke C.W., Gulari E., System and method of preparing a reinforced polymer by supercritical fluid treatment, *US Patent* 6,753,360 (2004)

Nguyen Q.T., Baird D.G. An improved technique for exfoliating and dispersion nanoclay particles into polymer matrices using supercritical carbon dioxide, *Polymer* 48 (2007), 6923-6933

Ottaviani R. A., Rodgers W. R., Fasulo P. D., Okonski D. A.. *US Patent* 7,462,666 B2, Dec. 9, 2008

Paul D.R., Robeson L.M., Polymer nanotechnology: Nanocomposites, *Polymer* 49 (2008), 3187

Pavlidou S., Papaspyrides, C.D. A review on polymer layered silicate nanocomposites, *Prog. Polym. Sci.* 33 (2008), 1119, C.D., A review on polymer layered silicate nanocomposites, *Prog. Polym. Sci.* 33 (2008), 1119

Reutergardh L.B., Parkpian P., Chaiyaraksa C. Supercritical fluid extraction of planar and mono-ortho PCB in selected tropical soils, *Chemosphere* 36(7) (1998), 1565-1573

Schmidt D. et al., *Current Opinion in Solid State and Mater. Sci.*, 6 (2002), 205

Shelley J.S., Mather P.T., De Vries K.L., Reinforcement and environmental degradation of nylon-6/clay nanocomposites, *Polymer* 42 (2001), 5849

Shah R.K., Paul D.R., Organoclay degradation in melt processed polyethylene nanocomposites, *Polymer* 47 (2006), 4075

Shi D., Yang J., Yao Z., Wang Y., Huang H., Jing W., Yin J., Functionalization of isotactic polypropylene with maleic anhydride by reactive extrusion: mechanism of melt grafting, *Polymer* 42 (2001), 5549

Stretz H.A., Paul D.R., Li R., Keskkula H., Cassidy P.E., Intercalation and exfoliation relationships in melt-processed poly(styrene-*co*-acrylonitrile)/montmorillonite nanocomposites, *Polymer* 46 (2005), 2621

Taylor L.T. Supercritical Fluid Extraction, Wiley, New York, 1996

Thompson M.R., Liu J., Krump H., Kostanski L.K., Fasulo P.D., Rodgers W.R., *J. Colloid Interf. Sci.* 2008, 324, 177-184

Thompson M.R., Balogh M.P., Speer R.L. Jr., Fasulo P.D., Rodgers W.R., *J. Chem. Phys* 2009, 130 (044705), 1-8

Tomasko D.L., Li H., Kiu D., Han X., Wingert M.J., Lee L.J., Koelling K.W., A Review of CO_2 Applications in the Processing of Polymers, *Ind. Eng. Chem. Res.* 42 (2003), 6431-6456

Ton-That M.-T., Perrin-Sarazin F., Cole K.C., Bureau M.N., Denault J., Polyolefin nanocomposites: Formulation and development, *Polym. Eng. Sci.* 44 (2004), 1212

Treece M.A., Oberhauser J.P., Processing of polypropylene–clay nanocomposites: Single-screw extrusion with in-line supercritical carbon dioxide feed versus twin-screw extrusion, *J. Appl. Polym. Sci.* 103 (2007) 884-891

Usuki A., Kojima Y., Kawasumi M., Okada A., Fukushima Y., Kurauchi T., Kamigaito O., Synthesis of nylon 6-clay hybrid *J. Mater. Res.* 8 (1993), 1179

Vaia R.A., Ishii H., Giannelis E.P., Synthesis and properties of two-dimensional nanostructures by direct intercalation of polymer melts in layered silicates, *Chem. Mater.* 5 (1993) 1694

Vaia R.A., Jandt K.D., Kramer E.J., Giannelis E.P., Kinetics of Polymer Melt Intercalation, *Macromolecules*, 28 (1995), 8080

Vaia R.A., Jandt K.D., Kramer E.J., Giannelis E.P., Microstructural Evolution of Melt Intercalated Polymer--Organically Modified Layered Silicates Nanocomposites, *Chem. Mater.* 8 (1996), 2628

Vaia R.A., Giannelis E.P., Lattice Model of Polymer Melt Intercalation in Organically-Modified Layered Silicates, *Macromolecules* 30 (1997), 7990

West B.L., Kazarian S.G., Vincent M.F., Brantley N.H., Echert C.A. Supercritical fluid dyeing of PMMA films with azo-dyes, *J. Appl. Polym. Sci.* 69 (1998), 911-919

Yang K., Ozisik R. Effects of processing parameters on the preparation of nylon 6 nanocomposites, *Polymer* 47 (2006), 2849-2855

Yoo Y., shah R.K., Paul D.R., Fracture behavior of nanocomposites based on poly(ethylene-*co*-methacrylic acid) ionomers, *Polymer* 48 (2007), 4867

Zax D.B., Yang D.-K., Santos R. A., Hegemann H., Giannelis E. P., Manias E., Dynamical heterogeneity in nanoconfined poly(styrene) chains *J. Chem. Phys.* 112 (2000), 2945

Zhao Y., Huang H.-X. Dynamic rheology and microstructure of polypropylene/clay nanocomposites prepared under sc-CO_2 by melt compounding, *Polymer Testing* 27 (2008), 129-134

Chapter 3

Influence of Supercritical CO_2 on the Interactions between Maleated Polypropylene and Alkyl-Ammonium Organoclay

This chapter is a paper accepted as:

J. Liu, M.R. Thompson, M. P. Balogh, R. L. Speer Jr., P. D. Fasulo, and W. R. Rodgers. Influence of Supercritical CO_2 on the Interactions between Maleated Polypropylene and Alkyl-Ammonium Organoclay, *Journal of Applied Polymer Science*, in press, 2010. Jinling Liu is the major contributor to this work.

In this chapter, influence of $scCO_2$ on the compatibilizer/organoclay intercalation was examined *by varying maleated propylenes (3 in total)* in their molecular weight and content of grafted anhydride. Influence of pre-treatment of an organoclay (Cloisite 20A) using $scCO_2$ on the intercalation was also investigated.

ABSTRACT

Supercritical carbon dioxide ($scCO_2$) has been proposed as an effective exfoliating agent for the preparation of polymer-layered silicate nanocomposites, though there is limited fundamental understanding of this mechanism. The present study looks at the interactions of this unique green solvent with three maleated polypropylenes of varying anhydride content and molecular size with an alkyl-ammonium organoclay. Mixtures of compatibilizers and organoclay were melt-annealed in a high pressure batch vessel at 200°C and subjected to either a blanket of nitrogen or $scCO_2$ at a pressure of 9.7 MPa. The structures and properties of these melt-annealed mixtures were characterized by X-Ray Diffraction (XRD), Transmission Electron Microscopy (TEM), Fourier Transform Infrared Spectroscopy (FTIR), Nuclear Magnetic Resonance Spectroscopy (NMR), Differential Scanning Calorimetry (DSC), and contact angle measurement. The results indicate that the plasticizing influence of $scCO_2$ aided intercalation and exfoliation for intercalants of moderate molecular size and anhydride content which would otherwise have limited diffusion into the clay galleries.

3.1 INTRODUCTION

For the polymer components that make a polymer-layered silicate (PLS) nanocomposite, it is well recognized in the foams literature that supercritical carbon dioxide ($scCO_2$) has a plasticizing effect, provided sufficient CO_2-philicity is demonstrated [1-3]. For olefinic polymers like polyethylene and polypropylene, $scCO_2$ demonstrates modest solubility in the range of 1-10wt%, depending on the system

conditions [4]. The result of this plasticizing effect during compounding, or other polymer processing operations, is most generally associated with a reduction of viscosity on the order of 10-30%, which can be attributed to the increased free volume of the melt [5]. Conversely, the compatibilizing additive commonly used with current polyolefin nanocomposite formulations still remains poorly understood with regard to its function in the mechanism of clay delamination, and its interactions with $scCO_2$ have thus far not been reported in the literature.

The term *compatibilizer,* when used in commercial nanocomposite literature, refers to a functionalized polymer with its backbone structure similar to the matrix resin and containing chemical groups suited to interfacial association with organo-modified clays. Due to its reasonable affinity with the matrix and clay species, minimal influence on final material properties, and ready availability, a popular example of a compatibilizer is maleic anhydride-grafted polypropylene (MA-PP) [6-9]. It is believed that the anhydride moiety coordinates with the broken plane of the silicate tactoids which contains hydroxyl groups and other oxidative functionalities [9-11]. The exact influence of MA-PP on forming a nanocomposite remains a contentious subject in the literature since both its molecular weight and degree of functionalization are thought to contribute to the delamination mechanism of melt intercalation [9-10, 12]; but, these two factors are highly correlated due to the degradation reaction used in its preparation [13]. It has been found that higher grafted concentrations of maleic anhydride lead to greater intercalation capacity [9], but miscibility of the compatibilizer with the polymer matrix decreases and eventually domain segregation occurs [10]. On the other hand, as the degree of

functionalization increases there is a corresponding decrease in the molecular weight of the MA-PP which reportedly improves clay dispersion but subsequently deteriorates the mechanical properties of the nanocomposite [12]. With regard to $scCO_2$, we consider its possible effects on the compatibilizer to include plasticization, improved interfacial association of the anhydride with the clay, or direct chemical reaction/association between the CO_2 and anhydride. Most evidence regarding $scCO_2$ interactions with maleic anhydride (MA) can be found in studies looking at Diels-Alder reactions conducted under supercritical conditions. Glebov et al. [14] found that the rate of reaction between maleic anhydride and isoprene under supercritical conditions was substantially increased when the MA concentration was below its CO_2 solubility limit and only a single phase existed. At higher concentrations of MA, multiple phases existed in their reaction system and the rate of reaction was decreased correspondingly closer to those trials without CO_2. Unfortunately, the literature in this area never hypothesized how the increase in reaction rate occurred. Extraction of MA from prepared MA-PP under $scCO_2$ was found by Clark and Lee [15], but they provided little analysis on the mechanism. In the work of Liu et al. [16], the authors attempted to prepare MA-PP by a solid-state free radical reaction aided by $scCO_2$. They found a maximum in the grafted maleic anhydride content in relation to CO_2 pressure, which was attributed to the partitioning of MA between different phases within the mixture.

This paper presents our studies looking at the influence of $scCO_2$ on the diffusion-controlled interactions between an organoclay and various maleated polypropylenes.

This is the third paper in a series attempting to understand the benefits of $scCO_2$ as a processing aid for producing highly exfoliated polyolefin nanocomposite materials.

3.2 EXPERIMENTAL

3.2.1 Materials

Three commercial maleated polypropylenes (MA-PP) were selected for this work in order to examine the influence of the maleic anhydride (MA) content and molecular weight on the intercalation of organoclays. These resins were Polybond® 3002 and Polybond® 3200 from Chemtura Corporation, and Licocene® PP MA 6252 provided by Clariant Corporation. Table 3.1 summarizes the properties of the three compatibilizers as well as lists the abbreviated terms used in this paper to refer to each material. The measured MA content for each compatibilizer found in the table was determined by KOH titration.

The organoclay, Cloisite® 20A (C20A) supplied by Southern Clay Products was selected based on its demonstrated favorable interactions with $scCO_2$ in our previous studies [17]. The clay species is a montmorillonite modified with dimethyl-dihydrogenated tallow ammonium chloride. Hydrogenated tallow is a mixture comprised largely of dimethyl-dioctadecylammonium chloride with minor components of dimethyl-octadecylhexadecylammonium chloride and dimethyl-dihexadecylammonium chloride. The properties of the organoclay are listed in Table 3.2. The calculated spreading coefficients for the clay with each compatibilizer are listed in Table 3.3 which showed

Table 3.1 Properties of the three compatibilizers

Compatibilizer	Name	Melting Range (°C)	Zero Shear Viscosity† (Pa-s)	M_N (g/mol)	M_W (g/mol)	MA Content (wt%)
Licocene® PP MA 6252*	Li6252	105-138	0.7	2,420	5,490	4.7 ± 0.2
Polybond® 3200**	PB3200	134-168	200	27,360	87,670	1.1 ± 0.1
Polybond® 3002**	PB3002	135-172	3600	51,830	254,350	0.4 ± 0.1

* supplied by Clariant

** supplied by Chemtura

† measured at 200°C

Table 3.2 Properties of the Organic Modified Montmorillonite

Surfactant structure	Surfactant content (wt %)	Surfactant melting range (°C)	*d*-spacing (Å)
$(CH_3)_2 (HT^*)_2N^+Cl^-$	38.5 ± 0.2	25-60	25.8

* HT= hydrogenated tallow (C_{18} ~65%; C_{16} ~30%; C_{14} ~5%).

Table 3.3 Surface energy of the three compatibilizers and C20A and interfacial tension between them at 50°C.

Species	Dispersive contribution*	Polar contribution*	Total surface energy	Interfacial tension with C20A	Spreading coefficient	
	γ^d (mJ/m^2)	γ^p (mJ/m^2)	γ (mJ/m^2)	γ_{sl} (mJ/m^2)	λ_{12}	λ_{21}
Licocene 6252	35.8	0.9	36.7	0.0	1.3	-1.5
Polybond 3200	35.8	0.2	36.0	17.4	1.8	-2.4
Polybond 3002	36.1	0.1	36.2	28.4	1.4	-2.4
Cloisite 20A	37.34	0.7	38.1	—	—	—

* standard deviation 0.8 % (maximum)

that spontaneous spreading should be expected at the selected operating temperature of 200°C used in our experiments. The interfacial properties of each clay-compatibilizer combination used in the spreading coefficient were determined from contact angle measurements, following the method disclosed in reference [18]. Surface tension values of the clay and compatibilizers were determined using the sessile drop contact angle method at 50°C with 1-bromonaphthalene (dispersive component δ^d = 42.517 mJ/m^2, polar component δ^p = 0.283 mJ/m^2) and glycerin (δ^d = 35.541 mJ/m^2, δ^p = 25.359 mJ/m^2). The values were corrected to 200°C assuming a decrease in surface tension with temperature at a rate of 0.1 mJ/(m^2 °C) [19].

The carbon dioxide and nitrogen used in the experiments were supplied by Air Liquide Canada Inc. at 99.5% and 99.995% purity, respectively.

3.2.2 Procedures

In preparation for the experiments, all three compatibilizers were first converted into fine powder from their pellet form in order to minimize segregation while being mixed with the clays. Li6252 was cryogenically ground into a fine powder of approximately 50 μm. The powders of PB3200 and PB3002 were prepared by precipitation from hot xylene using acetone due to difficulties with grinding, even under cryogenic conditions. The prepared materials were thoroughly washed with acetone, vacuum dried overnight at 80°C, and reduced to a fine powder in a blender to reach a particle size of 10-100 μm, similar to the clay. FT-IR analysis confirmed that after powder formation the major absorbances for the grafted anhydride remained, namely

carboxylic acid vibrations at 1715 cm^{-1} and the anhydride ring at 1781 cm^{-1} and 1790 cm^{-1}; the absorption pattern changed little when compared to the as-supplied compatibilizers. The MA-PP powder and clay powder were mixed manually to a ratio of 2:1 by weight. In certain instances, an organoclay that had been pretreated by exposure to $scCO_2$ (s-C20A) was used in place of C20A for the experiments. The pretreatment of the clay was performed by soaking the C20A under 9.7MPa of $scCO_2$ at 200°C in a batch vessel for 3 hours followed by a rapid depressurization at ~10 MPa/s.

Trials were run varying the compatibilizer, clay type, or gas type present. As typical conditions, each prepared polymer mixture of MA-PP and organoclay was first dried at 40°C under vacuum overnight and then directly placed into a high pressure batch vessel that had been heated to 200°C. The duration of an experiment was 30 minutes once pressurization was achieved. The apparatus has been described in detail in an earlier paper [17]. For those runs involving $scCO_2$, the gas was injected and maintained at 9.7MPa over the course of the trial with a Teledyne-ISCO 260D syringe pump. At the end of the run, the gas was removed by depressurization at 4.8 MPa/s. For each trial condition performed with $scCO_2$, a corresponding trial run under a nitrogen blanket was prepared for comparison and to establish the temperature effects while minimizing oxidative degradation. Upon removal from the batch vessel, each sample was ground using a mortar and pestle for subsequent analyzes.

3.2.3 Characterization

Thermal properties of the clay and polymers were measured in a TA Instruments Q200 differential scanning calorimeter (DSC). Thermograms of the different MA-PP by DSC were collected under a nitrogen atmosphere during the second heating cycle at a ramp rate of 10°C/min. The melting ranges for the three compatibilizers are given in Table 3.1. The thermal shielding of the intercalated surfactant in the clay required a more sensitive approach; therefore the modulating option of the DSC was used with a modulated period and amplitude of 60 seconds and ± 1°C, respectively at a heating rate of 1°C/min. The determined melting transition for the surfactant of the organoclay is included in Table 3.2.

The molecular weight moments of each compatibilizer listed in Table 3.1 were determined using a high temperature gel permeation chromatograph (GPC) manufactured by PolymerChar and equipped with IR, viscosity and light scattering detectors (15 and 90 degrees). The analysis was conducted at the Institute of Polymer Research (University of Waterloo, Waterloo, ON). The columns were PLgelOlexis made by Polymer Laboratories, and the chromatograph was operated at 145°C. A sample was dissolved in trichlorobenzene and passed through the columns at a flow rate of 1 ml/min.

Direct observations of gallery spacing for the clay were made by powder x-ray diffraction (XRD) using Cu Kα radiation ($\lambda = 1.541$ Å). Both ex-situ and in-situ analyses was conducted by XRD. The apparatus used for the in-situ XRD study was described in detail in an earlier paper [20]. Briefly, the cell containing the clay samples for the in-situ

tests was a 1 mm diameter quartz capillary tube (10 μm wall thickness) with its open end affixed to a high pressure manifold. The CO_2 gas was pressurized to above 13.9 MPa in an attached batch vessel and then supplied at the appropriate pressure by a series of control valves to the sample cell. The clay sample was heated by a small furnace encompassing the capillary tube. Two 90° conical windows cut into the furnace wall allowed observation of the 2θ ranges ± 45° at 0° incidence angle. The temperature of the system was controlled by a thermocouple mounted in the wall of the furnace while the actual temperature of the sample in the field of view of the X-ray beam was calibrated using a series of melting point standards. The XRD data was collected over a period of 300 seconds with consecutive scans taken to study the influence of the gas on the clay/compatibilizer system for a 30 minute duration.

Transmission electron microscope (TEM) analyses of the processed mixtures were performed using a JEOL 1200 EX TEMSCAN microscope operating at an accelerating voltage of 80kV and a magnification of 200,000x. For TEM observations, each sample was first embedded in epoxy resin and microtomed with a diamond knife into thin sections approximately 70 nm thick.

Interactions between the organoclay with the different compatibilizers affected by the $scCO_2$ were determined by Fourier transform infrared (FT-IR) and solid-state ^{13}C nuclear magnetic resonance (^{13}C NMR) spectroscopy.

Transmission infrared absorbance spectra of the neat compatibilizers and prepared samples from the high pressure vessel involved collection of 64 scans at 2 cm^{-1} resolution

over a range of 500-4000 cm^{-1} using a Bio-Rad FTS-40 spectrometer. The neat compatibilizers were prepared as films in a hot press at 165°C under 0.13 MN compressive force for 5 minutes. Powder clay or powdered clay/polymer samples were mixed with dry KBr and compressed into tablets.

The 125 MHz solid-state ^{13}C NMR analysis was performed with a Bruker 500 MHz NMR spectrometer at 23°C and 50°C. The higher probe temperature used was higher than the melting point of the surfactant (45°C) for C20A. Both single-pulse direct-polarization (Bloch-decay) and cross-polarization methods were used with ^{1}H decoupling. All experiments employed a 24 kHz spectral window centered on the main peaks, a 5 kHz magic-angle spinning frequency, and a 41 ms acquisition time. A cross-polarization (CP MAS) contact time of 3 ms and repetition delay of 5 s were used for the spectra as determined by a variable contact-time experiment. A 4.5 μs (90°) ^{13}C pulse and a repetition delay of 40 s were used in the Bloch-decay (BD MAS) analysis. All chemical shifts were referenced to tetramethylsilane (TMS) at 0 ppm.

3.3 RESULTS AND DISCUSSION

Previous works by the present authors have examined the influence of $scCO_2$ on the organoclay individually, both after treatment in the supercritical solvent [17] and in-situ [20]. Both experiments found the supercritical solvent primarily acted as a plasticizer with alkyl ammonium-modified montmorillonite, overcoming the 'barrier effect'. The barrier effect normally limits the cation exchange reaction used in their preparation to the outer edges of the clay galleries. The barrier is created by the presence of van der Waals

attractive forces between bound and free intercalated surfactant species, thereby preventing the organic modifier from fully penetrating into the central region of the silicate sheets, and hence sodium ions remain present in the prepared organoclays. Supercritical CO_2 along with elevated temperatures allowed greater chain mobility for the surfactant molecules and as a result, further cation exchange reactions were observed to occur [17]. Generally, this unique solvent afforded rearrangement of the surfactant and greater organic coverage over the silicate surface, which brought about either basal expansion or partial collapse depending on the original surfactant arrangement in the galleries. With rapid depressurization of the clay suspension in $scCO_2$, a small but further increase in basal spacing was detected, though the work of Horsch et al [21] suggested instead that the particles were fractured. In the studies of the present paper, these rapidly depressurized $scCO_2$-treated organoclays are simply referred to as *pretreated* and the species included in the study is denoted as s-C20A. With the introduction of a compatibilizer to the system of organoclay and $scCO_2$, it is expected that both polymer intercalation and surfactant rearrangement will proceed simultaneously.

3.3.1 XRD, Interlayer Spacing of the Mixtures

Direct evidence of intercalation by the compatibilizers was obtained from analysis of the XRD patterns for the melt-annealed mixtures and neat C20A under $scCO_2$ or N_2 conditions. First, the basal spacings of the neat organoclays as determined by ex-situ XRD analyses are shown in Figure 3.1. The as-supplied C20A showed a characteristic broad, moderate intensity peak centered at $2\theta = 3.4°$ corresponding to a nominal basal spacing of 26 Å. It is noted that the same clay material showed only minor

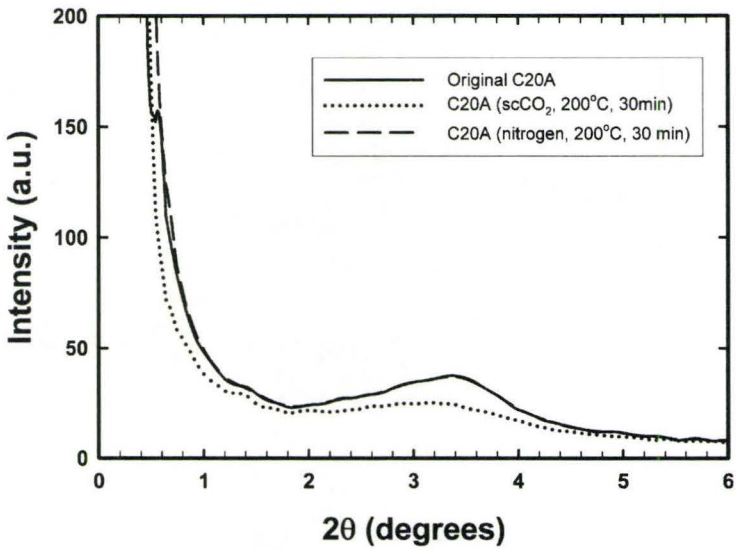

Figure 3.1 XRD patterns of C20A as-supplied in its original state, processed for 30 min in a $scCO_2$ atmosphere (200°C and 9.7 MPa), or processed for 30 min in a N_2 environment (200°C)

basal expansion while heated to 200°C (while observed in-situ, data not shown) due to melting of the surfactant with the characteristic peak shifted to $2\theta = 3.0°$ as well as showing greater layer-to-layer uniformity. Layer-to-layer uniformity in this case refers to a reduction in the full-width half-maximum (FWHM) measure of peak breadth which diminished from 1.9° at room temperature to 1.2° once the system reached 200°C. Yet as noted in Figure 3.1 once removed from heat and measured ex-situ the diffraction pattern for the clay conditioned at 200°C under nitrogen for 30 minutes matched that of the as-supplied sample. Conversely, the ex-situ diffraction pattern of C20A after its suspension in $scCO_2$ at 200°C for 30 minutes and then removed, showed persistent expansion with a

nominal peak position of $2\theta = 2.8°$ and a broader peak breadth (FWHM = 1.2°). With the increased packing density of surfactant gained by the organoclay while under the plasticizing influence of the supercritical solvent, the $scCO_2$ treated C20A retained its heat-expanded morphology upon cooling. The reduced intensity of the peak is attributed to the disturbed tactoid arrangement in the particles as the gas was released [17]. In comparison to these neat organoclay materials, the intercalated clay structures with the different compatibilizers showed much greater variance in the detected basal reflections.

Mixed with the low viscosity, highly maleated Li6252, the periodic structure of C20A was no longer detected by ex-situ XRD analyses for either $scCO_2$ or N_2 environments as seen in Figure 3.2. This oligomeric compatibilizer was found to be highly effective for clay intercalation but raised concerns for end-use suitability due to its low molecular weight. For the mixture of PB3002 and C20A, the diffraction peak shifted from a 2θ angle of 3.4° for the as-supplied organoclay to a lower 2θ angle of 3.0° with the aid of $scCO_2$, indicating that the nominal basal spacing of the clay increased to 29Å. This increase in spacing was similar to the $scCO_2$-treated clay discussed in Figure 3.1, leaving doubts that intercalation occurred. Under the N_2 atmosphere, the basal spacing of the clay mixed with PB3002 was only 27Å showing little difference from the as-supplied C20A. These outcomes indicated that the supercritical fluid continued to change the surfactant morphology of the organoclay within the mixture but the resulting expansion was insufficient to accommodate the large molecular size of the PB3002 intercalant. The TEM micrographs in Figure 3.3 for the $scCO_2$-treated mixtures with Li6252 and PB3002 support the observations by XRD. In the micrographs, the clay demonstrated an

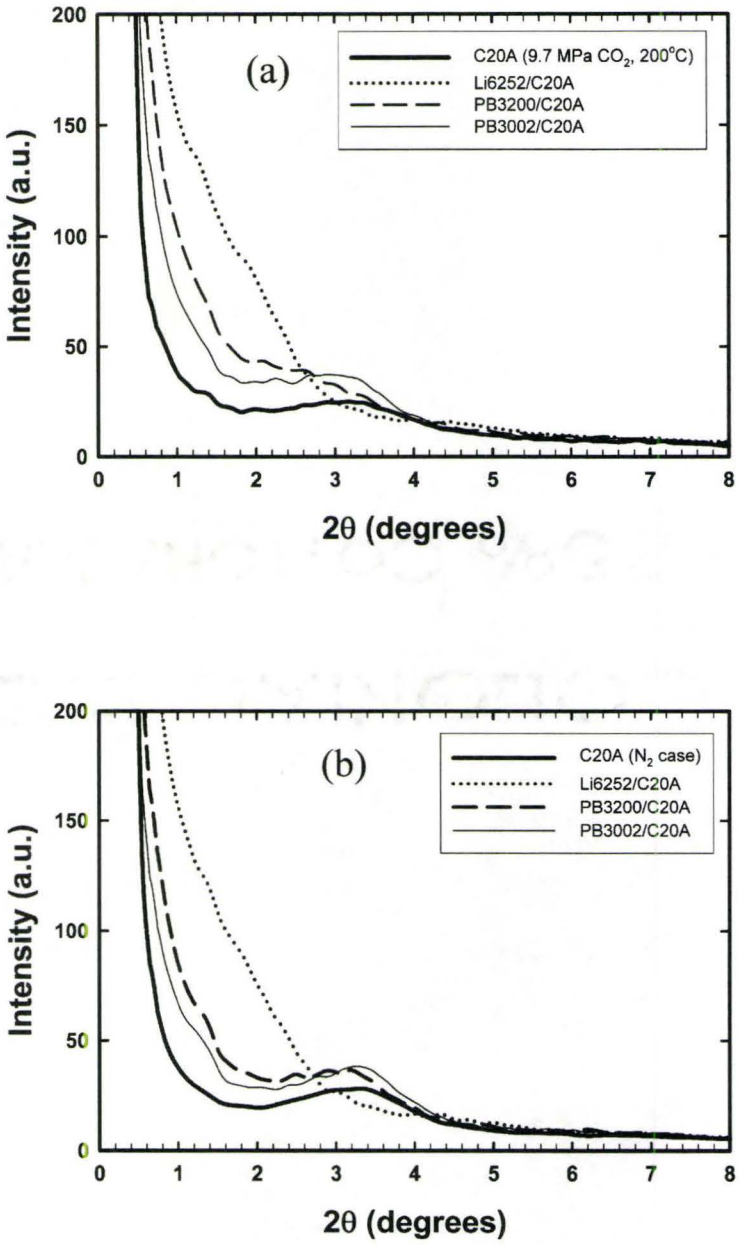

Figure 3.2 XRD patterns of C20A mixtures with Licocene 6252, Polybond 3200, and Polybond 3002 processed at 200°C for 30min for either (a) $scCO_2$ or (b) N_2, compared to their respective C20A processed under the same conditions.

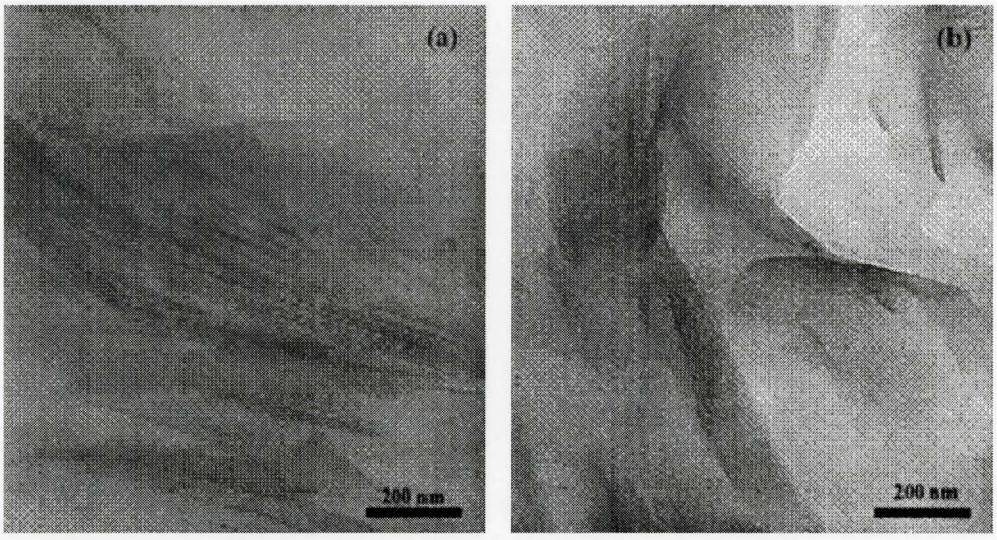

Figure 3.3 TEM micrographs for (a) Li6252/C20A mixture and (b) PB3002/C20A mixture, both processed under $scCO_2$

expanded sheet stack arrangement in the case of Li6252 while for the PB3002 mixture the ordered layer structure of the clay remained dense.

For the compatibilizer in the mid-range with respect to MA content and molecular weight, PB3200, the effect of $scCO_2$ on the mixture of C20A and compatibilizer was easily observed and significant. As shown in Figure 3.2, after annealing under nitrogen, the clay from this melt-annealed mixture showed a shift in its ex-situ diffraction peak to a 2θ angle of 3.0° (basal spacing of 29 Å) indicating that even without $scCO_2$ partial intercalation by this polymer species was possible. After annealing under $scCO_2$, the (001) peak for C20A appeared only as a shoulder at $2\theta = 2.5°$ but had became so wide

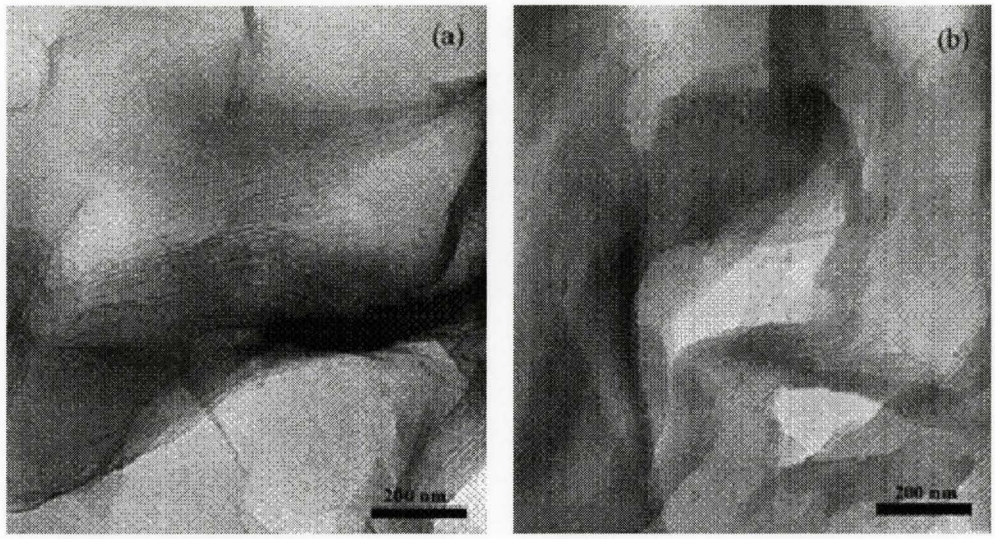

Figure 3.4 TEM micrographs for (a) PB3200/C20A, and (b) PB3200/s-C20A, both processed under $scCO_2$

that the 2θ position of the highest scattering intensity was almost indistinguishable from the background. The majority of the clay had lost its periodic stacked arrangement, which we attributed to substantial intercalation by the compatibilizer into the galleries of the clay The structure of the system was analyzed further by FT-IR and NMR and will be discussed in a later section. TEM micrographs of the $scCO_2$ treated PB3200 mixtures with C20A and s-C20A (which is discussed later in this section) are shown in Figure 3.4. The clay galleries seen in the micrograph for the mixture with C20A show good dispersion, though tactoids rather than platelets are observed.

To complement the ex-situ analysis above, the PB3200 mixture with C20A was evaluated using a specially constructed apparatus to observe the structure of the clay by XRD over time while under heat and pressure. Due to the fragile nature of the quartz

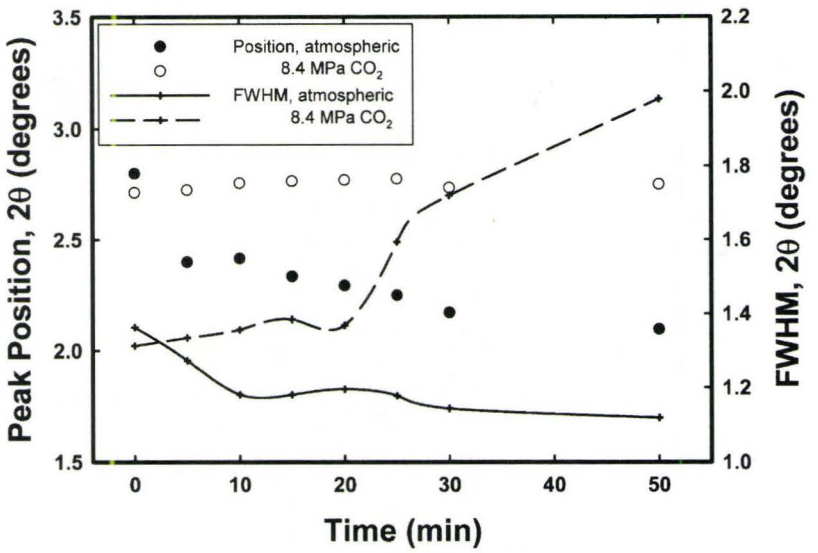

Figure 3.5 Changes in the nominal peak position and peak breadth (as measured by FWHM) while heated at 200°C for 30 minutes and then cooled to 50°C between 30-50 minutes for the PB3200/C20A mixture, with and without $scCO_2$.

tube used in the apparatus, the system could only reach a pressure of 8.4 MPa CO_2 at 200°C; however, such a condition still corresponds to the supercritical state of CO_2 and was felt to be sufficiently close to conditions used in the batch vessel to be meaningful. Figure 3.5 plots the nominal 001 peak position and its breadth (FWHM) for the clay within the mixture over time, either under atmospheric pressure or supercritical conditions. In the absence of high pressure, steady diffusion of the compatibilizer into the clay is assumed as the (001) peak shifted from $2\theta = 2.8°$ to 2.2° over 30 minutes. During this period, an improvement in layer-to-layer uniformity was seen over the first 10 minutes of the test as the peak became narrower and then no further changes in its breadth

occurred though the peak continued to shift to lower 2θ angles. Between 30 minutes and 50 minutes, the sample was cooled to 50°C over which time no further changes in structure were observed. Comparatively, under $scCO_2$ the (001) peak for C20A remained nearly constant in position over the 30 minutes while at 200°C. At the same time, the peak breadth broadened significantly, particularly after an induction period of 20 minutes. The peak appeared to continuously broaden through the cooling stage between 30-50 minutes. The final peak position was 0.2° higher by these in-situ experiments compared to the ex-situ analysis in Figure 3.2 but the peak broadening corresponds well. Though not included in the paper, the same in-situ trends for peak position and breadth, with and without $scCO_2$, were observed by the authors with a clay-compatibilizer mixture having a 50/50 w/w% composition.

Some of the discussion in the literature suggests that using a pretreated organoclay in place of the as-supplied species can further clay exfoliation in the final prepared nanocomposite without needing $scCO_2$ to be injected into the compounding process. This pretreated material should, in theory, remove the necessity for compounders to design and operate a supercritical gas delivery system. Figure 3.6 compares the ex-situ XRD diffraction patterns for the melt-annealed mixture of PB3200 with either the $scCO_2$ pre-treated C20A (s-C20A) or the as-supplied C20A, processed under either N_2 or $scCO_2$ conditions. The two mixture compositions retrieved from the supercritical solvent displayed similar diffraction patterns with their (001) peaks seen only as shoulders from the baseline at $2\theta = 2.5°$. According to the TEM micrographs in Figure 3.4 the extent of exfoliation for the s-C20A mixture under $scCO_2$ was also similar to the C20A counterpart,

with mostly clay tactoids visible and the largest interlayer expansion noted being approximately 92Å. In general, qualitative observations afforded by TEM showed little difference between the two clay systems. The same two materials annealed under nitrogen showed more clearly defined peaks centered at $2\theta = 3.0°$ by XRD. However, the peak in Figure 3.6 appears broader for the mixture with the pre-treated clay suggesting more ready disruption of the silicate stacking even under nitrogen. This was attributed to the more disordered tactoid arrangement of s-C20A creating more paths for intercalating polymer chains to enter the clay galleries.

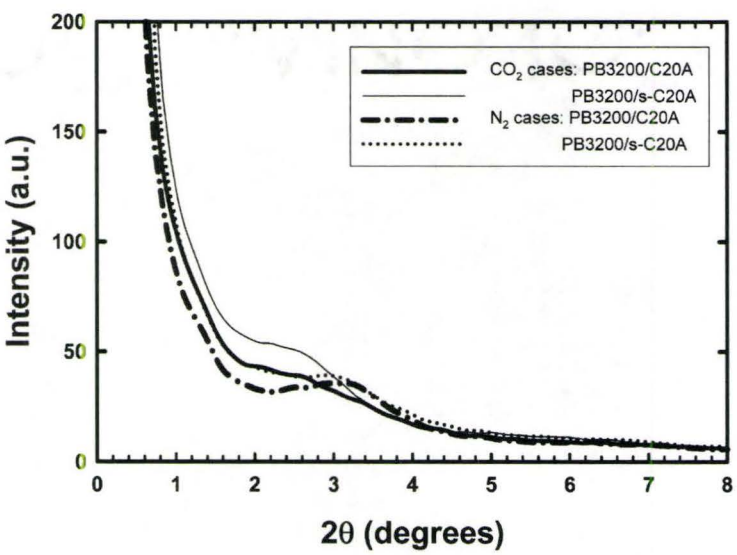

Figure 3.6 XRD patterns of PB3200 prepared mixtures with C20A and s-C20A under $scCO_2$ and N_2 conditions.

3.3.2 Infrared Spectroscopy

The FTIR spectra of the individual constituents are shown in Figure 3.7. The pretreated s-C20A was not included as its spectra matched that of C20A. The vibrations in the frequency ranges of 1400-1520 cm^{-1} and 2800-3000 cm^{-1} pertaining to CH_2 bending and stretching modes respectively, have been of interest to researchers attempting to identify structural changes in the clay pertaining to the surfactant and intercalating molecules [22-24]. From the figure it can be seen that C20A had methylene modes centered at 1468, 2852, and 2921 cm^{-1} whereas for the MA-PP species, the detectable modes corresponded to 1460 (very broad), 2838, and 2917 cm^{-1}. The peaks at 2838 cm^{-1} for MA-PP and 2852 cm^{-1} for C20A were relatively sharp and remained well differentiated in the spectra for the mixtures, so these vibrations related to symmetric CH_2 stretching were selected to monitor changes in the systems as a result of $scCO_2$ treatment. The FTIR spectra of the three melt-annealed mixtures from the different compatibilizers, under N2 or scCO2 are shown in Figure 3.8. For the Li6252 derived mixtures, where the compatibilizer was observed by XRD to have fully intercalated into the galleries of C20A regardless of the supercritical fluid being present, the band at 2852 cm^{-1} could no longer be detected in the spectra. On the other hand, the band showed the least change for the mixture with PB3002 whose high molecular weight chains were noted by XRD as being restricted from entering the galleries of the organoclay. However, the band still showed a markedly reduction with PB3002 when the mixture was processed with $scCO_2$ compared to N_2. The band intensity for the nitrogen case with PB3200 bore close similarity to the $scCO_2$ case for the PB3002-based mixture, in the same way as the XRD diffraction

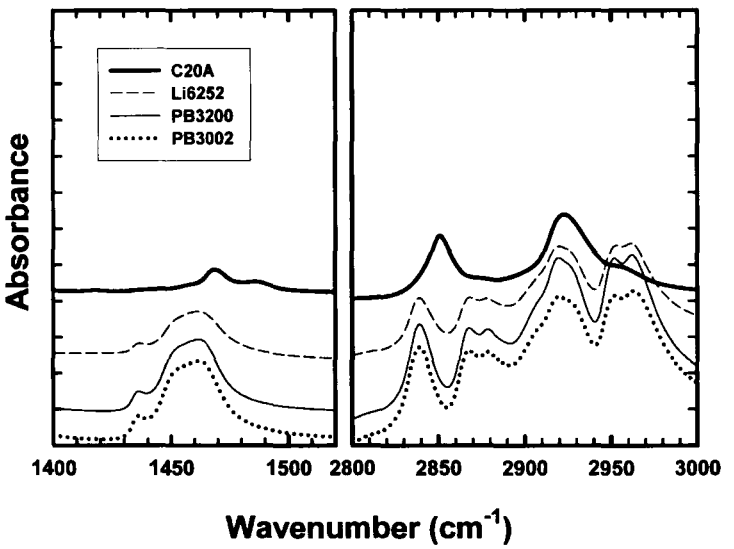

Figure 3.7 FT-IR spectra at bands 1400-1520 cm^{-1} and 2800-3000 cm^{-1} for C20A and the three individual compatibilizers

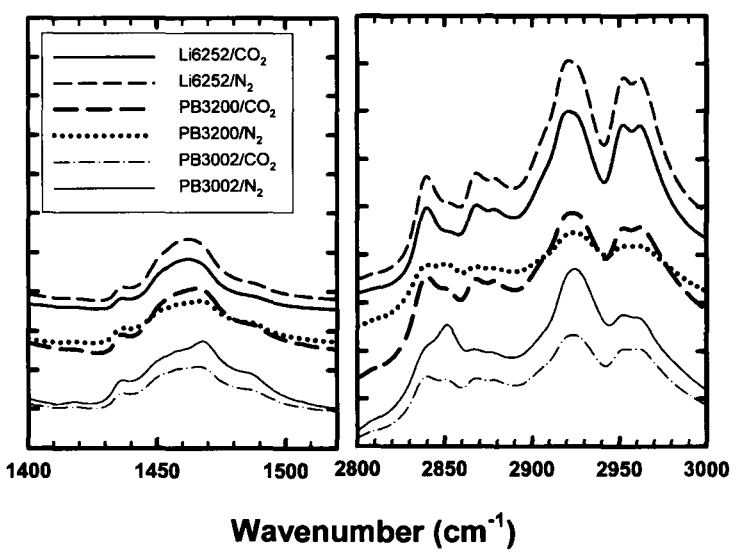

Figure 3.8 FT-IR spectra at bands 1400-1520 cm-1 and 2800-3000 cm^{-1} for Li6252, PB3200, and PB3002 mixtures with C20A processed with and without $scCO_2$

patterns between these two materials reported similar clay structures. In the presence of the supercritical solvent, the mixture prepared with PB3200 under $scCO_2$ showed the band at 2852 cm^{-1} to still be present though its intensity was almost negligible, similar to the Li6252-based material.

The band at 2852 cm^{-1} showed a marked correspondence with the extent of intercalation revealed in the diffraction patterns from the XRD results. The band decreased in its intensity as more chains intercalated into the galleries of C20A, disrupting the solid-like environment of the near *all-trans* alkyl surfactant [22-24]. The NMR analysis in the following section shall examine this change in microstructure more closely, enough to postulate a cause for the loss of this vibrational band in the spectra. The FTIR spectra for the melt-annealed mixtures in the frequency ranges of 400-1300cm^{-1} and 1600-1900cm^{-1} revealed no significant information which could discern the changes brought about by the gases within the resolution of the measurement (i.e. 2 cm^{-1}). The absorbance bands for the carboxylic acid groups (1715 cm^{-1}) and anhydride groups (1780-1792 cm^{-1}) of the compatibilizer did not significantly change in position or intensity after exposure to the two gases at 200°C. Therefore, no analysis regarding the hydrogen bonding of the anhydride moiety with the oxygen plane of the clay or the exfoliated silicate structure could be made by this technique. This could, in part, be attributed to the fact that the mixtures were poorly dispersed in the absence of shear.

3.3.3 NMR analysis

The conformation of the intercalated molecules (i.e. surfactant and compatibilizer) related to the use of the supercritical solvent in the preparation of nanocomposite materials was studied by variable-temperature solid-state ^{13}C NMR experiments. Both common techniques, cross polarization (CP) MAS and Bloch decay (BD) MAS were used to probe the structural differences in the melt-annealed PB3200 mixtures and neat organoclay species prepared from the batch vessel. This allowed the products from the $scCO_2$ and N_2 environments to be compared. For clarity, this was an ex-situ analysis. The initial variable contact-time CP MAS experiments with the mixtures showed little difference between the samples processed with and without $scCO_2$. With varied contact times, both samples showed a rapid increase in signal intensity up to 1.2 ms contact time, and then a gradual decrease in intensity out to 5 ms which was set as the maximum contact time. The lack of differentiation in the spectra for the two samples was attributed largely to inefficient cross-polarization of the surfactant intercalated within the clay in comparison to the detected chemical shifts assigned to isotactic polypropylene (22 ppm CH_3, 26 ppm CH, and 44 ppm CH_2) at both temperatures.

Comparatively, the Bloch-decay (BD MAS) technique showed discernable differences between the $scCO_2$ and N_2 processing conditions, most notably for the PB3200 mixture. The lengthy recycle delay for the direct-pulse technique (Bloch-decay) provided considerably more signal related to the confined surfactant compared to cross-polarization. The ^{13}C spectra prepared using the Bloch-decay method are shown in Figures 3.9 and 3.10 for the organoclay species and for the melt-annealed PB3200

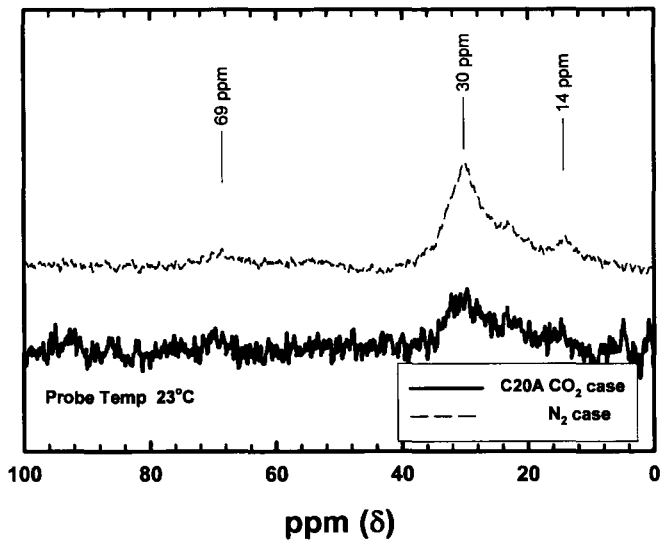

Figure 3.9 ^{13}C NMR spectra of collected C20A processed under $scCO_2$ and N_2 using a probe temperature of 23°C.

mixtures, respectively. The spectra of the two neat organoclays after annealing in one of the two gas environments are shown in Figure 3.9. Both spectra showed similar detectable chemical shifts, though the poor signal-to-noise ratio for the neat paramagnetic material made quantitative assertions difficult. The majority of the surfactant was considered to be in the paraffin-type arrangement exhibiting solid-like mobility attributed to an *all-trans* chain conformation, agreeing with the corresponding XRD-detected gallery heights for the $scCO_2$-treated and nitrogen-treated C20A of 28Å and 25Å, respectively [17]. The signals for the interior methylene groups in the alkyl chains of the surfactant were the most sensitive to the conformer state and in this regards, the peak at 30 ppm was assigned to the mixed conformation of trans and gauche of the internal

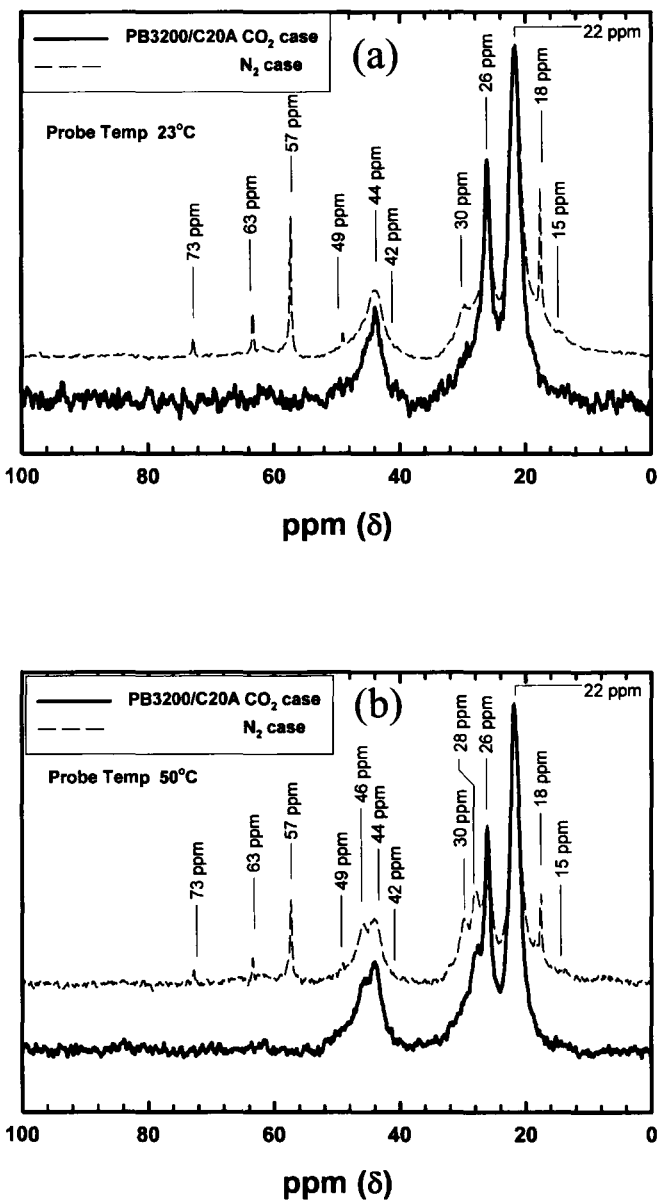

Figure 3.10 ^{13}C NMR spectra for the PB3200/C20A mixture processed under $scCO_2$ and N_2, using a probe temperature of a) 23°C and b) 50°C

methylenes and shoulder peak at ~33 ppm to the *all-trans* state of these groups [23, 25]. The chemical shift observed at 14 ppm corresponded to the terminal methyl groups (C-CH_3) for both C_{18} and C_{16} alkyl chains. Both C_{18} and C_{16} chain lengths were present as the quaternary ammonium surfactant used for C20A was mainly composed of dimethyl-dioctadecyl-ammonium salt but included minor components of dimethyl-octadecyl-hexadecyl-ammonium and dimethyl-dihexadecyl-ammonium salts, and very low concentrations of dimethyl-octadecyl-ammonium and dimethyl-hexadecyl-ammonium salts. Several other peaks were identified but were much more difficult to distinguish from the baseline noise of the spectra, most likely due to the close proximity of these carbon groups to the paramagnetic influence of the montmorillonite sheets. Not seen in the plot were the terminal group signals due to their low intensity, though the resonance at 69 ppm corresponding to the methylenes attached to the nitrogen was just barely detected in this case. The weaker signal for the $scCO_2$ treated organoclay compared to nitrogen was attributed to both paramagnetic interference from the silicate and the lower mobility of surfactant chains due to their greater packing density within the interlayer region [17].

Figures 3.10(a) and (b) show the spectra for the PB3200 melt-annealed mixture using the BD MAS technique at NMR probe temperatures of 23°C and 50°C, respectively. The spectra do not include the anhydride carbonyl resonances at 172-174 ppm which could not be distinguished from the baseline noise by this technique. The three isotactic polypropylene resonances were the most intense signals, but the resonance peaks attributed to the surfactant were clearly observable in the poorly intercalated mixture (i.e. sample processed with N_2). For this nitrogen-processed PB3200/C20A mixture, the

signal for the interior methylene groups was observable as an overlapped shoulder peak with highest intensity at 30 ppm, similar to the neat clay shown in Figure 3.9, indicating that most of the surfactant remained in its original conformation in the presence of the compatibilizer. At the elevated probe temperature, 50°C, new methyne and methylene signals were detected at 28 ppm and 46 ppm, respectively, indicating an increased liquid-like state for the surfactant/compatibilizer mixture. A weak peak corresponding to the terminal propyl end group of the compatibilizer was observed at 15 ppm whereas a strong terminal methyl signal for the surfactant was found downfield at 18 ppm. The peak at 57 ppm indicated that the nitrogen-bound methyl groups (-N-CH_3) were unaffected by the presence of the compatibilizer yet the peak representing the N-CH_2- was shifted downfield to 73 ppm. The peaks at 49 ppm and 63 ppm were assigned to the CH_2 and CH groups of the grafted anhydride ring [26]. In general, the spectra for the nitrogen-processed PB3200/C20A mixture indicated little disruption of the methylene conformation for the surfactant by the compatibilizer, confirming the XRD results of minimal intercalation by the MA-PP. The downfield shift of the carbon groups around the nitrogen group suggests the partial influence of hydrogen bonding by the anhydride moiety.

The spectrum for the more highly exfoliated PB3200/C20A mixture prepared under $scCO_2$ was included in Figure 3.10. At a probe temperature of 23°C, the chemical shifts at 22 ppm, 26 ppm, and 44 ppm were the strongest, corresponding to the compatibilizer, with an additional shoulder peak at 46 ppm and a barely detectable shoulder peak at 28 ppm. At the elevated probe temperature of 50°C the shoulder peaks

at 28 ppm was more clearly defined. The resonances corresponding to the alkyl surfactant were not detected in the ^{13}C spectra for either probe temperature. The disappearance of these alkyl-related resonances can be explained by the surfactant being forced into a disorganized lateral bilayer arrangement to accommodate the inclusion of the intercalated compatibilizer species. In the molecular simulations of Toth et al. [27] it was observed that in the presence of a maleated polypropylene in the galleries of organically-coated clay, the surfactant flattens over the silicate surface to shield the clay from the polymer despite its functional moiety. In such a case, paramagnetic interference by the silicate towards the carbon groups of the surfactant in close proximity would severely broaden and weaken any related peaks.

3.4 GENERAL DISCUSSION

It has been well established in the literature that achieving an intercalated silicate structure does not readily predispose the clay mineral to exfoliation [28-29], but rather intercalation is a necessary mechanism towards overcoming the barriers of exfoliation. XRD results in this work have indicated that the modified clay, in the presence of a maleic anhydride grafted polypropylene compatibilizer, exhibited varying degrees of basal expansion; however, only those composite materials exhibiting major microstructural changes to the confined surfactant were notably exfoliated. With favorable interfacial interaction for all the compatibilizer species selected for this study, the constraint in their capacity to intercalate into the galleries of the clay can largely be related to their molecular size. This was most evident by the extensive intercalation and partial exfoliation of the organoclay by the oligomeric MA-PP, Li6252. For all

conditions examined, this compatibilizer readily entered the galleries of the clay without aid from the supercritical solvent. However, if the intended use of a nanocomposite requires enhanced mechanical properties, then the lower molecular weight compatibilizer species would appear undesirable.

In comparison, the larger molecular size of PB3200 and PB3002 largely restricted their entry to only the outer edges of the silicate stack without $scCO_2$ aid, yielding only minor basal expansion. Most likely, the majority of associations with the clay in such cases would be confined to the broken plane of the clay which possesses suitable sites for hydrogen bonding with the compatibilizer. In the absence of $scCO_2$, the NMR and FTIR analyses suggests that these higher molecular weight compatibilizers have little or no effect on the surfactant arrangement within the clay galleries. The in-situ XRD analysis revealed that under these conditions without $scCO_2$ greater uniformity in the ordered structure of the silicate sheets resulted along with a small increase in basal spacing. The annealing conditions would seem to have afforded more reorganization of the surfactant in the galleries and possibly some chains of the compatibilizer entered, probably from the lower molecular weight fractions of these compatibilizers. The poor extent of exfoliation for these higher molecular weight species was comparable to the reported results by other researchers [9, 10, 12].

Larger molecules could be afforded entry to the clay galleries when annealed in the presence of the supercritical CO_2, which demonstrates the capacity of this unique solvent to act as an exfoliating agent in the synthesis of a nanocomposite. For moderate molecular sizes such as PB3200, the plasticizing features of the supercritical fluid

allowed a similar extent of exfoliation as witnessed with the oligomeric species, Li6252. ^{13}C NMR and FTIR results appear to indicate that the chains of PB3200 could become fully intercalated into the galleries of the clay, so much so that the surfactant arrangement was dramatically altered. The in-situ XRD characterization of the phenomenon showed substantial heterogeneity in the clay structure arising from this processing condition, though the lack of shift in the diffraction peak position suggests intercalation was localized to only a few galleries. Once a chain pushes aside the surfactant to fully intercalate and expand a gallery there is a greater tendency for subsequent intercalating chains to enter at the same location rather than randomly approaching any gallery in the stack. The length of chains for PB3002 appeared to have exceeded the upper bounds in capacity of the $scCO_2$ to aid in penetrating the galleries of C20A.

The unexpected finding in this work was that the usefulness of $scCO_2$ appeared to be constrained to the manner by which the clay was exposed to the solvent. Pretreatment of the clay with $scCO_2$ (i.e. s-C20A) offered no benefit towards greater diffusion of the compatibilizer into the clay galleries compared to an as-supplied organoclay. The basal spacing gained by pretreatment was not sufficient to afford easier access of the macromolecules into the confined spaces within the clay. Rather, annealing the two components, clay and compatibilizer, together in the presence of the $scCO_2$ was far more beneficial towards exfoliation. However, a cautionary point should be made that as these trials did not include shear, it was not possible to exclude the possibility that $scCO_2$ pre-treated clays may still be more easily delaminated. This concern will be addressed in future work.

3.5 CONCLUSIONS

All three compatibilizers in this study contained sufficient polarity to interact with the silicate structure of C20A, but their abilities to intercalate varied significantly. The short chain oligomeric MA-PP, Li6252, readily entered the galleries of the clay, leading to extensive intercalation and exfoliation for all conditions examined, including those without the supercritical solvent. The larger molecular sizes of PB3200 and PB3002 had their entry into the interlayer regions restricted without $scCO_2$ assistance, yielding only minor basal expansion. The moderate molecular weight PB3200 mixture showed the strongest evidence for $scCO_2$ providing aid toward compatibilizer intercalation and achieved a similar extent of exfoliation as observed with the oligomeric species. The length of chains for PB3002 appeared to have exceeded the upper bounds in molecule size for the $scCO_2$ to aid in penetrating the galleries of C20A. Pretreating the C20A with $scCO_2$ in place of its use with both clay and compatibilizer present, did not improve intercalation. The benefit of $scCO_2$ for intercalation and exfoliation was proposed to be due to its plasticizing effect on the alkyl chains of the clay surfactant and the polymer chains.

REFERENCES

1. Manke, C. W.; Gulari, E.; Mielewski, D. F.; Lee, E. C. (Ford Global Technologies, Inc.; Wayne State University). US Patent 6,468,073, October 22, 2002.
2. Zerda, A. S.; Caskey, T. C.; Lesser, A. J. Macromolecules 2003, 36, 1603.

3. Mielewski, D. F.; Lee, E. C.; Manke, C. W.; Gulari, E. (Ford Global Technologies, LLC; Wayne State University). US Patent 6,753,360, June 22, 2004.
4. Sato, Y.; Fujiwara, K.; Takikawa, T.; Sumarno, S.; Takishima, S.; Masuoka, H. *Fluid* Phase Equil 1999, 162, 261.
5. Nalawade, S. P.; Picchioni, F.; Janssen, L. P. B. M. Chem Eng Sci 2007, 62, 1712.
6. Kim, D. H.; Fasulo, P. D.; Rodgers, W. R.; Paul, D. R. Polymer 2007, 48, 5960.
7. Wang, Y.; Chen, F.-B.; Wu, K.-C.; Wang, J.-C. Polym Eng Sci 2006, 46, 289.
8. Hong, C. H.; Lee, Y. B.; Bae, J. W.; Jho, J. Y.; Nam, B. U.; Hwang, T. W. J Ind Eng Chem 2005, 11, 293.
9. Kato, M.; Usuki, A.; Okada, A. J Appl Polym Sci 1997, 66, 1781.
10. Kawasumi, M.; Hasegawa, N.; Kato, M.; Usuki, A.; Okada, A. Macromolecules 1997, 30, 6333.
11. Vaia, R. A.; Giannelis, E. P. Macromolecules 1997, 30, 7990.
12. Wang, Y.; Chen, F.-B.; Li, Y.-C.; Wu, K.-C. Composites: Part B 2004, 35, 111.
13. Shi, D. ; Yang, J.; Yao, Z.; Wang, Y.; Huang, H.; Jing, W.; Yin, J.; Gosta, G. Polymer 2001, 42, 5549.
14. Glebov, E. M.; Krishtopa, L. G.; Stepanov, V.; Krasnoperov, L. N. J Phys Chem A 2001, 105, 9427.
15. Clark, K.; Lee, S. Polym Eng Sci 2004, 44, 1636.
16. Liu, T.; Hu, G.-H.; Tong, G.-S.; Zhao, L.; Cao, G.-P.; Yuan, W.-K. Ind Eng Chem Res 2005, 44, 4292.
17. Thompson, M. R.; Liu, J.; Krump, H.; Kostanski, L. K.; Fasulo, P. D.; Rodgers, W. R.

J Colloid Interf Sci 2008, 324, 177.

18. Rogers, K.; Takacs, E.; Thompson, M. R. Polymer Testing 2005, 24, 423.
19. Gokel, G. W. Dean's Handbook of Organic Chemistry; McGraw-Hill: New York, 2004.
20. Thompson, M. R.; Balogh, M. P.; Speers, R.; Fasulo, P. D.; Rodgers, W. R. The J Chem Phys 2009, 130, 044705.
21. Horsch, S.; Serhatkulu, G.; Gulari, E.; Kannan, R. M. Polymer 2006, 47, 7485.
22. Vaia, R. A.; Teukolsky, R. K.; Giannelis, E. P. Chem Mater 1994, 6, 1017.
23. Wang, L.-Q.; Liu, J.; Exarhos, G. J.; Flangan, K. Y.; Bordia, R. J Phys Chem B 2000, 104, 2810.
24. De Rosa, C.; Auriemma, F.; Capitani, D.; Caporaso, L.; Talarico, G. Polymer 2000, 41, 2141.
25. Russell, K. E.; Mcfaddin, D. C.; Hunter, B. K.; Heyding, R. D. J. Polym. Sci. B 1996, 34, 2447
26. Walter, P.; Mäder, D.; Reichert, P.; Mülhaupt, R. J Macromol Sci A 1999, 36, 1613.
27. Toth, R.; Coslanich, A.; Ferrone, M.; Fermeglia, M.; Pricl, S.; Miertus, S.; Chiellini, E. Polymer 2004, 45, 8075.
28. Bharadwaj, R. K.; Vaia, R. A.; Farmer. B. L. In Polymer Nanocomposites, Krishnamoorti, R.; Vaia, R. A. Eds. ACS Symposium Series 804, American Chemistry Society: Washington DC, 2002, chap. 16.
29. Sinsawat, A.; Anderson, K. L.; Vaia, R. A.; Farmer, B.L. J Polym Sci Part B: Polym Phys 2004, 41, 3272.

Chapter 4

Evaluating Compatibilizer Interactions with Different Alkyl Ammonium Modified Organoclays

This chapter is a paper formatted as:

J. Liu, M.R. Thompson, P. D. Fasulo, W. R. Rodgers, Evaluating Compatibilizer Interactions with Different Alkyl Ammonium Modified Organoclays, which is under review by GM and intended to be submitted to *Applied Clay Science*. Jinling Liu is the major contributor to this chapter.

In this chapter, influence of $scCO_2$ on the compatibilizer/organoclay intercalation and effect of the $scCO_2$-affected intercalation on morphology of the TPO nanocomposite were investigated *by varying surfactant that modifies montmorillonite (5 in total)*.

ABSTRACT

Five organically modified montmorillonites with different surfactants were examined in thermoplastic polyolefin nanocomposites prepared by a two-step method. Chain length and the number of alkyl chains attached to the quaternary ammonium surfactant were the main variables of study towards the CO_2 treatment with the goal being improvement of exfoliation in the dispersed organoclay. The intermediate masterbatch containing organoclay and compatibilizer as well as the final TPO nanocomposite were characterized using X-Ray Diffraction (XRD), Transmission Electron Microscopy (TEM), Fourier Transform Infrared Spectroscopy (FTIR) and rheological analysis. The results showed that significant changes in the state of exfoliation after processing with the supercritical fluid occurred only for surfactants possessing dialkyl tails and exhibiting a paraffin type arrangement within the montmorillonite.

4.1 INTRODUCTION

Selection of an alkyl ammonium surfactant for an organoclay has a major influence on the effectiveness of a compatibilizer in exfoliating the mineral during nanocomposite preparation (Dennis et al. 2001). The concentration of an appropriate surfactant in the clay (relative to the cation exchange capacity (CEC) of the natural clay mineral) and the structure of the surfactant (i.e. chemical moieties and presence of bulky side groups) affect its arrangement in the interlamellar regions (Lagaly et al. 1976; Lagaly, 1994; Xi et al. 2007; He et al. 2005). The complex molecular arrangements of organic species within the silicate stack determines basal expansion, with wider galleries thought

to lower the entropic penalty related to intercalation of a large compatibilizer molecule (Heinze et al. 2007). However, it has only recently been considered in the literature that the amount of organic mass required to bring about substantial basal expansion (i.e. 2-3 nm interlamellar spaces) may also sterically interfere with entry of the compatibilizer into the clay stack (Li et al. 2006; Rohlmann et al. 2008; Toth et al. 2004; Kim et al. 2004). These opposing effects need closer examination since newer processes using supercritical carbon dioxide ($scCO_2$) to aid exfoliation have been found to create greater surfactant coverage over some organoclay species (Thompson et al. 2008, 2009) and the resulting polyolefin nanocomposites are showing lower mechanical properties than would be anticipated by their increased exfoliated morphologies.

Rohlmann et al. (2008) studied the interaction of a maleated polypropylene compatibilizer with six different organoclays in the preparation of a polypropylene nanocomposite. They used the trends in interaction energies predicted by the simulations of Toth et al (2004) to explain the higher tendency for favored intercalation into dialkyl modified clays with paraffinic arrangement versus organoclay species with lateral bilayer surfactant arrangements. However, there were not enough similarities in the chemical structures of the surfactants used to establish trends from their study. The work of Li et al (2006) focused on a smaller set of surfactants, i.e. a quaternary ammonium salt versus a primary amine, and looked at the influence of surfactant concentration in the clay galleries. Li reported that properties of their nanocomposites improved with increased surfactant concentration for the primary amine, stating that basal spacing was more

important than access to the oxygen layer of the clay for the compatibilizer. However, the opposite was found with the bulkier alkyl ammonium surfactant, finding that basal spacing was large enough even at their lowest surfactant concentration to not pose an issue for intercalation. So they found that a lower surfactant concentration was favored for that surfactant as it left more of the oxygen plane exposed to the compatibilizer. Experimentally, it is difficult to separate the effect of gallery spacing versus surface coverage on compatibilizer intercalation, especially since the latter can not be determined readily. Through molecular simulations, Toth et al. (2004) and Kim et al. (2004) have both shown that unhindered regions of the silicate's oxygen plane are necessary for effective interaction with a compatibilizer species.

Despite the few studies mentioned, further efforts are necessary to investigate this potentially ill-determined facet of organoclay intercalation, to validate molecular simulations such as those by Toth et al. (2004) and Kim et al. (2004), and to assist the development of newer technologies such as those using $scCO_2$ to aid in the preparation of highly exfoliated nanocomposites. This paper will experimentally investigate the chemical, rheological and morphological differences between nanocomposite materials prepared with different organoclays while influenced by supercritical CO_2. The work seeks to better understand the importance of association sites between a compatibilizer and the clay mineral, and now how an external additive like $scCO_2$ can influence such sites.

4.2 EXPERIMENTAL

4.2.1 Materials

A 13 MFR thermoplastic polyolefin (TPO) supplied by LyondellBasell was selected for this study. Pellets of the TPO material were used directly without any further treatment. A commercial maleated polypropylene (MA-PP) compatibilizer, Polybond® 3200 (PB3200) from Chemtura Corporation was selected. This compatibilizer has sufficient molecular weight to minimize any losses in mechanical properties by its addition to the polymer matrix and demonstrated plasticization in the presence of supercritical CO_2 sufficient to aid intercalation (Liu et al. 2010). Pellets of the MA-PP were ground cryogenically into powder to minimize segregation as it was mixed with the different organoclay species. Other properties of the MA-PP have been reported in a previous study (Liu et al. 2010).

Table 4.1 lists the five organoclays supplied by Southern Clay Products, prepared from montmorillonite (MMT) using different quaternary ammonium surfactants. The organoclays were used as-supplied in the preparation of the PLS nanocomposite, with their properties summarized in Tables 4.1 and 4.2. Three of the alkyl ammonium organoclays mentioned in the tables have been discussed in detail within earlier studies (Thompson et al. 2008, 2009; Liu et al. 2010), namely DODA, ODTA, and THMA. The

Table 4.1 Properties of the quaternary ammonium modified montmorillonite

Name	Surfactant structure	CEC content (meq/100g)	Surfactant content (wt %)	Surfactant melting range (°C)	*d*-spacing (Å)
Na^+ MMT					12.1
DODA	$(CH_3)_2 (HT)_2N^+Cl^-$	100	38.5 ± 0.2	25-60	25.8
ODTA	$(CH_3)_3(C_{18}H_{37})N^+Cl^-$	95	26.8 ± 0.2	55-135	17.3
THMA	$(CH_3)(C_{16}H_{33})_3N^+Cl^-$	100	44.2 ± 0.3	25-55	33.5
DDDA	$(CH_3)_2(CC)_2N^+Cl^-$	95	30.6 ± 0.3	N/A	20.6
C30B	$(CH_3)(C_2H_4OH)_2(HT)N^+Cl^-$	90	29.5 ± 0.1	20-110	18.6

*HT= hydrogenated tallow (C_{18} ~65%; C_{16} ~30%; C_{14} ~5%); CC = coco (C_{12} ~56%; C_{14} ~18%; C_{18} ~7%; C_{16} ~7%; C_{10} ~7%; C_8 ~5%)

Table 4.2 Surface energy of the five organoclays and compatibilizer and interfacial intension between them at 50°C.

Species	Dispersive contribution*, γ^d (mN/m)	Polar contribution*, γ^p (mN/m)	Total surface energy, γ (mN/m)	Interfacial tension with PB3200, γ_{sl} (mN/m)	Spreading coefficient	
					λ_{12}	λ_{21}
PB3200	35.8	0.2	36.0	-	-	-
DODA	37.3	0.7	38.1	17.4	1.8	-2.4
ODTA	39.9	4.8	44.7	24.2	4.3	-13.2
THMA	37.8	0.01	37.9	20.5	1.6	-2.1
DDDA	37.7	1.63	39.3	18.7	2.1	-4.5
C30B	40.2	2.2	42.4	7.4	4.5	-8.3

* standard deviation 0.8 % (maximum)

main difference between the three organoclays was the number of C_{16-18} alkyl chains attached to the nitrogen moiety of the surfactant. DODA (commercially known as Cloisite 20A®) was repeatedly observed in those earlier studies to demonstrate the greatest changes in microstructure under the influence of $scCO_2$. The alkyl-based organoclay, DDDA has a di-alkyl surfactant similar to DODA yet with shorter chains. Similar to the previous three alkyl organoclays, the surfactant in DDDA lacked any polar groups besides its ammonium salt. The basal spacing of the as-supplied organoclay was 20.6 Å suggesting a bilayer surfactant arrangement according to the interlamellar classifications of Lagaly (1976, 1994), meaning that the alkyl chains lay flat across the silicate surface, in a similar manner to ODTA. Alternatively, the surfactants of DODA and THMA are considered to assume a paraffin arrangement (Thompson et al. 2008, 2009) where the alkyl chains extend away from the silicate surface. The final organoclay was C30B (commercially known as Cloisite 30B®) which was included in the study to offer the potential of a different chemical interaction between the clay and compatibilizer, namely through the hydroxyl groups in the surfactant, during intercalation. The basal spacing of this polar supplied organoclay was 18.6Å suggesting once again a bilayer surfactant arrangement.

4.2.2 Preparation of the organoclay/compatibilizer masterbatch

For the first step in preparation of a polymer nanocomposite, PB3200 and a selected organoclay were mixed at equal weight ratio by tumble blending and dried at 40°C under vacuum overnight before use. This will be referred to as the *intercalation step* in future discussions. The dried powder mixture was annealed in a high pressure batch

vessel under supercritical CO_2 (200°C and 9.7 MPa) or under a blanket of N_2 (200°C and ambient pressure) for 3 hours. The melting transition ranges for the different surfactants used by the clays are listed in Table 4.1 whereas the melting range of PB3200 was 134-168°C (determined by differential scanning calorimetry). Upon conclusion of the experiment, the vessel was rapidly depressurized at 4.8 MPa/s and the sample was removed to cool and then be stored in a dessicator till ready for the compounding step.

4.2.3 Compounding of the TPO nanocomposites

The prepared masterbatch from the intercalation step was ground with a mortar and pestle and then melt-blended with TPO at a ratio of 10:90 (%w/w) using a ThermoScientific HAAKE Minilab II micro-compounder. This preparation was referred to as the *exfoliation step* in future discussion. The operating conditions required a barrel temperature of 180°C and screw speed of 200 RPM. The material was recycled for 2 minutes within the mixer before being extruded. The prepared nanocomposite was ground and subsequently analyzed.

4.2.4 Characterization

Characterization of the pristine organoclay species was done to understand their original microstructures prior to contact with the polymers and $scCO_2$. The organic content was evaluated by measuring the residual ash content where a fully dried organoclay sample was heated in muffle furnace at 600°C for 1 hour. The detected melting temperature of the surfactant present for each modified clay was evaluated by a Q200 modulating differential scanning calorimeter (DSC) from TA Instruments. DSC

was used to evaluate the melting transition of the surfactants used in the different organoclays. Two consecutive heating/cooling cycles with a ramp rate of 10°C/min were performed on a specimen over a temperature range from -20°C to 150°C under a nitrogen atmosphere. To improve peak resolution of the detected transition a modulated heating condition of ±1°C /60 s was selected.

The interfacial properties of each clay-compatibilizer combination were determined by calculating the spreading coefficients from contact angle measurements, following the method disclosed in reference (Liu et al. 2010). The method was used to calculate the spreading coefficient of the molten compatibilizer over the clay (λ_{12}) and conversely, the spreading coefficient of the clay over the melt (λ_{21}). Surface tension values of the clays and compatibilizer were determined using the sessile drop contact angle method at 50°C with 1-bromonaphthalene (dispersive component δ^d = 42.517 mJ/m^2, polar component δ^p = 0.283 mJ/m^2) and glycerin (δ^d = 35.541 mJ/m^2, δ^p = 25.359 mJ/m^2).

The crystal structure of the modified clay, clay/compatibilizer masterbatch and prepared nanocomposite was characterized by powder X-ray diffraction (XRD) and transmission electron microscopy (TEM). XRD analyzes were performed using a Bruker D8 diffractometer with Cu K_α radiation (λ = 1.5407 Å). This analysis was carried out using an accelerating voltage of 40kV and a current of 20mA. TEM micrographs were collected from a JEOL 1200 EX TEMSCAN microscope operating at an accelerating voltage of 80kV and magnifications of 60,000x and 200,000x. Samples were microtomed

with a diamond knife into thin sections approximately 70 nm thick and mounted on a carbon grid.

Transmission infrared absorbance spectra of the neat compatibilizer and organoclays as well as prepared samples involved collection of 64 scans at 2 cm^{-1} resolution over a range of 500-4000 cm^{-1} using a Bio-Rad FTS-40 spectrometer. The prepared TPO nanocomposite materials were prepared as films in a hot press at 165°C under 0.13 MN compressive force for 2 minutes. Powder clay or powdered clay/polymer samples were mixed with dry KBr and compressed into tablets.

The viscoelastic properties of the nanocomposite samples were evaluated using an ARES parallel plate rheometer (TA Instruments). A constant strain of 5% was chosen for the measurements based on the determined linear viscoelastic region from strain sweep testing. The tests were conducted at 200°C over a frequency range of 0.1–100 rad/s.

4.3 RESULTS AND DISCUSSION

The positive λ_{12} values listed in Table 4.2 indicated that the compatibilizer should be expected to spontaneously spread over each of the organoclay species examined in the study. The higher spreading coefficients for ODTA, C30B and DDDA indicated more favorable wetting by the compatibilizer, an outcome related to their higher polar contributions to the interfacial energy of the system. The negative λ_{21} values indicate that the organoclays will not spontaneously spread over the compatibilizer, though they may interact at isolated contact points. Based on this thermodynamic interpretation of the

compatibility, the chosen organoclays should show little differentiation towards their association with the compatibilizer.

4.3.1 X-ray Diffraction Analysis

The small-angle diffraction patterns determined by XRD for samples prepared with each organoclay species are shown in Figures 4.1. The samples shown in each plot include the neat organoclay, masterbatches prepared by batch annealing under either nitrogen or $scCO_2$, and the resulting nanocomposites formed from compounding those masterbatches into TPO. All organoclay species experienced some changes in both basal spacing and reflection intensity as a result of annealing and compounding, indicating disruption of the crystal structure for montmorillonite in each sample.

The industrial preference for using DODA in polyolefin formulations is understandable from these XRD results as it appeared more readily swollen and destructured compared to other organoclays in these tests. It also appeared that its crystal order was most sensitive to the inclusion of $scCO_2$ during preparation of its masterbatch (Figure 1a). The basal spacing of DODA in the annealed masterbatch under $scCO_2$ was 29.8 Å whereas for the N_2 case the galleries showed no difference from the pristine clay, i.e. 25.8 Å spacing. For the TPO nanocomposites prepared from these two masterbatches of DODA, further expansion and destructuring of the clay was indicated by their XRD patterns. These changes could be indicative of intercalation and exfoliation, but the technique alone does not allow such suppositions to be made. The $scCO_2$ case displayed a small, well defined d_{001} diffraction peak (positioned at $2\theta = 2.6°$), whereas the N_2 case

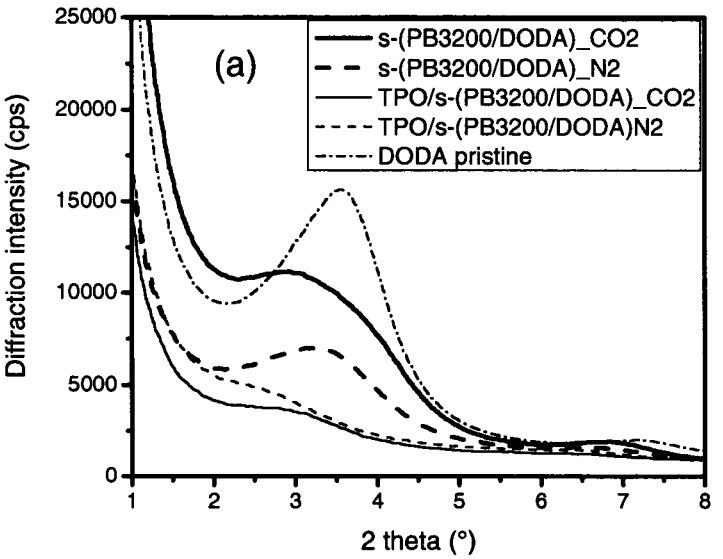
(a)
s-(PB3200/DODA)_CO2
s-(PB3200/DODA)_N2
TPO/s-(PB3200/DODA)_CO2
TPO/s-(PB3200/DODA)N2
DODA pristine
Diffraction intensity (cps)
2 theta (°)
25000
20000
15000
10000
5000
0
1
2
3
4
5
6
7
8

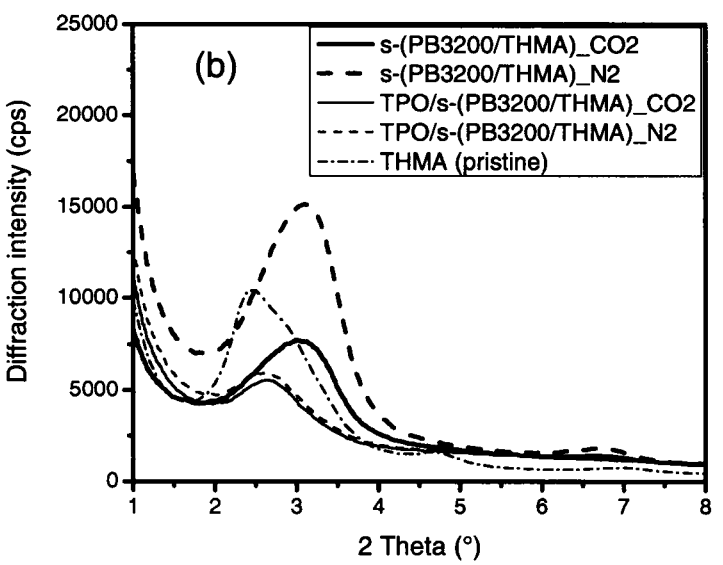
(b)
s-(PB3200/THMA)_CO2
s-(PB3200/THMA)_N2
TPO/s-(PB3200/THMA)_CO2
TPO/s-(PB3200/THMA)_N2
THMA (pristine)
Diffraction intensity (cps)
2 Theta (°)
25000
20000
15000
10000
5000
0
1
2
3
4
5
6
7
8

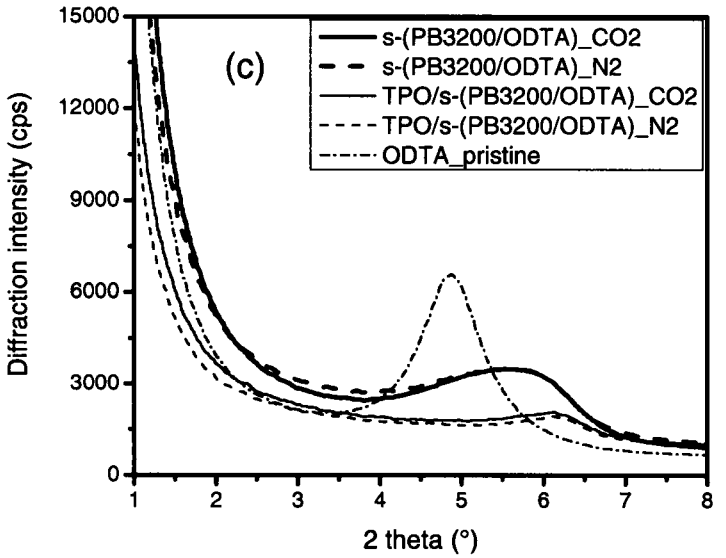
(c)
s-(PB3200/ODTA)_CO2
s-(PB3200/ODTA)_N2
TPO/s-(PB3200/ODTA)_CO2
TPO/s-(PB3200/ODTA)_N2
ODTA_pristine
Diffraction intensity (cps)
2 theta (°)
15000
12000
9000
6000
3000
0
1
2
3
4
5
6
7
8

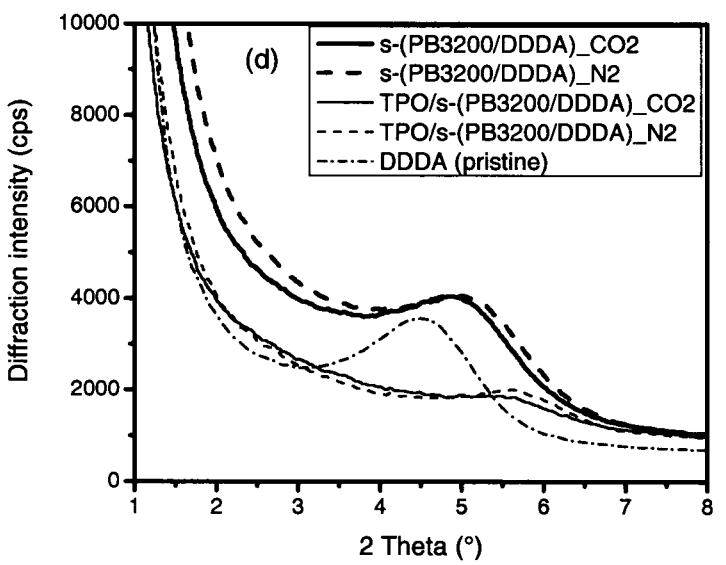
(d)
s-(PB3200/DDDA)_CO2
s-(PB3200/DDDA)_N2
TPO/s-(PB3200/DDDA)_CO2
TPO/s-(PB3200/DDDA)_N2
DDDA (pristine)
Diffraction intensity (cps)
2 Theta (°)
10000
8000
6000
4000
2000
0
1
2
3
4
5
6
7
8

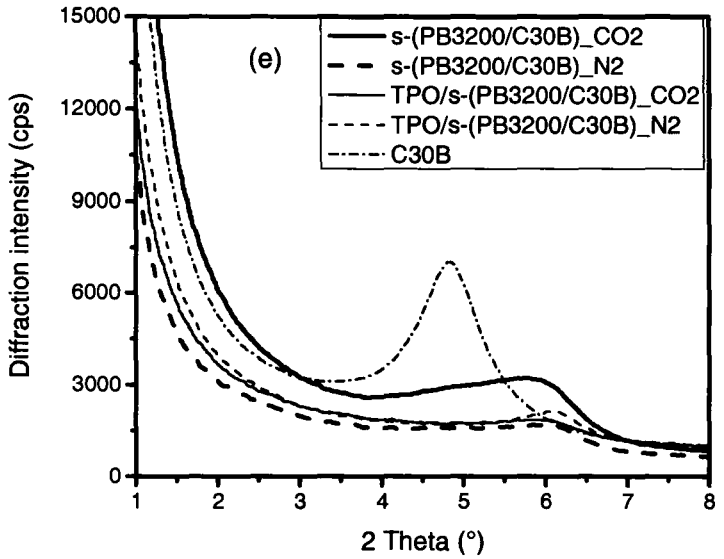

Figure 4.1 XRD patterns of an organoclay, its masterbatch with PB3200 and the TPO nanocomposite: (a) DODA, (b) THMA, (c) ODTA, (d) DDDA and (e) C30B

displayed a broad shoulder with higher intensity in the same region. The more swollen clay structure found in the $scCO_2$ prepared masterbatch led to similarly greater destructuring in the subsequent compounding step. The observable structural differences between these two nanocomposites based on DODA would appear minor, though the subsequent TEM and rheology do reveal greater distinctions; it should not surprising that XRD does not fully convey the extent of dispersion achieved (Eckel et al. 2004).

The (001) diffraction peak of THMA in the analyzed masterbatches and corresponding TPO nanocomposites samples, shown in Fig. 4.1b, was well defined showing a lesser extent of basal expansion and destructuring compared to results for the

other organoclays. The diffraction peak for as-supplied THMA was characteristically broad with nominal positioning at $2\theta = 2.7°$ (32.7 Å) though the crystal order appeared quite heterogeneous based on its skewness with suggested preferential spacing at both 2.4^{o} and 3.0^{o}. The organoclay in both masterbatches remained highly ordered after annealing with a broad basal reflection centered at $2\theta = 3.1°$ (28.5 Å) noted by XRD but showed no difference between the $scCO_2$ and N_2 cases. The absence of any effect by $scCO_2$ on the organoclay was consistent with previous studies examining the same species (Thompson et al. 2008, 2009). The (001) diffraction peak of the two produced TPO nanocomposites showed a minor shift from $2\theta = 3.1°$ for the masterbatches to 2.6°, possibly indicating some effect of the compounding with regards to expansion and destructuring of the organoclay. Once again there was no apparent difference based on the gas used, $scCO_2$ versus N_2.

The (001) diffraction peaks for samples prepared with ODTA, DDDA and C30B under both $scCO_2$ and N_2 are shown in Fig. 4.1c-e. Their as-supplied organoclays are shown displaying basal spacings (~20 Å) indicative of *lateral bilayer* surfactant arrangements whereas the previously mentioned DODA and THMA have *paraffin-type* arrangements (Favre and Lagaly, 1991). This means the long chain alkyl groups of the surfactant species lay flat along the silicate surface for the bilayer arrangement whereas for the paraffin-type arrangements, the alkyl groups extend into the open gallery regions. For these three organoclays, there was no observable influence of $scCO_2$ on the detected basal reflection for each masterbatch or final composite produced. The masterbatches showed broader d_{001} diffraction peaks than their respective neat clays and a shifted peak

position to higher 2θ values. The peak (centered at 2θ = 5.5-6.1°) suggests an increasingly monolayer arrangement to the surfactants resulted from annealing. Based on in-situ XRD studies for ODTA reported in an earlier paper (Thompson et al. 2008), the change to the monolayer arrangement is known to occur almost instantly once the temperature of the system exceeds the melting transition of the surfactant. Comparable reports of collapsed silicate stacks in the literature are often attributed to thermal degradation or surfactant leaching (Rohlmann et al. 2008; Shah and Paul, 2006; Horsch et al. 2006; Ton-That et al. 2004) but such a change in spacing can only occur once substantial amounts of mass have been lost, as demonstrated by other authors for ODTA (Lagaly et al. 1976; Lagaly, 1994; Bonczec et al. 2002). Having in-situ knowledge of the clay structure under temperature and pressure and knowing the immediacy of this change in basal spacing, it seems more likely that the bilayer-to-monolayer transition seen for our three organoclays was largely attributed to increased mobility of their surfactants during annealing. We are not disregarding the thermal sensitivity of these surfactants but merely suggest that degradation could only be a small contributor to the observed change in basal spacing.

The XRD patterns for subsequently prepared nanocomposites with TPO from the masterbatches with ODTA, C30B and DDDA indicated substantial disordering but a small well defined peak was still noted indicating that some crystal order remained. The fact that the clay structure found in both masterbatch and nanocomposite materials were comparable for all three organoclay species notes that the hydroxylethyl moiety in C30A was not beneficial to basal expansion or clay destructuring in our case; an observation bearing further examination by infrared spectroscopy in a subsequent section.

4.3.2. TEM analysis

TEM micrographs were taken to directly observe the morphology of the prepared TPO nanocomposite materials. In order to see details on delamination among the five organoclays and the effect of the supercritical fluid, particles in each image were analyzed using image analysis software (SigmaScan Pro 5, SYSTAT Software Inc.). The normalized size distribution for tactoid thicknesses within each nanocomposite is summarized in Figure 4.2, distinguished based on the gas used during annealing.

The DODA-derived TPO nanocomposite prepared from the $scCO_2$ treated masterbatch had the highest incidence of tactoids less than 2 nm in thickness (individual platelet of montmorillonite) as well as tactoids appearing between 2-4 nm compared to all other clays. The nitrogen case for the DODA-based material showed little difference from the other clay materials tested. The distributions for nanocomposites using THMA were broader than DODA, but similarly had a relatively high fraction of particles below 4 nm. The main difference between the two organoclays was that samples prepared under $scCO_2$ had smaller tactoids in their particle distribution compared to N_2 for DODA whereas for THMA the opposite was true, indicating the supercritical fluid was interfering rather than aiding exfoliation in that case. The TEM data confirmed the XRD results – just gave a clearer understanding of the changes in microstructure correlated to the gas present during annealing. Bousmina (2006) estimated through 'energy of adhesion' modeling that clay layer separation could be most readily achieved in a non-polar matrix by shear when its original basal spacing was greater than 34 Å. Stoeffler et al. (2008) suggested that this

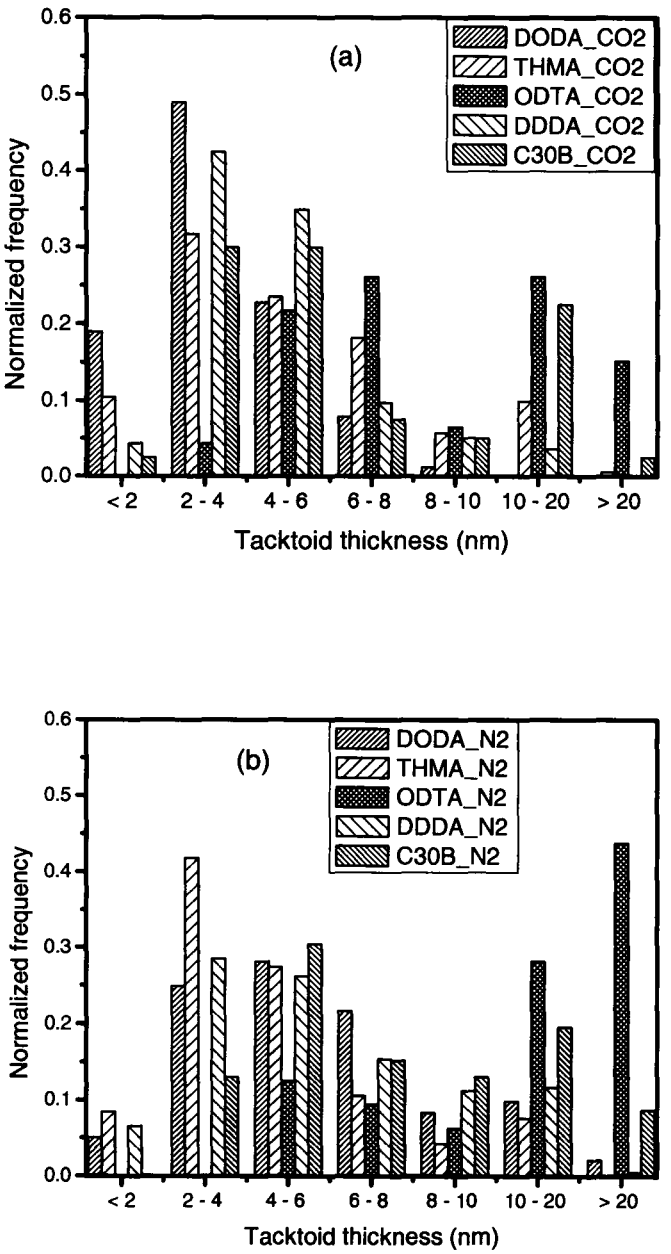

Figure 4.2 Histograms of frequency of tactoid thickness present in TEM images for TPO nanocomposites based on selected organoclays and gases of $scCO_2$ (a) and N_2 (b)

minimum value was closer to 25 Å based on a review of experimental results in the literature and from their experiments of delamination in polyolefins without compatibilizer. The particle distributions of our samples seem to support the lower value of Stoeffler as DODA and THMA appeared to have more readily exfoliated compared to the other three organoclays.

ODTA and C30B showed greater sensitivity to $scCO_2$ than eluded by XRD results or later rheological measurements but under either gas both had the highest content of large tactoids (> 6 nm) compared to other organoclay species. Comparatively, the nanocomposites with DDDA showed greater exfoliation than found with C30B or ODTA despite XRD results indicating little difference. For both gases used there was a distinct preference for tactoids in the 2-4 nm and 4-6 nm ranges yet comparatively, for $scCO_2$ there was a notable improvement in exfoliated particles in the 2-4 nm range for this organoclay. The supercritical fluid appeared to have been an effective exfoliating aid in the cases of both DDDA and DODA, both organoclays with dialkyl surfactants.

4.3.3. Infrared Spectroscopy

Infrared analysis was used to evaluate coordination of the maleic anhydride moiety with the surfactant and clay surface for the different organoclay species. It would have been desirable to obtain chemical information on both the masterbatch and nanocomposite samples for each organoclay; however, this analysis discusses only the masterbatch samples since the diluted concentrations of anhydride and surfactant within the TPO matrix of a nanocomposite were too low to make meaningful interpretations.

Spectra for the organoclays and maleated polypropylene compatibilizer in their pristine state are shown in Figure 4.3a for the frequency range of 1500-2000 cm^{-1}. The strong absorbances by the organoclays versus compatibilizer in this region are well differentiated, except for a small broad peak for both components in the region of 1820-1870 cm^{-1}. For the organoclays, the principal peak of interest in the figure was seen at ~1640 cm^{-1} for bending vibrations of the hydroxyl groups along the broken edges (octahedral Al-OH and tetrahedral Si-OH) of montmorillonite. This peak was strongest for the unmodified sodium montmorillonite (NaMMT, Cloisite Na^+ from Southern Clay Products), which was included in this section for reference, but also C30B whose surfactant included hydroxyl groups. The peak was weakest for THMA and DDDA. The original compatibilizer (PB3200) presented two well defined peaks in the region, i) a broad anhydride absorbance centered at ~1780 cm^{-1} with a distinct shoulder at 1790 cm^{-1} corresponding to the different ring conformations found for grafted anhydride and poly(maleic anhydride) grafted species on the polypropylene; and ii) a strong absorbance at ~1715 cm^{-1} for the carboxylic acid groups resulting from hydrolysis.

Spectra of the masterbatch materials are shown in Figure 4.3b to highlight changes to the grafted anhydride groups, and this time included an annealed mixture with NaMMT for comparison. In order to eliminate differences in film thickness, all curves in the figure were normalized using a band of 840 cm^{-1}, a typical wagging vibration of CH_3/CH_2 in the polypropylene. After melt annealing with the different organoclays, the absorbance centered at 1780 cm^{-1} for the different anhydride moieties in MA-PP was

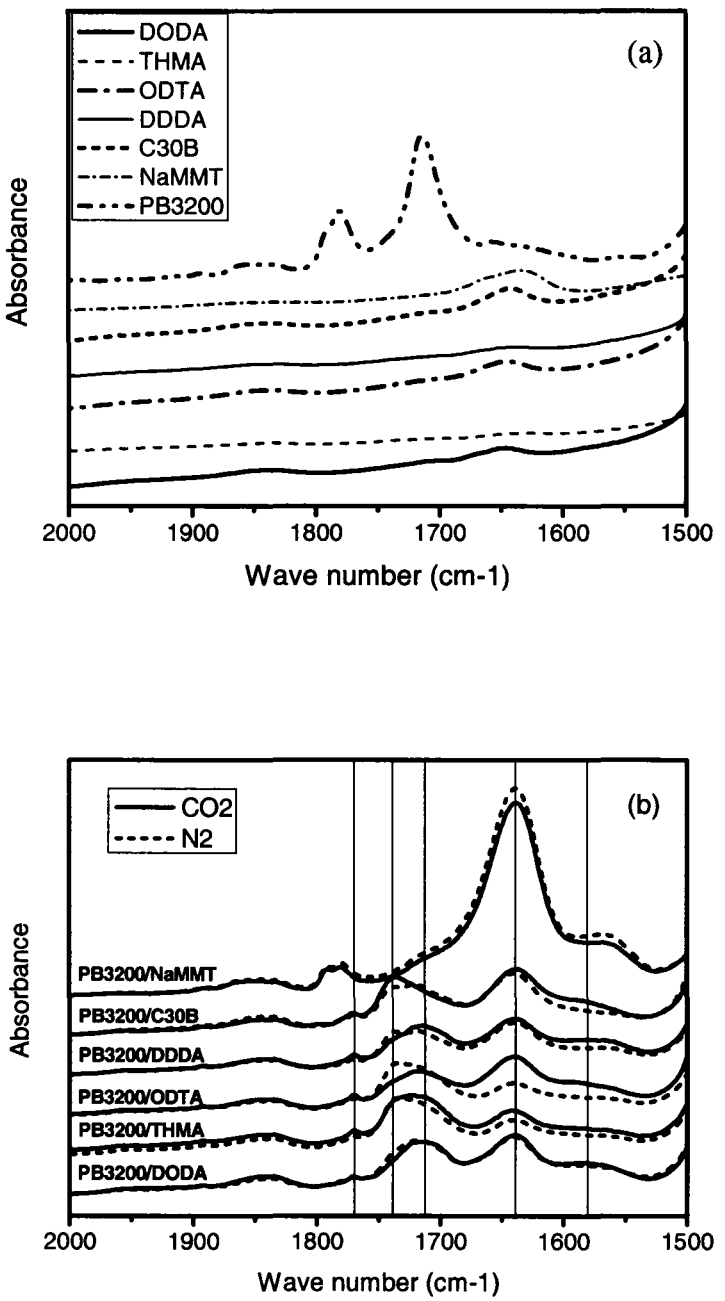

Figure 4.3 FT-IR spectra of (a) PB3200 and organoclays at their pristine state and (b) masterbatches of organoclays with PB3200

significantly reduced. A residual anhydride absorbance at ~1770 cm^{-1} remained but all other conformations of the functional group in MA-PP were no longer detected. It was felt in the case of NaMMT that its poor interfacial interaction with the compatibilizer made it more difficult for associations with the anhydride group and hence the limited change in absorbance at ~1780 cm^{-1}; however, this does not imply that no interactions occurred. The peak at ~1715 cm^{-1} for MA-PP persisted in the organoclay masterbatches, though broadened in comparison of the original compatibilizer. Under normal conditions at the temperatures of this study the dicarboxylic acid group for hydrolyzed MA-PP should dehydrate, reverting back to its anhydride moiety unless at least one of the acid groups undergoes reaction. The broadening of this peak indicated ester formation by reaction of at least the one of the carboxylic groups with hydroxyls, most notably found at the broken edges of montmorillonite. The ester absorbance at ~1740 cm^{-1} was strongest for C30B which is understandable due to the additional presence of hydroxyl groups in the surfactant. For the other organoclay species the ester formation would reasonably only be expected at the broken plane of the formed tactoids. Sterically, it would be unlikely both acid groups of the opened anhydride ring form an ester and hence the mixture of carboxylic acid and ester in the final masterbatch materials.

The hydroxyl group detected at 1640 cm^{-1} for the different organoclays was observed to increase in intensity as a result of annealing with MA-PP, most notably for NaMMT but now THMA and DDDA also showed absorbances in this region not seen for their pristine clays. With the broken plane of montmorillonite being the primary source of hydroxyl species for these mixtures and no foreseeable reaction creating such moiety,

the increase in absorbance intensity pointed to greater exposure of this plane by exfoliation. The smaller but persistent presence of hydroxyls within the organoclay masterbatches indicated insufficient concentration of the anhydrides to fully convert all groups to esters or alternatively indicating steric hindrance limited access of both acids in the opened ring moieties to reaction. The larger peak at 1640 cm^{-1} for NaMMT corresponded once again to the fact that esterification would not proceed in the case of this masterbatch.

The broad absorbance peak between 1550-1600 cm^{-1}, strongest for NaMMT but notable for all organoclays as well, corresponded to vibrational bands for asymmetric stretching of a carboxylate. The dicarboxylic acid species in coordination with MMT formed outer-sphere (~1560 cm^{-1}) and inner-sphere (~1580 cm^{-1}) complexes (Kang and Xing, 2007) for the NaMMT, DODA and DDDA masterbatches while the other masterbatch materials showed only the inner-sphere complex. Outer-sphere adsorption for the maleic/succinic acid groups with MMT likely involved complexation through the sodium ion since NaMMT has a high sodium content (2.84g Na^{+}/100g clay) but comparatively DDDA also had a high content (0.46g Na^{+}/100 g clay) in regards to the other organoclay species (0.22-0.25g Na^{+}/100g clay); elemental analysis for sodium was conducted using a Perkin-Elmer 5100 ZL atomic absorption spectrometer. Inner-sphere complexation implies direct bonding between the formed carboxylate group of the maleic/succinic acid and the metal ions at the silicate surface. The small intensity of this absorbance shows dominance for ester formation between the organoclays and compatibilizer.

The gas present during annealing had only a small effect on the associations between organoclay and compatibilizer. Compared to the $scCO_2$ cases, those masterbatches annealed under nitrogen showed slightly higher intensity of the esterification absorption at 1740 cm^{-1} (except C30B). This can be explained by the surfactant rearrangement that occurs to a higher extent in the $scCO_2$ environment (Thompson et al. 2008). More organic coverage over the silicate surface due to surfactant rearrangement would reduce exposure of the broken plane of montmorillonite and therefore, less esterification was possible between the carboxylic acid and the hydroxyl groups in the case of the $scCO_2$-based masterbatches. Correspondingly, there was a higher tendency of MA-PP coordination with MMT for the $scCO_2$ cases through carboxylate complexation for all clay species except NaMMT. The differences between bond associations for the $scCO_2$ case and N_2 case were most notable for ODTA among all organoclays tested.

4.3.4 Rheological analysis

Rheological measurements tends to be more sensitive to the bulk nanoscale features of a nanocomposite compared to other techniques like XRD and TEM, and are directly related to the final mechanical properties of the material which are being optimized. Figure 4.4 compares the storage modulus (G′) for the TPO nanocomposites prepared with the five different organoclays and under the two gases, over a frequency range between ω = 0.1-100 rad s^{-1}. The error in these measurements was quite small and the error bars are only distinguishable in these plots at lower frequencies. In general, our

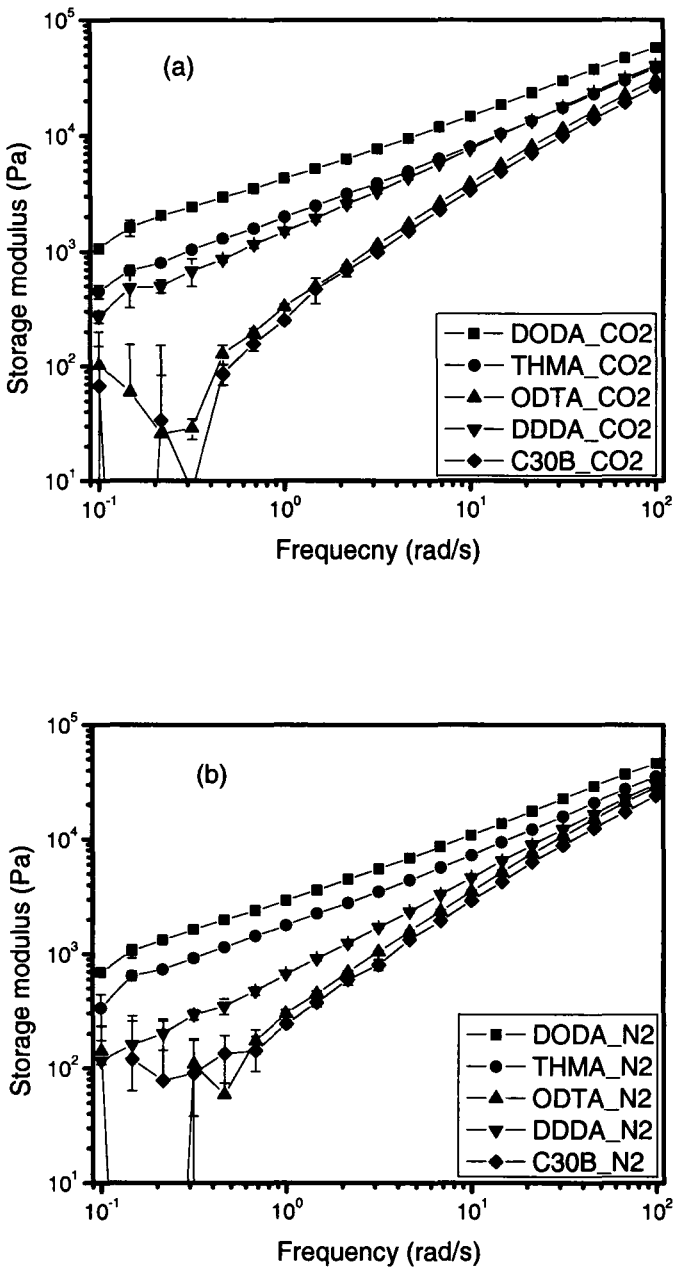

Figure 4.4 Storage moduli of the TPO nanocomposites in which masterbatches were prepared under atmosphere of (a) $scCO_2$ and (b) N_2

focus lies in the terminal region below $\omega = 1$ rad s^{-1} where large-scale segmental motion of the polymer chains are observable and interference to that motion by short-range filler-filler interactions is most readily noted. The change in the slope of the curve within this terminal region of the graph and the corresponding increase in modulus resulting from exfoliation have been identified by others (Krishnamoorti and Giannelis, 1997; Galgali et al. 2001; Lele et al. 2002; Solomon et al. 2001; Ren et al. 2003) as being related to a percolating network of silicate nanoparticles formed within the material. From the figure it can be noted that there was a general correspondence in trends between the measured G′ for the different organoclays and the frequency of smaller tactoids found by TEM analysis, though some features were certainly better distinguished rheologically.

The nanocomposites with highest storage moduli prepared in this study corresponded to those containing DODA. The higher modulus of these nanocomposites was reconciled by the higher extent of destructuring to the clay that occurred by intercalation during the annealing step. Supercritical CO_2 had a small beneficial effect on the modulus, reflecting an improvement in exfoliation seen earlier by particle size analysis. Previous work by the group (Liu et al. 2010) has postulated that the change in intercalation for this organoclay-compatibilizer system was related to the plasticizing effect of $scCO_2$ on both oleophilic polymer and surfactant. Larger molecules were found to intercalate into this clay's galleries than occurred when $scCO_2$ was not present. These larger chains were envisioned as extending outwards from the clay into the matrix to more effectively transfer stresses during shear delamination and produce these more highly exfoliated silicate structures.

The storage moduli of the nanocomposite materials prepared with THMA were lower than those prepared with DODA yet greater than the other three organoclays. DODA did possess more tactoids below 4 nm to explain this difference. Neither N_2 nor $scCO_2$ showed any significant effect on the measured G′ for THMA; however based on particle size, the N_2 case should have shown a higher modulus value than the $scCO_2$ case and been more comparable to DODA. Here we see an excellent example for the case that particle size can not be the only criteria for improved mechanical properties. THMA had the highest organic content, largest basal spacing, and lowest surface energy – it should theoretically have demonstrated the highest frequency of exfoliation by its better compatibility with the matrix and therefore, provided the highest reinforcement in the rheological tests. The fact that it did not match expectation points to the validity of the molecular simulations of Toth et al (2004) where the large molecular volume of its surfactant shielded the MMT from forming complexes with the compatibilizer. A similar explanation for the negative effects of the surfactants on affinity of the polymer chains was given by Paul and Robeson (Paul and Robeson, 2008).

The storage modulus curves for nanocomposites prepared with either of the mono-alkyl ammonium modified clays, namely ODTA or C30B, demonstrated similar rheological behavior to one another and the lowest set of stiffness values in the study. The unsteady stress data noted in the displayed G′ curves at low strain rate (i.e. below 1 rad s^{-1}) for C30B, ODTA as well as DDDA (nitrogen case only) were interpreted as indicators of poor filler dispersion within the TPO matrix. A higher polar contribution ($\gamma^p > 1$ mN/m) was noted to correlate with the unsteady stress response. No influence of

$scCO_2$ was seen for either of these two clays (i.e. ODTA and C30B). The similarity in rheology for these two materials was in agreement with their XRD patterns though not the TEM results. Here again was an example case highlighting the importance of compatibilizer interactions. The performance of ODTA was understandable in light of the other evidence in this work; collapsed galleries and large tactoids pointed to a poorly intercalated and exfoliated material system offering little enhanced surface area development for reinforcement of the polymer matrix. For C30B, the particle size distribution found implied the available surface area for stress transfer was comparable to DODA and THMA, and having the lowest interfacial energy of tested clay-compatibilizer systems there should be good wetting by the PB3200, so the low modulus was unexpected being so similar to ODTA. The presence of the strong ester FTIR absorbance band for the C30B composites indicated a high extent of coordination by the compatibilizer with the organoclay which translated to greater extent of delamination than for the comparable basal spacing of ODTA. The poor reinforcement of C30B demonstrated in the rheological analysis suggested that bonding with the surfactant was less desirable than direct bonding with the broken edges of MMT. This could again be demonstrating a negative outcome by shielding the anhydride from direct coordination with the MMT.

The nanocomposites prepared with the only other bilayer-arranged organoclay, namely DDDA, exhibited rheological differences depending on whether $scCO_2$ was used, just like DODA. In fact, the response to $scCO_2$ was more dramatic on a relative basis than seen with DODA – the sample prepared with $scCO_2$ demonstrated a storage modulus

similar to THMA, while the sample prepared with N_2 exhibited a much lower modulus closer to those found with ODTA or C30B.

4.4 INFLUENCE OF $scCO_2$ ON DIALKYL MODIFIEC ORGANOCLAYS

Supercritical carbon dioxide produced a small change to the microstructure of any of the organoclays tested; however, significant improvements in material reinforcement as probed by rheological testing, were only noted with two species, DODA and DDDA. The supercritical fluid has been noted in earlier works to cause change to the surfactant arrangement of DODA (Thompson et al. 2008, 2009) and when in the presence of the compatibilizer as well, allow intercalation of larger compatibilizer chains deeper into the galleries of DODA (Liu et al., 2010). The new finding in this work was the similar responsiveness to $scCO_2$ being noted for DDDA. The $scCO_2$-treated TPO nanocomposites from these two organoclays showed a higher fraction of silicate particle sizes less than 4 nm and higher G' than their nitrogen counterparts. However, besides both containing dialkyl quaternary salts there were few similarities noted. The two organoclays possessed different alkyl chain lengths, different polar interfacial contributions, different original basal spacing and different surface coverage over montmorillonite (if the sodium ion content can be taken as an indicator). These two did share similar dispersive interfacial contributions though (but then so did THMA). There seems little comparable between the two species besides their dialkyl structure and with only these two positive outcomes to $scCO_2$ among the tested organoclays it is unclear whether the structure is relevant.

The data in this paper has shown that the state of clay dispersion and the properties of the final material are not directly related. An association between the compatibilizer and silicate surface appears necessary to increase stiffness yet bonding with the surfactant instead (i.e. C30B) does not bring comparable improvement. Infrared analysis has suggested that these interactions are slightly different when $scCO_2$ was present with more carboxylate complexes formed, though ester formation remained the dominant association. There is limited literature on quaternary ammonium salts being used with supercritical CO_2 to aid in this analysis but the work of Fernandez et al. (1996) offers a possible explanation to our work. Those authors found that supercritical fluid has limited capacity to extract alkyl-type quaternary ammonium cations based on their strong ion-dipolar interactions with clay and that the extent of extraction increased with decreased alkyl chain length. It is possible that in the case of the present work that the solvating capacity of $scCO_2$ for DODA and DDDA was sufficient to allow an exchange within the galleries of the montmorillonite for the anhydride moiety of the compatibilizer. Further studies are merited in this regards to verify the hypothesis.

4.5 CONCLUSIONS

The experiment results showed that paraffinic arrangements for an alkyl surfactant appeared to offer more effective access of the compatibilizer functionality to the silicate than lateral monolayer or bilayer arrangements. This appears to validate computational results by other researchers regarding the shielding effect of some surfactants limiting potential interaction of the compatibilizer with the silicate surface. Poor exfoliation and reduced reinforcement by the silicate filler was noted for the final materials when

shielding was assumed to occur. The effectiveness of supercritical CO_2 on the intercalation and exfoliation was also strongly related to properties of a surfactant. Intercalation and exfoliation of DODA and DDDA, their surfactant having two long alkyl tails, in the TPO matrix were significantly improved due to presence of the supercritical gas whereas those other organoclays did not. It seems that $scCO_2$ significantly altered the physical and chemical environment of the two organoclays, which allowed them to more actively coordinate with the compatibilizer. As a result, $scCO_2$-treated masterbatches for these two organoclays were found more compatible with the matrix polymer and experienced a higher level of exfoliation in the prepared TPO nanocomposite.

REFERENCES

Bonczek, J.L., Harris, W.G., Nkedi-Kizza, P., 2002. Monolayer to bilayer transitional arrangements of hexadecyltrimethylammonium cations on Na-montmorillonite. Clays Clay Miner. 50, 11-17

Bousmina, M., 2006. Study of intercalation and exfoliation processes in polymer nanocomposites. Macromolecules 39, 4259-4263

Dennis, H.R., Hunter, D.L., Chang, D., Kim, S., White, J.L., Cho, J.W., Paul, D.R., 2001. Effect of melt processing conditions on the extent of exfoliation in organoclay-based nanocomposites. Polymer 42, 9513-9522

Eckel, D.F., Balogh, M.P., Fasulo, P.D., Rodgers, W.R., 2004. Assessing organo-clay dispersion in polymer nanocomposites. J. Appl. Polym. Sci. 93(3), 1110-1117

Favre, H., Lagaly, G., 1991. Organo-bentonites with quaternary alkylammonium ions. Clay Miner. 26, 19-32

Fernandez, P., Alder, A. C., Suter, M. J.-F., Giger, W., 1996. Determination of the quaternary ammonium surfactant ditallowdimethylammonium in digested sludges and marine sediments by supercritical fluid extraction and liquid chromatography with postcolumn ion-pair formation. Anal. Chem. 68, 921-929

Galgali, G., Ramesh, C., Lele, A., 2001. A rheological study on the kinetics of hybrid formation in polypropylene nanocomposites. Macromolecules 34, 852-858

He, H., Duchet, J., Galy, J., Gerard, J.-F., 2006. Influence of cationic surfactant removal on the thermal stability of organoclays. J. Coll. Interf. Sci. 295, 202-208

Heinz, H., Vaia, R. A., Krishnamoorti, R., Farmer, B. L, 2007. Self-assembly of alkylammonium chains on montmorillonite: effect of chain length, head group structure, and cation exchange capacity. Chem. Mater. 19, 59-68

Horsch, S., Serhatkulu, G., Gulari, E., Kannan, R.M., 2006. Supercritical CO_2 dispersion of nano-clays and clay/polymer nanocomposites. Polymer 47, 7485-7496

Kang, S., Xing, B., 2007. Adsorption of dicarboxylic acids by clay minerals as examined by *in situ* ATR-FTIR and *ex situ* DRIFT. Langmuir 23, 7024-7031

Kim, K., Utracki, L.A., Kamal, M.R., 2004. Numerical simulation of polymer nanocomposites using self-consistent mean-field model. J. Chem. Phys. 121, 10766-10777

Krishnamoorti, R., Giannelis, E.P., 1997. Rheology of end-tethered polymer layered silicate

Nanocomposites. Macromolecules 30, 4097-4102

Lagaly, G., Gonzalez, F., Weiss, A., 1976. Problems in layer-charge determination of montmorillonites. Clay Miner. 11, 173-187

Lagaly, G., 1994. In Clay Minerals Society Workshop Lectures 6, Layer Charge Characteristics of 2 : 1 Silicate Clay Minerals, A.R. Mermut (Ed.), Boulder, Colorado

Lele, A., Mackley, M., Galgali, G., Ramesh, C., 2002. *In situ* rheo-x-ray investigation of flow-induced orientation in layered silicate–syndiotactic polypropylene nanocomposite melt. J. Rheol. 46, 1091-1110

Li, J., Ton-That, M.-T., Tsai, S.-J., 2006. PP-based nanocomposites with various intercalant types and intercalant coverages. Polym. Eng. Sci. 46, 1060-1068

Liu, J., Thompson, M.R., Balogh, M.P., Speer Jr., R.L., Fasulo, P.D., Rodgers, W. R., Nov. 2010. Influence of supercritical CO_2 on the interactions between maleated polypropylene and alkyl-ammonium organoclay. J. Appl. Polym. Sci. (accepted)

Paul, D.R., Robeson, L.M., 2008. Polymer nanotechnology: nanocomposites. Polymer 49, 3187-3204

Ren, J., Casanueva, B.F., Mitchell, C.A., Krishnamoorti, R. Disorientation kinetics of aligned polymer layered silicate nanocomposites Macromolecules, 36 2003., 4188-4194

Rohlmann, C.O., Fernanda Horst, M., Quinzani, L.M., Failla, M.D., 2008. Comparative analysis of nanocomposites based on polypropylene and different montmorillonites. European Polym. J. 44, 2749-2760

Shah, R.K., Paul, D.R., 2006. Organoclay degradation in melt processed polyethylene nanocomposites. Polymer 47, 4075-4084

Solomon, M.J., Almusallam, A.S., Seefeldt, K.F., Somwangthanaroj, A., Varadan, P., 2001. Rheology of polypropylene/clay hybrid materials, Macromolecules 34, 1864-1872

Stoeffler, K., Lafleur, P.G., Denault, J., 2008. Effect of intercalating agents on clay dispersion and thermal properties in polyethylene/montmorillonite nanocomposites, Polym Eng Sci, 48, 1449-1466

Thompson, M.R., Liu, J., Krump, H., Kostanski, L.K., Fasulo, P.D., Rodgers, W.R., 2008. Interaction of supercritical CO_2 with alkyl-ammonium organoclays: changes in morphology. J. Colloid Interf. Sci. 324, 177-184

Thompson, M.R., Balogh, M.P., Speer Jr., R.L., Fasulo, P.D., Rodgers, W.R., 2009. *In situ* x-ray diffraction studies of alkyl quaternary ammonium montmorillonite in a CO_2 environment. J. Chem. Phys. 130, 044705

Ton-That, M.-T., Perrin-Sarazin, F., Cole, K.C., Bureau, M.N., Denault, J. Polyolefin nanocomposites: formulation and development. Polym Eng Sci 44(7) (2004), 1212-1219

Toth, R., Coslanich, A., Ferrone, M., Fermeglia, M., Pricl, S., Miertus, S., Chiellini, E., 2004. Computer simulation of polypropylene/organoclay nanocomposites: characterization of atomic scale structure and prediction of binding energy. Polymer 45, 8075-8083

Xi, Y., Frost, R. L., He, H., 2007. Modification of the surfaces of Wyoming montmorillonite by the cationic surfactants alkyl trimethyl, dialkyl dimethyl, and trialkyl methyl ammonium bromides, J. Coll. Interf. Sci. 305, 150-158

Chapter 5

Use of supercritical CO_2 as an intercalation/exfoliation aiding agent in the preparation of a polymer layered silicate nanocomposite

J. Liu, W. R. Rodgers, P. D. Fasulo, and M. R. Thompson

This chapter is paper formatted to be consistent with the previous ones but has not been submitted to a technical journal. Jinling Liu is the major contributor to this chapter.

In this chapter, the role of $scCO_2$ in the processing of TPO nanocomposites was examined through three different combination manners of the organoclay, compatibilizer and matrix materials during their melt annealing. The organoclay used included its pristine state and its pretreated species using $scCO_2$.

ABSTRACT

A novel small scale mixer was successfully developed based on extensional flow mixing. Usefulness of supercritical CO_2 ($scCO_2$) in the processing of thermoplastic elastomer nanocomposites was investigated using this device. An organoclay (Cloisite 20A), a maleated polypropylene (Polybond® 3200) and a thermoplastic olefinic polymer (TPO) were selected for this study. The three components were combined in different manner to evaluate how $scCO_2$ influenced microstructure of the final composite prepared by different mixing orders of the components. The organoclay was examined in its pristine state and having been previously conditioned under $scCO_2$. Analyses of the nanocomposites formed using X-ray diffraction (XRD), transmission electron microscope (TEM) and parallel plate rheology techniques showed that introduction of supercritical CO_2 in melt compounding significantly improved level of exfoliation and dispersion of the organoclay in the TPO nanocomposite. The aiding effect was more significant when the compatibilizer and organoclay formed a molten masterbatch under supercritical CO_2 before the extensional flow mixing with the matrix TPO. The $scCO_2$ pre-conditioned organoclay had not impact on its final extent of exfoliation in the TPO nanocomposite.

5.1 INTRODUCTION

Supercritical CO_2 ($scCO_2$) has been strongly involved in the developments of foaming thermoplastics for the past two decades. It was observed in the course of foaming polymer nanocomposites that the addition of this supercritical solvent to the compounding process resulted in higher exfoliation for the dispersed clay mineral. There are now research efforts underway to utilize $scCO_2$ as an exfoliating aid without

necessarily producing a foam. At issue with this new use for $scCO_2$ is the nature by which it contributes to the more highly exfoliated morphology in formation of a polymer layered silicate (PLS) nanocomposite. Several technologies have emerged in patents and published papers on this new utilization and these technologies can basically be divided into three categories. The first and most extensively pursued is direct gas injection into a mixing device where all components are melt compounded [1-3]. This approach aims at good solubility of surfactant and polymeric components in the supercritical fluid, expecting improved intercalation and exfoliation occurred during the shear-dominated melt mixing. Another approach focuses on pre-exfoliating the layered silicate filler using the supercritical fluid. Gulari et al. used a technique known as 'particles from gas-saturated solutions/suspensions (PGSS)' in the hopes of fracturing the layered structure of an organoclay before it was added to the compounding process [4, 5]. Baird et al. modified this technology from batch to a continuous process [6]. The third method was recently proposed by Rodgers et al. [7] who added the supercritical fluid and organoclay together into a highly pressurized zone of a compounding process which maintains the CO_2 gas in its supercritical state during mixing, at least for the initial stages. In the course of studying what the $scCO_2$ was contributing to the mixed nanocomposite prepared by these different systems, our own experiments started as batch processes, first examining the organoclay under $scCO_2$, and then the mixture of clay and compatibilizer with $scCO_2$ [8-9]. Intercalation was the primary focus for our earlier studies, with no possibility for convective (mechanical) mixing while the system was maintained in suspension with supercritical CO_2. The present work introduces a mixing device built to allow assessment

of the role of $scCO_2$ with inclusion of dispersive forces for the preparation of a thermoplastic elastomer nanocomposite. To be effective, the device had to allow examination of the mixing order by which the three components (i.e. organoclay, compatibilizer and matrix) were combined and evaluate effectiveness based on extent of exfoliation.

5.1.1 Designing a mixing device

The most commonly used compounding device for studies of exfoliation of a PLS nanocomposite are usually a twin- or single-screw extruder [10-12]. But these devices do not readily allow control over which material components are exposed to the $scCO_2$, especially if it is important that the highly pressurized gas be present before melting of either the compatibilizer or matrix polymer. For such a study a compartmentalized mixing system would be desirable. The mechanical action of organoclay dispersion into a PLS nanocomposite can originate from shear or extensional deformation and both are ideally found in compounding machinery, though studies generally show that extensional flow can generate better dispersive and distributive mixing results than that achieved by shear alone [13-15]. Again, as part of the study is intent on looking at powders while in contact with the supercritical fluid before they melt, it is difficult to conceive of a rotary shearing device which can maintain control over the gas pressure to a desired extent. A piston-driven mixer is ultimately proposed as suitable to the needs of the present work, a device where extensional mixing was produced by convergent-divergent flow through an orifice plate separating two heated compartments.

5.2 EXPERIMENTAL

5.2.1 Materials

A medium-to-high flow TPO (13 MFR) supplied by LyondellBasell was selected for this study. Pellets of the TPO material was used directly without any further treatment. Cloisite 20A (C20A), the organically modified montmorillonite, was supplied by Southern Clay Products which was found most sensitive to supercritical CO_2 among the three organoclays examined in our previous studies [16-18]. The $scCO_2$ pre-conditioned organoclay (s-C20A) was prepared in a high pressure batch vessel where the clay was annealed under an environment of CO_2 for 3 hours at 9.7MPa and 200°C before being collected by rapid depressurization at ~10 MPa/s. A commercial maleated polypropylene (MA-PP) compatibilizer, Polybond® 3200 (PB3200) from Chemtura Corporation was selected. This compatibilizer has sufficient molecular weight to minimize any losses in mechanical properties by its addition to the nanocomposite and demonstrated plasticization in the presence of supercritical CO_2 sufficient to aid intercalation [18]. Pellets of the MA-PP were ground cryogenically into powder by a local company, Ingenia Polymers, for improved blending with the clay. Other properties of the organoclay and MA-PP have been reported in previous studies [16-18]. The carbon dioxide and nitrogen used in the experiments were supplied by Air Liquide Canada Inc. at 99.5% and 99.995% purity, respectively.

5.2.2 Extensional flow mixer

The custom-built extensional flow (EF) mixer for this work is schematically shown in Figure 5.1. The mixer was comprised of two cylindrical chambers which could accommodate different components for the TPO nanocomposite formulation. The two chambers were aligned and joined by a flange containing an orifice plate. Each chamber had an inner diameter of 10mm and was 110mm long. The orifice plate was 2 mm thick and had a hole of 3 mm diameter. Heating was accomplished by suspending the device in a convective oven with a silicone heating tape wrapped around the flange region to increase its temperature ramp rate.

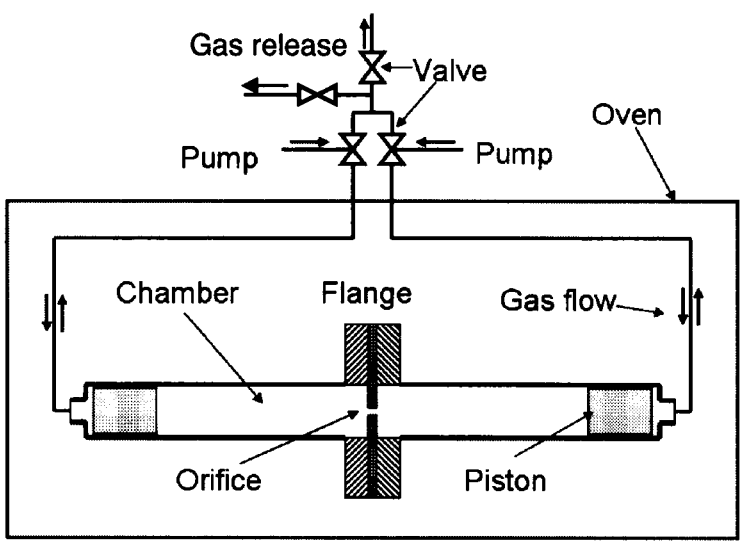

Figure 5.1 Schematics for the EF mixer

The large diameter difference (7 mm) between the chamber and orifice produced a convergent-divergent flow event each time the materials were pushed through the orifice. On the opposite ends of both chambers away from the orifice plate there were two pistons that were driven by the supplied gas to the system. A high pressure 260 ml syringe pump (ISCO Model 260D) connecting the two ends through two three-way ball valves to both the gas supply and relief valve. The relief valve maintained the system above the critical pressure for CO_2, i.e. 7.4 MPa, but allowed escape of sufficient gas to create a pressure gradient across the mixer. Incoming gas was supplied at 11.7 MPa by the pump whereas the exit pressure was normally ~ 8 MPa. An alternating pressure gradient was generated across the system through the use of the three-way ball valves to drive material from one chamber to the next across the orifice plate, resulting in repeated extensional deformation of the materials back and forth in the mixer. The duration of each extensional flow event took less than 2 s. Mixing resulted from the repeated extensional deformation across the orifice plate with optimal dispersion of the organoclay reached after 40 passes. Optimal dispersion was considered by the absence of detectable filler agglomerates under an optical microscope and reproducible determination of a storage modulus curve (G' vs. frequency) for at least three replicates of a sample.

5.2.3 Preparation of TPO nanocomposites

To evaluate the importance of $scCO_2$ as it contacted the different components of a TPO nanocomposite during the preparation, the three components were separated between the two chambers of the mixer in different combinations prior to heating. The different combinations of the three components, i.e. organoclay, compatibilizer and

polymer matrix, are listed in Table 5.1. To establish the naming convention for our samples, components that were put together in one chamber of the EF mixer were bracketed. For example, T/P/C, initial letter for TPO, PB3200 and C20A, respectiviely, refers to a sample prepared where all three components were put together in one chamber prior to mixing, while T(P/C) refers to a sample prepared such that PB3200 and C20A were first placed in one chamber and TPO in the other one. s-C20A was examined in same way as the pristine C20A. The composition for each nanocomposite was 90:5:5 (%w/w) for TPO, PB3200, and C20A (or s-C20A), respectively. Nitrogen gas was used for a reference to evaluate the role of $scCO_2$ in the process.

Table 5.1 Experimental trials for combination order

Sample name	Temp (°C)	Heat/Mixing time (min)	Contents in Chamber 1 during heating	Contents in Chamber 2 during heating
T/P/C	200	20/30	TPO/PB3200/C20A	—
T(P/C)	200	20/30	TPO	PB3200/C20A
(T/P)C	200	20/30	TPO/PB3200	C20A
T/P/s-C	200	20/30	TPO/PB3200/s-C20A	—
T(P/s-C)	200	20/30	TPO	PB3200/s-C20A
(T/P)s-C	200	20/30	TPO/PB3200	s-C20A

The compounding process was divided into two stages, i) 50-minutes for melting and annealing, and ii) 30-minutes for mixing. The heating/annealing stage was done

completely under a supercritical CO_2 (9.6 MPa) or nitrogen (3.5 MPa) environment, and included 30 minutes for heating the mixer from room temperature to 200°C and 20 minutes for isothermal equilibration. The following mixing stage corresponded to 40 extensional flow events, completed with the use of only nitrogen; due to rapid freezing of the relief valve due to expansion of gas it was not possible to operate the mixing stage under $scCO_2$ even when heating tape was tried.

5.2.4 Characterization

The crystal structure of the organoclay in the TPO composite was characterized using X-ray diffraction (XRD) and transmission electron microscopy (TEM). XRD analyses were performed using a Bruker D8 diffractometer with Cu K_α radiation (λ = 1.5407 Å) at an accelerating voltage of 40kV and a current of 20mA. TEM micrographs were collected from a JEOL 1200 EX TEMSCAN microscope operating at an accelerating voltage of 80kV and magnifications of 60,000x. Samples were microtomed with a diamond knife into thin sections approximately 70 nm thick and each mounted on a carbon grid. Viscoelastic properties of the nanocomposite samples were evaluated using an ARES parallel plate rheometer (TA Instruments). A constant strain of 5% was chosen for the measurements based on the determined linear viscoelastic region from strain sweep testing. The tests were conducted at 200°C over a frequency range of 0.1–100 rad/s.

5.3 RESULTS AND DISCUSSION

For clarification, it is pointed out that samples being referred in this section as prepared under $scCO_2$ corresponds only to the conditioning they received during

annealing. All samples were actually mixed under N_2 due to the freezing issue with the relief valve disclosed in Section 5.2.3.

5.3.1 XRD Analysis

Diffraction patterns of the six prepared nanocomposites listed in Table 5.1 for C20A are shown in Figure 5.2. The analysis method is being used to qualitatively identify structural changes, while recognizing XRD has questionable quantitative value in actually determining extent of intercalation or exfoliation of the organoclay. For the $scCO_2$ prepared samples, the (001) diffraction peak for T/P/C was significantly diminished (Figure 5.2a) and that for T(P/C) showed a peak shifted by 0.4° indicating a larger basal spacing (Figure 5.2b) compared to their corresponding N_2 cases. Differences for (T/P)C between the $scCO_2$ and N_2 case were not significantly apparent (Figure 5.2c). These results point to significant influence by the supercritical gas on dispersion of C20A and that the manner of combining the three components in the presence of the gas was a concern. The greater change in basal spacing for T(P/C) suggests the preferred method of combination favoured increased contact time between the compatibilizer and organoclay prior to mixing. Conversely, among the N_2 samples the manner of combination appeared to favour the case where maximum contact time was given to all three components prior to mixing, i.e. T/P/C.

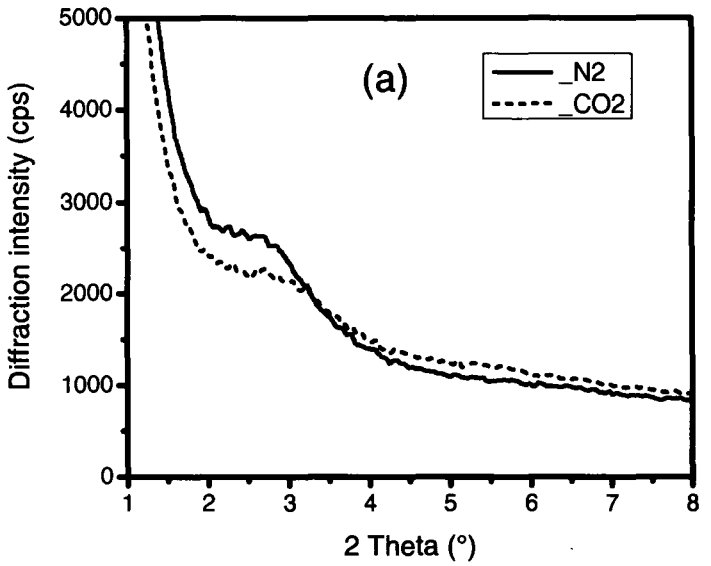
(a)
_N2
_CO2
Diffraction intensity (cps)
2 Theta (°)
0
1000
2000
3000
4000
5000
1
2
3
4
5
6
7
8

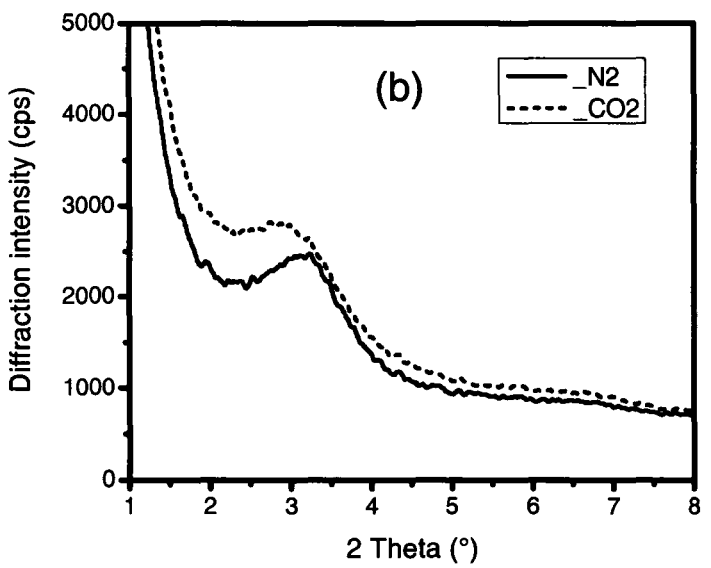
(b)
_N2
_CO2
Diffraction intensity (cps)
2 Theta (°)
0
1000
2000
3000
4000
5000
1
2
3
4
5
6
7
8

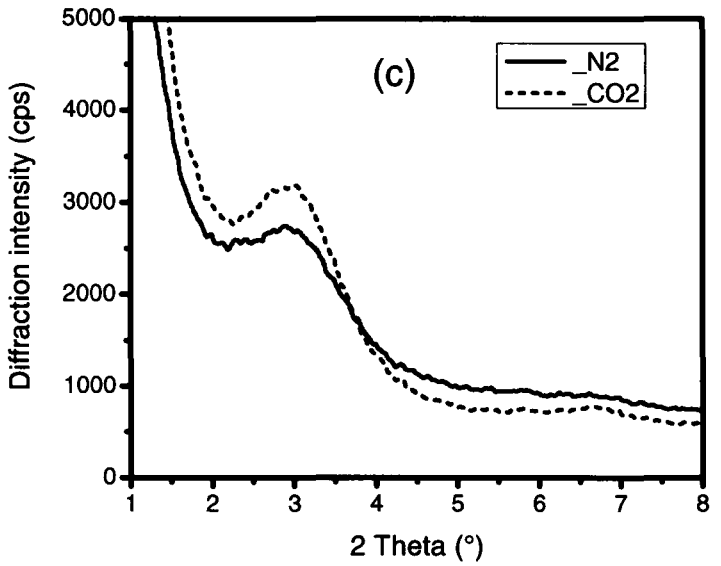

Figure 5.2 XRD patterns of the TPO nanocomposites prepared under $scCO_2$ and N_2 with formulation of T/P/C (a), T(P/C) (b) and (T/P)/C (c)

Similarly, diffraction patterns of the six prepared nanocomposites listed in Table 5.1 for s-C20A are shown in Figure 5.3. It can be seen from the figure that the clay diffraction peak corresponding to the (001) plane for each composite was difficult to distinguish from the baseline. The loss of ordered structure to the clay was attributed to the preparation method of the s-C20A particles, as reported in earlier papers [9, 18], and as such could not be related to the mixing. The technique does not provide sufficient information to determine the extent of dispersion but provides corroborating evidence to other techniques like TEM and rheological analysis.

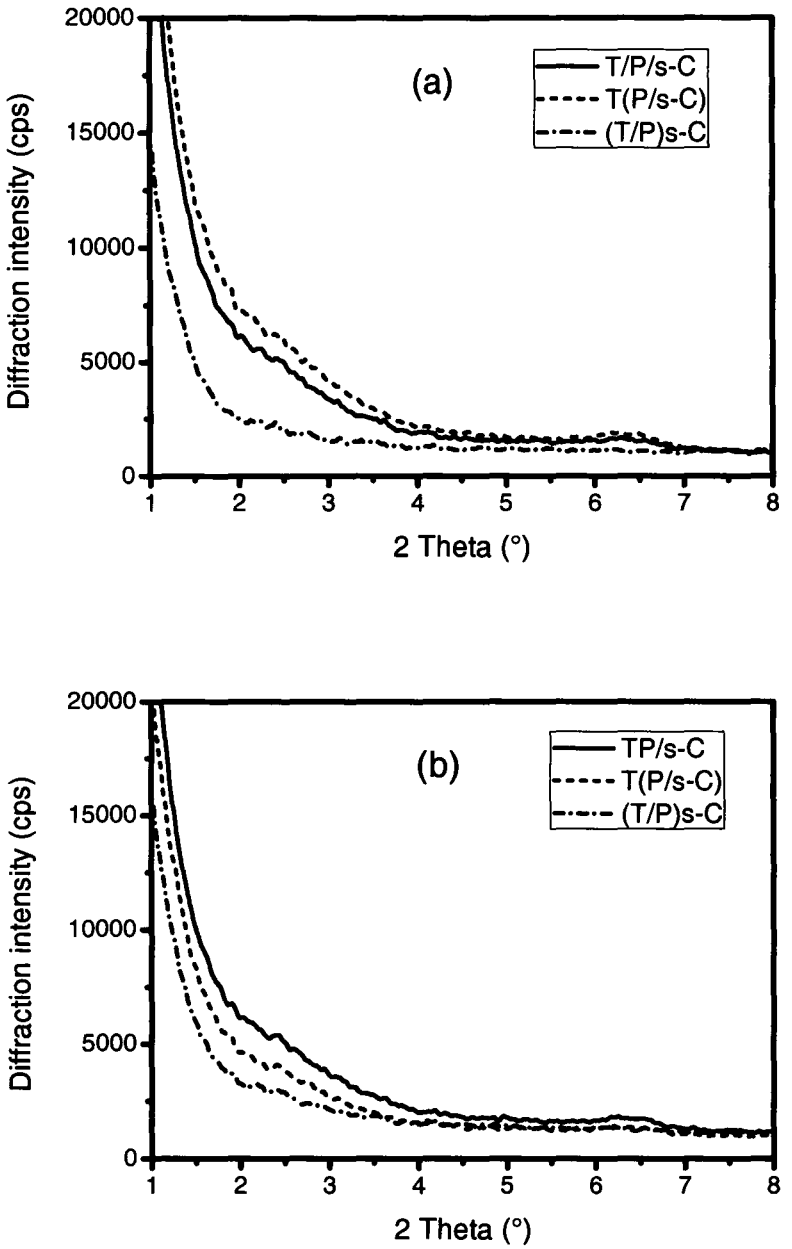

Figure 5.3 XRD patterns of the TPO nanocomposites prepared from s-C20A under environment of $scCO_2$ (a) and N_2 (b) with formulation of T/P/s-C, T(P/s-C) and (T/P)s-C

5.3.2. TEM

TEM images of the six C20A based nanocomposites are shown in Figure 5.4. In general for each method of combination, the CO_2 case showed clay tactoids structures that were less dense and dispersed more uniformly than their N_2 counterparts. Such observations are consistent with the XRD analysis; however, differences between the different combinations of the three components under a given gas system seem less distinct by TEM. For the three N_2 cases there was no perceivable difference and the small differences among the three CO_2 cases was only revealed by particle size analysis. Figure 5.5 shows the particle size distribution for the three CO_2-treated C20A-based nanocomposites. The particle size distributions among the N_2-case materials were not significantly different from one another and so only one example was included in the figure for comparison. The standard error for the analysis was 1.5%. The sample T(P/C)_CO_2 gave the smallest average tactoid thickness among all tested cases, showing that improvement in clay exfoliation arises when the scCO_2 mediates wetting of the organoclay by compatibilizer. Average tactoid thickness for the N_2-based composite was significantly higher than those for all the three scCO_2-based composite, indicating efficiency of the supercritical gas in aiding exfoliation and dispersion of the organoclay in our TPO nanocomposite. Assessing overall efficiency of mixing based on the frequency of large particles (i.e. thicknesses above 30 nm), the order of mixedness was T(P/C)_CO_2 (0%) < T/P/C_CO_2 (1%) < (T/P)C_CO_2 (3%) < T(P/C)_N_2 (11%), which was consistent with XRD observations.

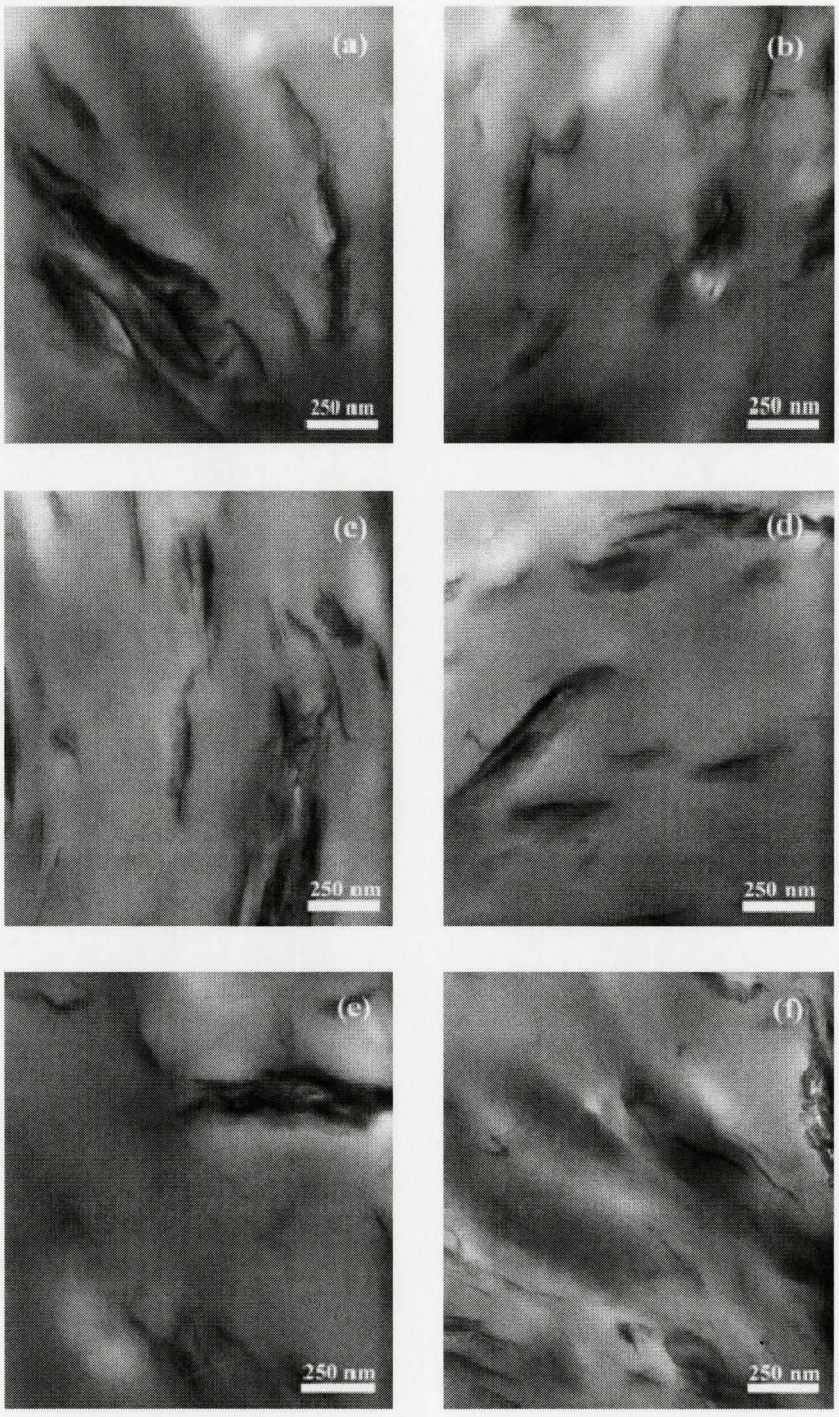

Figure 5.4 TEM images of the TPO nanocomposites from formula of T/P/C for N_2 (a) and CO_2 (b), T(P/C) for N_2 (c) and CO_2 (d), and (T/P)C for N_2 (e) and CO_2 (f)

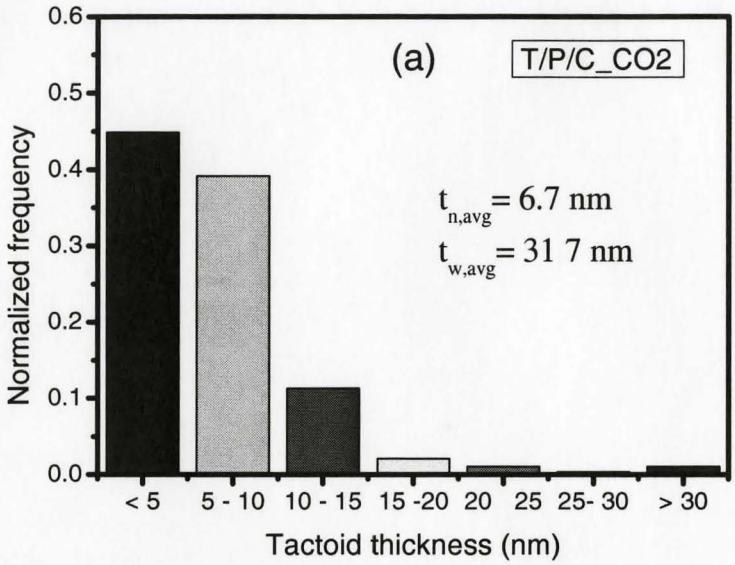
(a)
T/P/C_CO2
$t_{n,avg}$ = 6.7 nm
$t_{w,avg}$ = 31 7 nm
Normalized frequency
0.0
0.1
0.2
0.3
0.4
0.5
0.6
< 5
5 - 10
10 - 15
15 -20
20
25
25- 30
> 30
Tactoid thickness (nm)

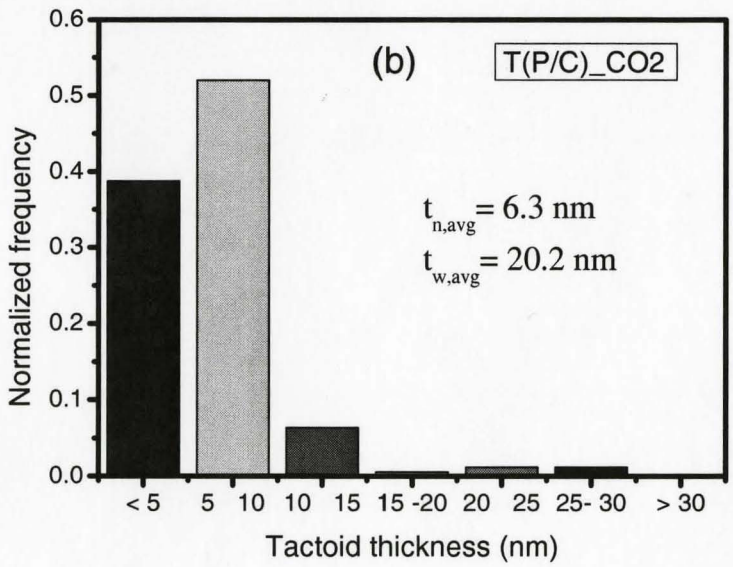
(b)
T(P/C)_CO2
$t_{n,avg}$ = 6.3 nm
$t_{w,avg}$ = 20.2 nm
Normalized frequency
0.0
0.1
0.2
0.3
0.4
0.5
0.6
< 5
5
10
10
15
15 -20
20
25
25- 30
> 30
Tactoid thickness (nm)

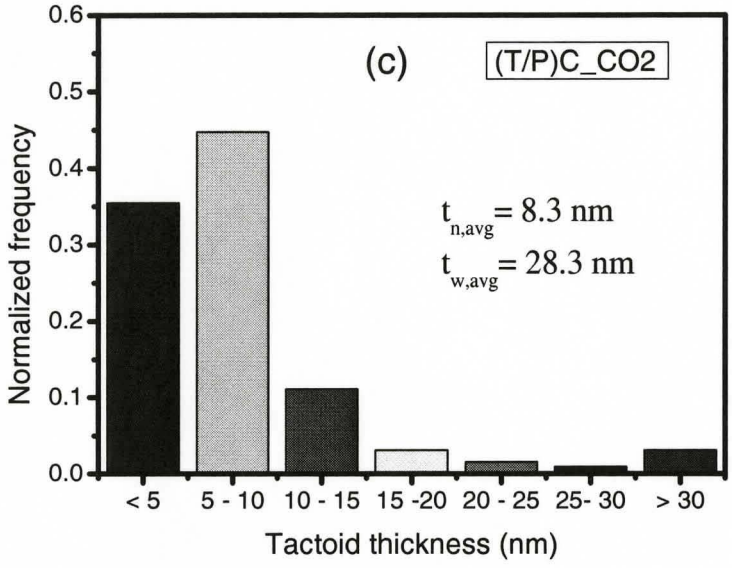

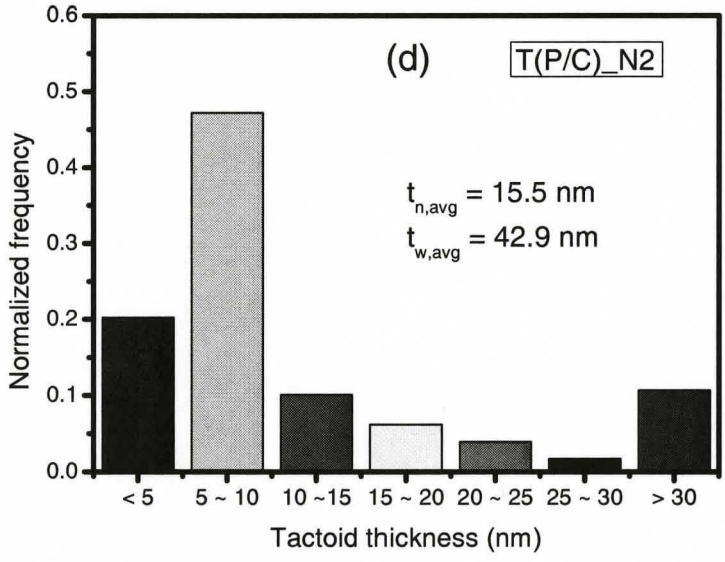

Figure 5.5 Histograms of normalized frequency of tactoid thickness by image analysis of TEM micrographs for the three $scCO_2$ cases. (a) T/P/C, (b) T(P/C), (c) (T/P)C; and one N_2 case: (d) T(P/C)

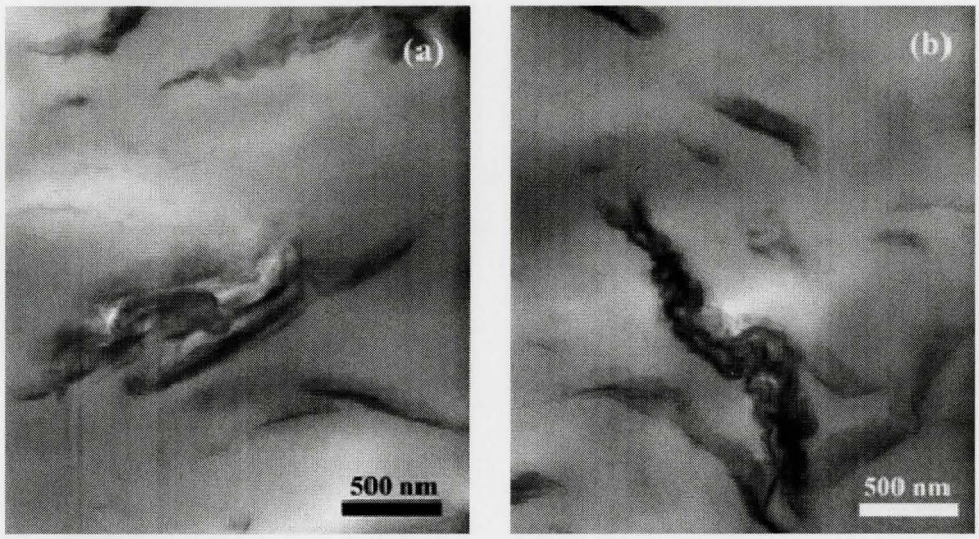

Figure 5.6 Micrographs for TPO nanocomposites made from s-C20A with formula of T(P/s-C) (a) and (T/P)s-C (b). Heating/annealing environment for both samples was $scCO_2$

XRD analytical results in Figure 5.3 indicated a high level of exfoliation for s-C20A in its nanocomposites, i.e. most of the clay in the nanocomposite samples lost its ordered structure. Considering the rheological data indicated that T/P/s-C and T(P/s-C) demonstrated no apparent differences, the TEM analysis focused only on T(P/s-C)_CO_2 and (T/P)s-C_CO_2 for the pre-treated clay samples. TEM images for these two nanocomposite samples are shown in Figure 5.6. It can be seen from the figure that the silicate layers were loosely packed, however, most of them agglomerated together. Tactoid size histograms were not included for these pre-treated clay nanocomposite samples as the results were not comparable to the C20A materials, distinguishing tactoids in the aggregrates shown in Figure 5.6 could not be quantitatively determined. Compared

with Figures 5.4(d and f) for C20A-based samples, the clay particles in the two s-C20A images were much larger than their C20A counterparts, indicating worse dispersion of s-C20A in its composite samples. In regards to comparison between the two s-C20A images, there were no significant difference in particle size distribution between T(P/s-C) (Figure 5.6a) and (T/P)s-C (Figure 5.6b), indicating that the mixing orders had little effect on dispersion of s-C20A in the TPO nanocomposite.

5.3.3. Rheological analysis

The rheological properties of the three pairs of C20A based TPO nanocomposites were expected to reflect their microstructures revealed by the TEM and XRD analyses. The storage moduli of these composite melts are shown in Figure 5.7. The data corresponding to low frequencies was the focus of attention for this analysis as this region is sensitive to interference in large-scale segmental motion of the polymer chains by short-range filler-filler interactions. The three $scCO_2$ prepared samples exhibited higher storage moduli in this low frequency region than their N_2 counterparts. Consistent with the reflected increase in smaller clay particles by TEM and XRD, the $scCO_2$ prepared sample T(P/C) demonstrated the highest storage modulus (G') among all tested conditions. In relative comparison, the improvement in G' related to use of $scCO_2$ was 39%, 122% and 40% for T/P/C, T(P/C) and (T/P)C, respectively at a frequency of 0.5 rad/s. Assuming G' in our case correlated to the increase in surface area afforded by exfoliation of our organoclay then $scCO_2$ is seen as an effective exfoliating aid in preparation of a PLS nanocomposite. The storage modulus of $scCO_2$-prepared samples T/P/C and (T/P)C

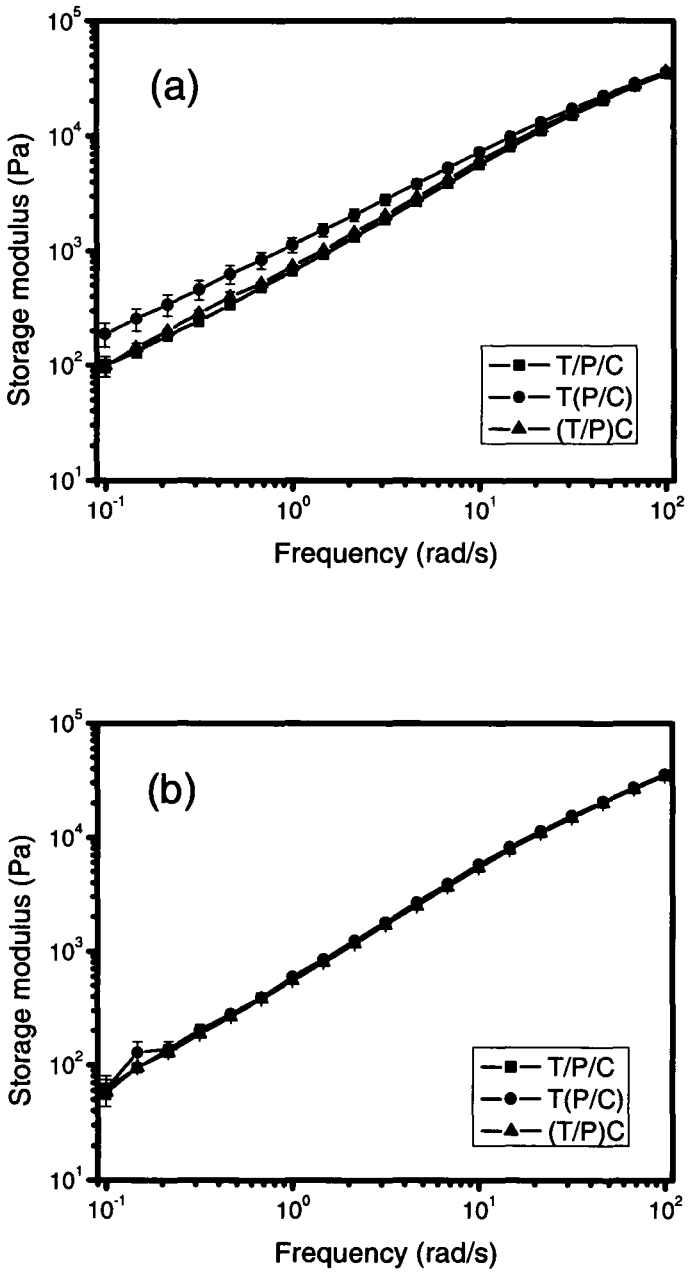

Figure 5.7 Comparisons in storage moduli of the TPO nanocomposites prepared from C20A using the home-made EF mixer under environment of (a) $scCO_2$ and (b) N_2

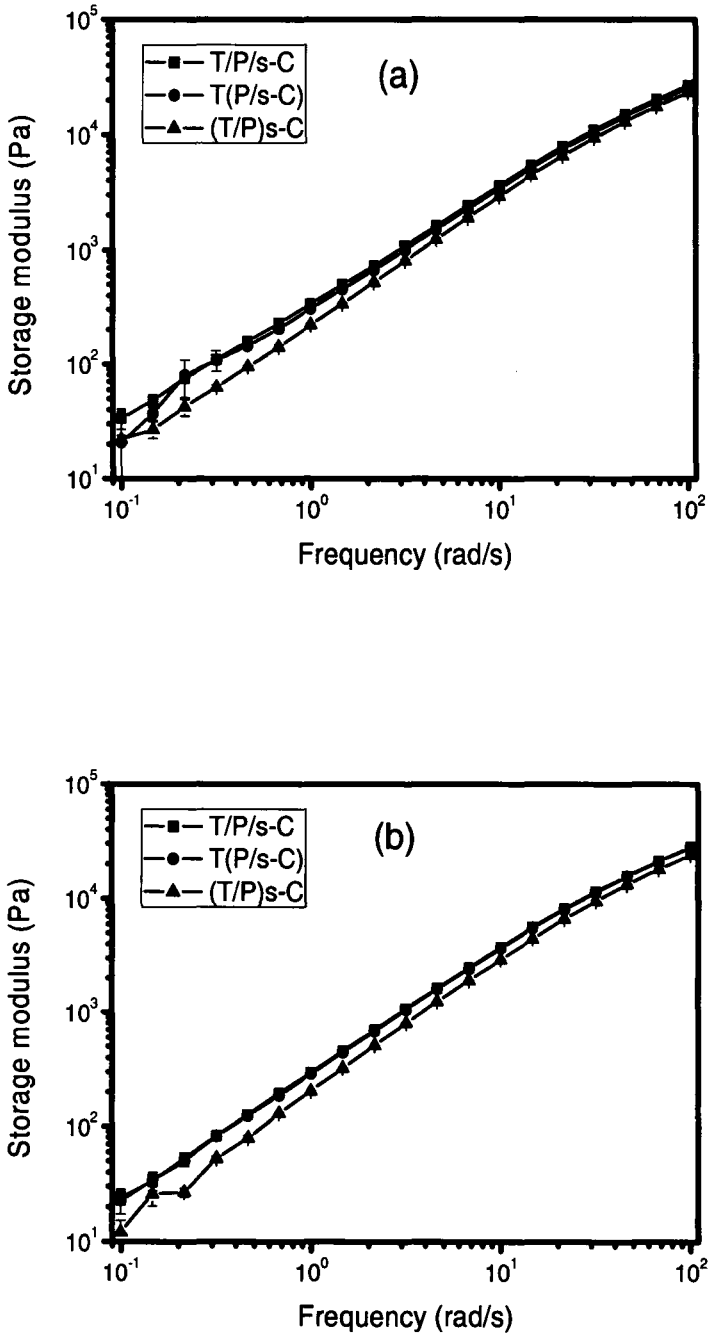

Figure 5.8 Comparisons in storage moduli of the TPO nanocomposites prepared from s-C20A using the home-made EF mixer under environment of (a) $scCO_2$ and (b) N_2

showed no apparent difference in value within the range of error. Figure 5.7b shows that there was no difference in storage modulus among the three N_2-based composites, correlating well with the TEM analysis.

Results of the rheological analysis for our six nanocomposites prepared with s-C20A are presented in Figure 5.8. Consistent with results obtained with the research group in other studies using different mixing equipment such as twin screw extrusion and batch mixing, it was found from our EF mixer that the G' of samples using this pre-conditioned organoclay was consistently lower than those noted for C20A. In comparison to the nitrogen case for samples based on C20A which is considered representative of conventional mixing conditions for PLS nanocomposites, it was seen that the modulus, e.g. at shear rate of 0.5 s^{-1}, was ~ 60% lower when using s-C20A in the composite structure. Gas type had no observable influence on the storage modulus on these materials based on s-C20A but it was an interesting point that the combination order also did not exhibit effect on clay dispersion. Comparable G' between the two combination orders was observed with either gas pointing to the fact that increased intimate contact between the compatibilizer and the $scCO_2$-pretreated organoclay did not improve dispersion of the pretreated clay in the TPO nanocomposite.

5.4 GENERAL DISCUSSION

The results of this work imply an effect by the different gases, which this section will explore, though the actual gas present during mixing was always nitrogen. The statement of gas effect is therefore specific to the intercalation stage as the components

were melted and annealed. However, it should be noted that $scCO_2$ was not evacuated from the mixer before mixing and therefore, at least the first extensional event was carried out under the influence of this gas when it was present.

The exfoliation-aiding effect of $scCO_2$ on the morphology of C20A-based TPO nanocomposites, especially for the beneficial mixing order of T(P/C), can be readily explained. First of all, plasticization of the compatibilizer by $scCO_2$ would be expected to increase the mobility of its chains, thereby increasing their effectiveness towards intercalation within the organoclay during the heating period. The pre-intercalated layers of the clay would more readily delaminate in the subsequent stress field [19-20], aiding losing their ordered arrangement. When the molten TPO chains were present with the other two components during annealing, as in the T/P/C case, the CO_2 was largely diluted due to the very high weight fraction of that polyolefin matrix (90 wt%) in the composition. In that case, plasticizer-aided PB3200/C20A intercalation would have been greatly reduced in comparison to the case of T(P/C). As for the case of (T/P)C, since there was no possibility for access between the compatibilizer and clay during the annealing stage, no intercalation occurred before mixing. Conversely, the clay was being pretreated with $scCO_2$ for this combination order in much the same manner as s-C20A was prepared except in this case without the rapid depressurization and cooling step. The similarity in storage modulus between the two mixing orders of T/P/C and (T/P)C shown in Figure 5.7a is an interesting finding as it implies the contact between clay and compatibilizer without high gas concentration was no more effective for intercalation than when the compatibilizer and clay were never in contact during annealing.

The $scCO_2$ pre-treatment of the tested organoclay has been established in earlier work to cause surfactant rearrangement, leading to basal expansion and increased organic coverage over the silicate surface [16, 17]. The rapid depressurization rate used by the pre-treatment method has also been reported by other researchers to cause clay exfoliation [4-6, 21]. Therefore, the swollen or pre-exfoliated clay particles would be expected to more readily delaminate in a shear- or extensional-flow field due to the diminished or negligible van der Waals forces between individual platelets (or small tactoid sections). The XRD results in the present work would tend to confirm that assessment. However, the importance of surfactant coverage is a new concept in the nanocomposite field and points to why only some organoclays are successful in commercialization of nanocomposites despite seemingly favourable oleophilic surfactants being used. Increased organic coverage over a silicate surface, in this case arising from surfactant rearrangement by $scCO_2$, would reduce exposure of the oxygen plane to a molecule of compatibilizer and consequently reduce the possibility of interaction [8]. This would seem the most plausible explanation for the aggregated structure for the clay in the TPO matrix seen by TEM and the relatively poor storage modulus found for materials based on s-C20A. For the two mixing orders of T/P/s-C and T(P/s-C), the annealing stage afforded time where heat and proximity of the compatibilizer to the clay provided increased opportunities for bonding to occur. However, from the lower storage modulus found for (T/P)s-C compared to the other two mixing orders it would seem the desired clay-compatibilizer associations now take considerable time to overcome the barrier formed by the surfactant.

5.5 CONCLUSIONS

Supercritical CO_2 has been found to be a significant aid to the level of exfoliation produced during mixing of Cloisite 20A into a TPO matrix. But its influence appears sensitive to which interactions may form while present during preparation of a nanocomposite. Concentrating CO_2 at the compatibilizer/clay interface appeared more effective in this regards than when these polymer components were annealed separately from the clay before mixing or when all components of the nanocomposite formulation were heated together. However, the combination order of the three components and whether supercritical gas was used had less effect on properties of a TPO nanocomposite as when the clay was pre-treated using supercritical CO_2 using a PGSS method. Though the pre-treatment led to an increased level of exfoliation for the organoclay, the G' of those nanocomposites was significantly lower than conventional (pristine) organoclay based materials.

REFERENCES

1. Y. Zhao, H.-X. Huang. *Polymer Testing* 2008, 27, 129-134
2. M.A. Treece, J.P. Oberhauser, *J Appl. Polym. Sci.* 2007, 103, 884-892
3. J. Ma, E. Bilotti, T. Peijs, J. A. Darr. *European Polym. J.* 2007, 43, 4931-4939
4. S. Horsch, G. Serhatkulu, E. Gulari, R.M. Kannan, *Polymer* 2006, 47, 7485-7496
5. C. W. Manke, E. Gulari, D. F. Mielewski, E.C. Lee. *US Patent* 6,469,073 (2002)
6. Q. T. Nguyen, D. G. Baird. *Polymer* 2007, 48, 6923-6933

7. R. A. Ottaviani, W. R. Rodgers, P. D. Fasulo, D. A. Okonski. *US Patent* US 7,462,666 B2, Dec. 9, 2008
8. J. Liu, M.R. Thompson, P. D. Fasulo, W. R. Rodgers. Evaluating Compatibilizer Interactions with Different Alkyl Ammonium Modified Organoclays prepared under Supercritical CO_2, to be submitted.
9. M.R. Thompson, Z. Zhuang, J. Liu, P. D. Fasulo, W. R. Rodgers. Supercritical CO_2 as an Exfoliating Aid for Nanocomposite Preparation: Comparison of Different Processing Methodologies, Polymer Engineering and Science, to be submitted
10. B. Finnigan, D. Martin, P. Halley, R. Truss, K. Campell, *Polymer* 45 (2004), 2249
11. R.K. Bharadwaj, et al. Polymer 43 (2002), 3699
12. J.S. Shelley, P.T. Mather, K.L. De Vries, *Polymer* 42 (2001), 5849
13. M. Tokihisa, K. Yakemoto, T. Sakai, L.A. Utracki, M. Sepehr, J. Li, Y. Simard. *Polym. Eng. Sci.* 46(8) 2006, 1040
14. M. Sentmanat, C. Stamboulides, S.G. Hatzikiriakos. *Polym. Eng. Sci.* 49(11) 2009, 2092
15. Yang, B.; Sato, M.; Kuriyama, T.; Inoue, T. *J. Appl. Polym. Sci.* 99(1) 2006, 1
16. M.R. Thompson, J. Liu, H. Krump, L.K. Kostanski, P.D. Fasulo, W.R. Rodgers, J. *Colloid Interf. Sci.* 2008, 324, 177-184
17. M.R. Thompson, M.P. Balogh, R.L. Speer, Jr., P.D. Fasulo, W.R. Rodgers, *J. Chem. Phys* 2009, 130 (044705), 1-8

18. J. Liu, M.R. Thompson, M.P. Balogh, R.L. Speer Jr., P.D. Fasulo, W. R. Rodgers, Influence of Supercritical CO_2 on the Interactions between Maleated Polypropylene and Alkyl-Ammonium Organoclay, *J. Appli. Polym. Sci.*, 2010, in press
19. N. Hasegawa, H. Okamoto, M. Kawasumi, M. Kato, A. Tsukigase, A. Usuki. *Macromol. Mater. Eng.* 280/281 (2000), 76
20. D.R. Paul, L.M. Robeson, *Polymer* 49 (2008), 3187
21. J. Liu, *Thesis for Masters Degree*, McMaster University, Aug. 2008

Chapter 6

Use of water or ethanol as a cosolvent to the supercritical CO_2 aided processing of TPO nanocomposites

J. Liu, M.R. Thompson, P. D. Fasulo, and W. R. Rodgers

This chapter is paper formatted to be consistent with the previous ones but has not been submitted to a technical journal. Jinling Liu is the major contributor to this chapter.

In this chapter, water and ethanol were examined to be used as cosolvent to $scCO_2$ to evaluate if the compatibilizer/organoclay intercalation and further exfoliation and dispersion of the TPO nanocomposite were improved.

ABSTRACT

Water or ethanol was tested as a possible cosolvent for supercritical CO_2 to aid exfoliation and dispersion of an organically modified montmorillonite in a thermoplastic polyolefin nanocomposite. Materials were prepared in two stages, where masterbatches of organoclay and compatibilizer were initially batch annealed in a cosolvent/supercritical CO_2 environment before being compounded into a thermoplastic elastomer (TPO) matrix by extrusion. The masterbatches and their TPO nanocomposites were analyzed using Fourier Transform Infrared Spectroscopy (FTIR), Nuclear Magnetic Resonance Spectroscopy (NMR), X-Ray Diffraction (XRD), Transmission Electron Microscopy (TEM), and a parallel plate rheometer. The cosolvents were both found to positively influence the effectiveness of supercritical CO_2 as an exfoliating aid of clay nanofillers with a TPO matrix. The results also indicated that ethanol or water could be effectively used as an exfoliating aid without $scCO_2$, especially ethanol which produced a higher extent of exfoliation than $scCO_2$.

6.1 INTRODUCTION

Studies on supercritical CO_2 ($scCO_2$) being used as an exfoliating aid agent in the processing of a polymer layered silicate (PLS) nanocomposite, have been reported in recent years [1-7]. Technologies used include *direct gas injection* [1-3], *pre-exfoliation* of the nanofiller using supercritical fluid [4-6] and addition of *organoclay/$scCO_2$ suspension* [7]. All claim that exfoliation and dispersion of the silicate nanofiller in the polymer

matrix is improved due to application of $scCO_2$. The mechanism for this exfoliating aid has been largely linked to the plasticizing capacity of $scCO_2$ to both surfactant of the organoclay and polymer compatibilizer during melt intercalation [1-3, 7]. Despite the improvement produced by this unique fluid, the persistent evidence of tactoids remaining in the final composite mandate exploring further approaches to maximize exfoliation.

In the literature, water and many organic solvents (e.g. acetonitrile, chloroform, toluene, methanol, ethanol, etc.) have been widely used to prepare PLS nanocomposites from solution [8-13]. Unfortunately, the solution method faces problems which include aggregation of dispersed silicate layers upon solvent removal and environmental concerns related to use of organic solvents. These studies show the good affinity of such solvents with silicates based on their polarity. Water and ethanol are industrially acceptable solvents, i.e. neither are harmful to workers or the environment, and each has considerable solubility in $scCO_2$ [14-16]. Excellent associations of water or ethanol with $scCO_2$ through dipole-dipole, dipole-induced dipole, induced dipole-induced dipole, and hydrogen bond interactions increase polarity of the solvent. Therefore, adding small amount of the cosolvents to $scCO_2$ can significantly increase the solvent power. The solvent/cosolvent system is usually used to extract non-volatile organic compounds. Their selection in the present study as cosolvents to the supercritical fluid is hoped to further aid compatibilizer/organoclay intercalation.

Different functionalities on water and ethanol allow them to possess different associating ability with $scCO_2$ and therefore polarity of the environment for the compatibilizer/organoclay annealing can be tuned. It was expected in this study that the

polarity-tuned annealing environment could help us to better understand the compatibilizer/organoclay intercalation mechanism. Selection of the two cosolvents was also to evaluate if exfoliation and dispersion of the TPO nanocomposite could be improved by the $scCO_2$-aided annealing-mixing (masterbatch) method [17-19].

6.2 EXPERIMENTAL

6.2.1 Materials

A medium-to-high flow TPO (13 MFR) supplied by LyondellBasell was selected for this study. Pellets of the TPO material was used directly without any further treatment. Cloisite 20A (C20A), the organically modified montmorillonite, was supplied by Southern Clay Products which was found most sensitive to supercritical CO_2 among the three organoclays examined in our previous studies [20-23]. A commercial maleated polypropylene (MA-PP) compatibilizer, Polybond® 3200 (PB3200) from Chemtura Corporation was selected. This compatibilizer has sufficient molecular weight to minimize any losses in mechanical properties by its addition to the nanocomposite and demonstrated plasticization in the presence of supercritical CO_2 sufficient to aid intercalation [20]. Pellets of the MA-PP were ground cryogenically into powder by a local company, Ingenia Polymers, for improved blending with the clay. Other properties of the organoclay and MA-PP have been reported in previous studies [20-23].

Deionized water and anhydrous ethyl alcohol supplied by Commercial Alcohols Inc. were used as cosolvents to supercritical CO_2. The carbon dioxide and nitrogen used

in the experiments were supplied by Air Liquide Canada Inc. at 99.5% and 99.995% purity, respectively.

6.2.2 Apparatus

The extensional flow mixing device suspended in a convection oven shown in Figure 6.1 was recently disclosed in a previous study (Chapter 5) [17] but now with a minor modification made for the cosolvents, i.e. the end of one chamber had a port added for liquid injection. A port cap allowed for injection of water or ethanol liquid and rapid re-sealing of the unit to prevent vapour loss. Details on the working principle of the extensional flow mixer remain the same as describe in that earlier work (Chapter 5).

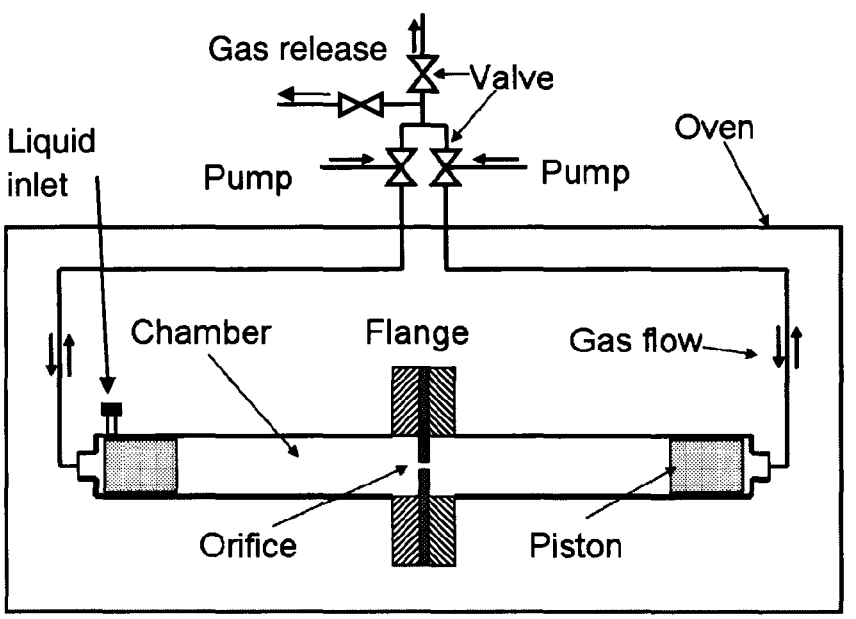

Figure 6.1 Schematics for the extensional flow mixer

6.2.3 Preparation of TPO nanocomposites

Studies in Chapter 5 on the order of combination for the three components making up a TPO nanocomposite formulation have shown that $scCO_2$ was most effective towards the final goal of increased clay exfoliation when localized to the molten compatibilizer/organoclay interface [17]. The current set of experiments investigating cosolvents followed this approach, which meant charging the mixer with PB3200 and C20A in one chamber, and TPO in the other one. Water or ethanol was injected into the device by a high precision syringe after the air in the mixing system had been purged with CO_2 or N_2. The mixer was heated to 200°C slowly over a span of 30 min and then maintained at this temperature for 20 min to fully equilibrate the system. In total the heating time for this annealing stage was 50 min. During the heating, pressure in the mixer was kept at 9.6 MPa for CO_2 and 3.5 MPa for N_2. Mixing was conducted in the same manner and for the same number of piston repetitions as described in Chapter 5.

Table 6.1 lists the prepared composite samples based on the variables under consideration in this study. The two concentrations tested for each cosolvent were below their solubility limit in $scCO_2$ [14]. N_2 gas was used as reference to $scCO_2$. The composition of each nanocomposite sample was 90:5:5 (w/w%) for TPO, PB3200 and C20A, respectively. The masterbatch samples were comprised of 50:50 (w/w%) for PB3200 and C20A, not including the TPO so the chemical associations between the two species under influence of the cosolvent could be clearly distinguished by infrared analysis.

Table 6.1 List of experimental trials for cosolvents

Sample name*	Temperature (°C)	Heat/mixing time (min)	Heating pressure (MPa)	Solvent type	Cosolvent type	Cosolvent content (w/w% $scCO_2$)
NCS1	200	20/30	3.5	N_2	—	—
NCS2	200	20/30	9.6	CO_2	—	—
NCS1W1	200	20/30	3.5	N_2	Water	10
NCS1W2	200	20/30	3.5	N_2	Water	30
NCS2W1	200	20/30	9.6	CO_2	Water	10
NCS2W2	200	20/30	9.6	CO_2	Water	30
NCS1E1	200	20/30	3.5	N_2	Ethanol	10
NCS1E2	200	20/30	3.5	N_2	Ethanol	30
NCS2E1	200	20/30	9.6	CO_2	Ethanol	10
NCS2E2	200	20/30	9.6	CO_2	Ethanol	30
MBS2	200	20/30	9.6	CO_2	—	—
MBS1W2	200	20/30	3.5	N_2	Water	30
MBS2W2	200	20/30	9.6	CO_2	Water	30
MBS1E2	200	20/30	3.5	N_2	Ethanol	30
MBS2E2	200	20/30	9.6	CO_2	Ethanol	30

* Sample name initiating with NC was referred to a TPO nanocomposite prepared while a sample labelling MB meant a PB3200/C20A masterbatch (without TPO).

6.2.4 Characterization

The masterbatch samples were analyzed using techniques of transmission mid-range infrared analysis (FTIR) and X-ray diffraction (XRD). For infrared measurements, the masterbatch samples were made into films with thickness of ~ 0.12 mm using a hot press at 200°C under 0.13 MN compressive force for 2 minutes. Spectra of the film samples were based on 64 scans collected using a Nicolet 6700 infrared spectrophotometer at 2 cm^{-1} resolution over a range of 400-4000 cm^{-1}. The same film samples were also analyzed by XRD using a Bruker D8 diffractometer with Cu K_α radiation (λ = 1.5407 Å) at an accelerating voltage of 40kV and a current of 20mA. The film was oriented vertical with the beam path through the thickness of the disk.

Test specimens were prepared from the TPO nanocomposites samples by hot pressing at 200°C under 0.13 MN compressive force for 4 minutes to make disks of 25 mm diameter and 1.5 mm thickness. These test specimens were characterized by XRD, transmission electron microscopy (TEM) and rheological analysis. XRD was conducted in the same manner as described for the film masterbatch specimens above. For TEM, a 70 nm thick microtomed section was cut from a disk by diamond knife and mounted on a carbon grid. The microtomed section was observed using a JEOL 1200 EX TEMSCAN microscope operating at an accelerating voltage of 80kV and magnifications of 60,000x. Viscoelastic properties of the nanocomposite samples were evaluated using an ARES parallel plate rheometer (TA Instruments). A constant strain of 5% was determined suitable from strain sweep testing for measurements within the linear viscoelastic region.

For each sample, four disk specimens were tested to get average value and error for the measurement. All testing was conducted at 200°C over a frequency range of 0.1–100 rad/s.

6.3 RESULTS AND DISCUSSION

6.3.1 PB3200/C20A masterbatches

FTIR analysis

In our previous study [21], infrared analysis was used to determine the manner which the maleic anhydride moiety of the compatibilizer differed in its coordination with the surfactant and clay surface for different organoclay species, and with supercritical CO_2. It was found in that work that the notable interactions occurring were esterification occurred between the grafted anhydride groups and the oxygen plane of silicate layers and carboxylation between the succinic groups and residual metallic cations of an organoclay and that the two chemical reactions were affected by $scCO_2$. In terms of C20A, presence of $scCO_2$ reduced generation of the ester but increased the carboxylate. That analysis also did not show evidence of new or shifted vibrational bands from use of $scCO_2$ which further fostered the authors' belief that the fluid was acting solely as a plasticizer for the organic components in the nanocomposite formulation, i.e. surfactant and polymer chains. Now in this study the analysis method was used to observed changes in those coordinations when either cosolvent was present.

FTIR spectra of the four PB3200/C20A masterbatches prepared using the two cosolvents (30% w/w) and two gases for the frequency range of 1500 – 2000 cm^{-1} are

shown in Figure 6.2, where absorbance for each spectrum was normalized using the 841 cm^{-1} vibration related to CH_3/CH_2 bending/stretching to eliminate effect of film thickness on the absorbance. Similar to our previous study discussed above, there was again no evidence of new peaks or shifted peaks due to the use of $scCO_2$ (Figure 6.2a, in which spectra for ethanol were staggered above the water's), suggesting the gas itself was not experiencing persistent chemical associations with the clay/compatibilizer. Between the two cosolvents a new chemical association at ~1725 cm^{-1} was observed for ethanol cosolvent and there were evident differences seen in the spectra based on absorption intensity, as shown in Figure 6.2b, where the spectra were not staggered and the species without a cosolvent was included for a reference. Table 6.2 lists the relative intensity of vibrational bands in the spectra (normalized but not staggered) based on gas type and cosolvent used. With water as a cosolvent, there was no apparent difference in carboxylate absorbance at ~1580 cm^{-1} between the two gases, but ester absorbance at ~1740 cm^{-1} for the CO_2-based masterbatch (MBS2W2) was higher than that its N_2-counterpart (MBS1W2), indicating that $scCO_2$ enhanced the silicate esterification when water was present. For the ethanol cosolvent, the strongest absorption appeared at 1725 cm^{-1} which was designed as ester covalent bonding occurring between ethanol and the grafted anhydride group. At this absorption band and the silicate ester band at ~ 1740 cm^{-1}, intensities for the CO_2-based sample (MBS2E2) were lower than those of the N_2-based masterbatch (MBS1E2). However, the carboxylate absorbance at 1580 cm^{-1} for MBS2E2 was higher than that of MBS1E2. The ethanol results indicated that presence of $scCO_2$ favoured the carboxylation but not the esterification.

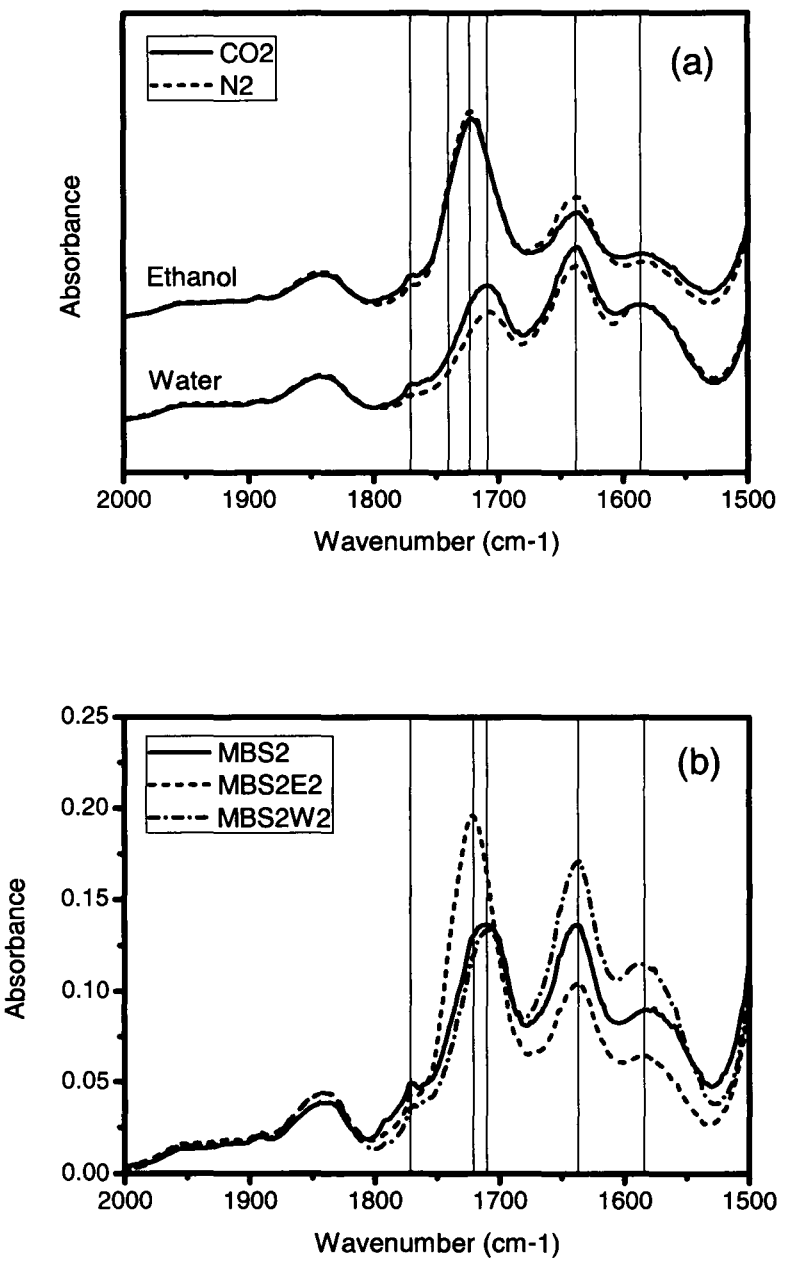

Figure 6.2 FTIR spectra of the PB3200/C20A masterbatches prepared at environment of $scCO_2$ and water or ethanol as cosolvent in comparisons of $scCO_2$ vs. N_2 for each cosolvent (a) and ethanol vs. water for $scCO_2$ (b)

Table 6.2 Relative intensity of vibrational bands in the spectra

Vibrational band (cm^{-1})	Water		Ethanol		—
	$scCO_2$	N_2	$scCO_2$	N_2	$scCO_2$
1580	0.11453	0.11449	0.06443	0.05632	0.08986
1640	0.17051	0.15242	0.10434	0.11943	0.1361
1725	—	—	0.19575	0.20346	0.12798
1740	0.0652	0.04843	0.12637	0.13192	0.07982
1770	0.03618	0.0255	0.04312	0.03278	0.04917

Compared to the no-cosolvent reference (MBS2), addition of water to the $scCO_2$-based mixing system did not improve the ester absorbance at 1740 cm^{-1}; however, the carboxylate interaction at 1580 cm^{1} was enhanced significantly. When ethanol was added to the $scCO_2$ mixing environment, the masterbatch absorbance at 1740 cm^{-1} increased but intensity at 1580 cm^{-1} decreased. The decrease in carboxylate for MBS2E2 relative to the other two, MBS2 and MBS2W2, can be attributed to a less number of acidic groups left for carboxylation after ethanol esterification. The small molecular size of ethanol and relatively high concentration allowed it to readily react with the residual acid group of the opened anhydride after silicate esterification. Essentially, the presence of water drove the reaction of the anhydride with the silicate surface towards carboxylate formation while ethanol promoted the silicate esterification. Additional ester covalent bonding generated in the case of ethanol.

XRD analysis

Diffraction patterns of the organoclay within the masterbatches detected by XRD are shown in Figure 6.3. It can be seen from the figure that only MBS1W2 showed a distinct diffraction peak corresponding to (001) reflection. The peak centered at $2\theta = 3.0°$ is identical to the previously reported XRD pattern of an annealed PB3200/C20A mixture prepared under $scCO_2$ alone at similar conditions [20]. However, diffraction intensity of the former (MBS1W2) was higher than the latter (MBS2), as shown in Figure 6.3, revealing that water alone can aid PB3200 intercalation but not as effective as $scCO_2$. When water was used as cosolvent to $scCO_2$, diffraction pattern of the prepared masterbatch (MBS2W2) at this reflection plane became broader and its intensity was significantly lower than MBS2 and MBS1W2, indicating that the intercalation was promoted by addition of the cosolvent.

When ethanol was used alone (MBS1E2), the diffraction intensity became smaller than the above three cases, i.e. $scCO_2$ without cosolvent (MBS2), water alone (MBS1W2) and water used cosolvent to $scCO_2$ (MBS2W2), indicating that the aiding effect of ethanol on the intercalation was over than $scCO_2$, water, and $scCO_2$ with water as cosolvent. Diffraction intensity for MBS2E2 was the smallest among the five masterbatches, indicating that the best mastermatch intercalation achieved when ethanol was used as cosolvent to $scCO_2$.

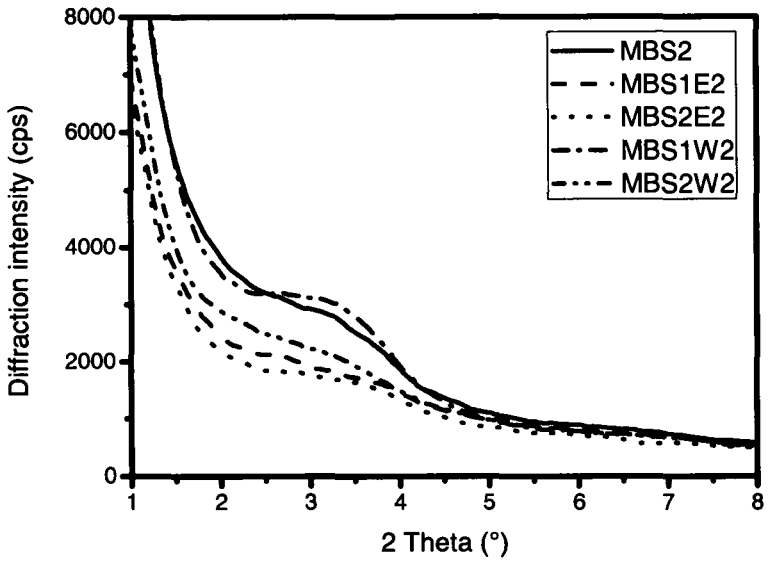

Figure 6.3 XRD patterns of masterbatches made from PB3200 and C20A at weight radio of 1:1

6.3.2 TPO nanocomposites

Whereas the chemical interactions and the physical intercalation between compatibilizer and clay related to $scCO_2$ and the cosolvents characterized by FTIR and XRD were more clearly observed in absence of TPO, the following analysis concerning features of exfoliation required the matrix polymer and the mixing under shear.

XRD analysis

Crystalline structures in the TPO nanocomposites related to the organoclay were detected by powder XRD. Figure 6.4 shows the diffraction patterns over a 2θ range of 1-8° for nanocomposites listed in Table 6.1. In all tested cases, a peak corresponding to

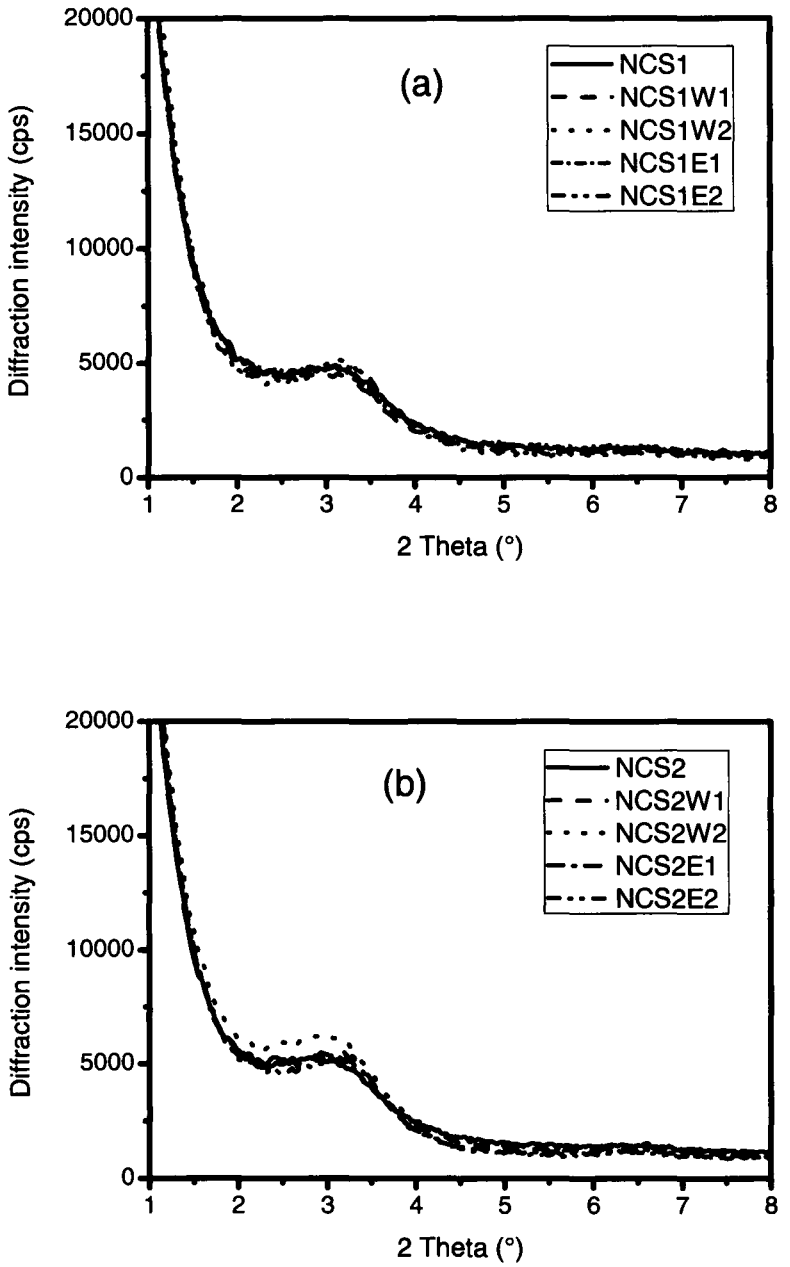

Figure 6.4 XRD patterns of TPO nanocomposites made from PB3200/C20A masterbatches prepared at environment of N_2 (a) or $scCO_2$ (b) with and without water or ethanol as cosolvent.

(001) reflection was noted in the diffraction pattern, indicating none of the examined samples experienced completed disorder of the organoclay. Without cosolvent, the (001) plane diffraction peak of C20A showed a shift to a lower 2θ angle value (i.e. from 3.1° to 2.7°) and became broader for the $scCO_2$ case (NCS2) in comparison with the N_2 counterpart, NCS1, consistent with earlier studies [17, 20-21]. The supercritical gas had a minor role in aiding changes to the organoclay once compounded into a TPO nanocomposite. Comparatively, the influence of water or ethanol cosolvents was not as apparent by the spectra of their samples included in Figure 6.4a and b. However, this analysis technique is rarely informative when seeking evidence of exfoliation or intercalation with organoclays due to presence of the matrix material [17-18, 21].

TEM results

Three pairs ($scCO_2$ vs. N_2) of the TPO composite samples were selected for the TEM analysis. These pairs corresponded to those without cosolvent, those with water at its highest tested concentration (i.e. 30% relative to $scCO_2$) and those with ethanol at its highest tested concentration (i.e. 30% relative to $scCO_2$). Micrographs of these samples are shown in Figure 6.5. It can be seen from the images that the particles including tactoids and individual platelets were uniformly dispersed and from the fact that the samples had been re-melted first before microtoming there are some indications the mixed state was thermodynamically stable. Differences between these images are discernable. In regard to the first pair without cosolvent, a higher frequency of large tactoids were noted for NCS1 (Figure 6.5a) compared to NCS2 (Figure 6.5b). A similar

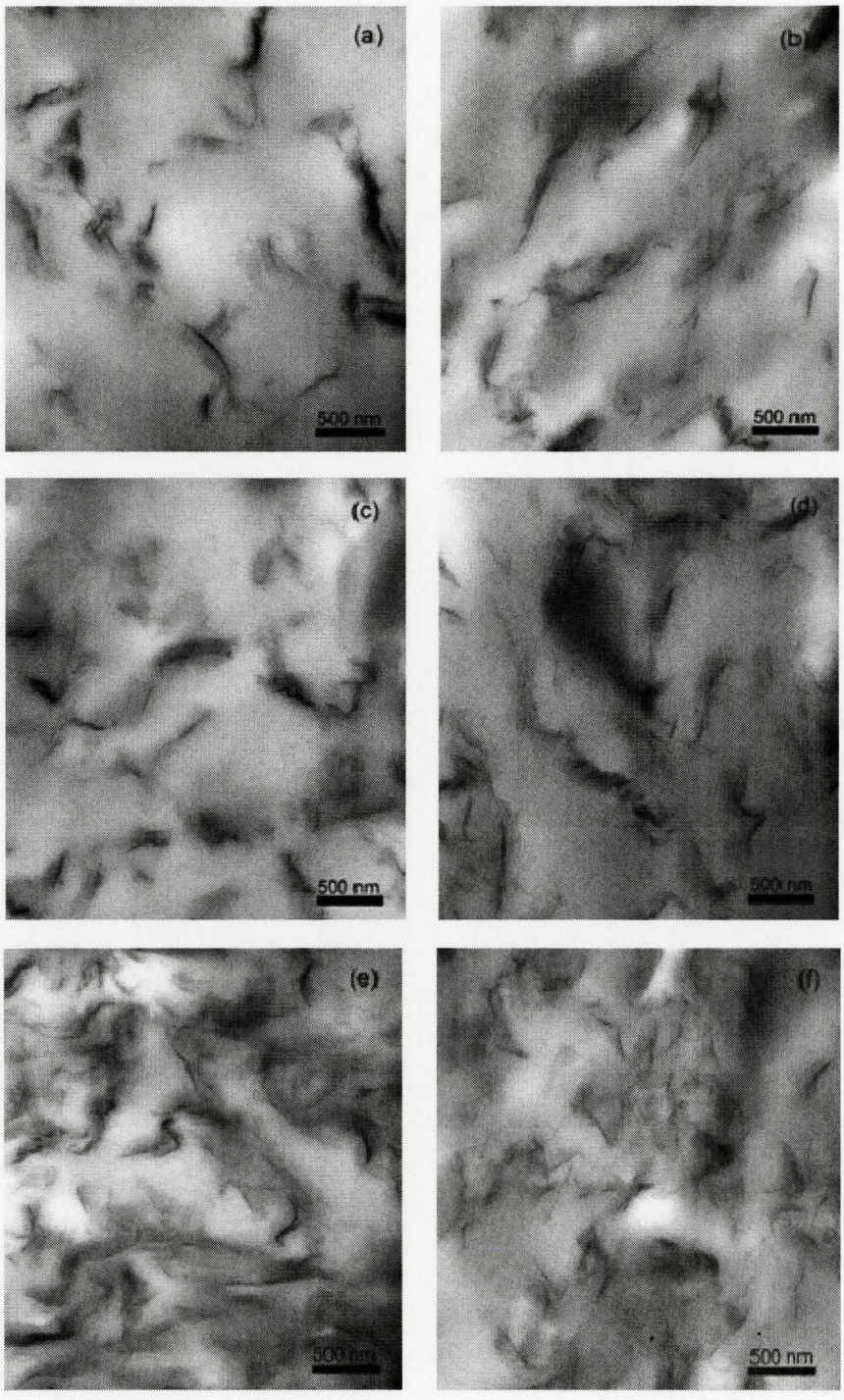

Figure 6.5 TEM images of TPO nanocomposites. (a) NCS1, (b) NCS2, (c) NCS1W2, (d) NCS2W2, (e) NCS1E2 and (f) NCS2E2

outcome based on gas type was found for the samples prepared with water cosolvent, Figures 6.5c and d. However, for samples prepared with ethanol cosolvent, Figures 6.5e and f, the opposite was noted with more uniform dispersion corresponding to the N_2-case. With use of a cosolvent, the samples showed a higher frequency of smaller particles in the TEM images, pointing to a higher extent of exfoliation. In order to quantify the extent of exfoliation in these composite samples, particles in each image were analyzed using an image analysis software (SigmaScan Pro 5, SYSTAT Software Inc.). The normalized size distribution of tactoid thickness within each nanocomposite is summarized in Figure 6.6, again distinguished based on the gas used during annealing. Number average particle thickness, $t_{n,avg}$, and weight average particle thickness, $t_{w,avg}$, were calculated in Table 6.3. Since a fixed magnification was used in these TEM observations, total particle number in each image (fixed unit area) reflects the extent of exfoliation if one assumes the bulk state and area under view are statistically correlated. The total particle number for each image was also included in Table 6.3.

In regards to the two annealing gases, neglecting the cosolvents for the moment, both number and weight average thickness values for the $scCO_2$-based composite were significantly smaller than those for the N_2-case, showing more highly delaminated tactoids, consistent with XRD data and our previous studies [12, 15]. For the water cosolvent, weight average thickness values for the two gas cases are identical, but the number average thickness for NCS2W2 was lower than NCS1W2. A larger number of particles with thickness less than 6 nm for NCS2W2 were the reason to its lower number

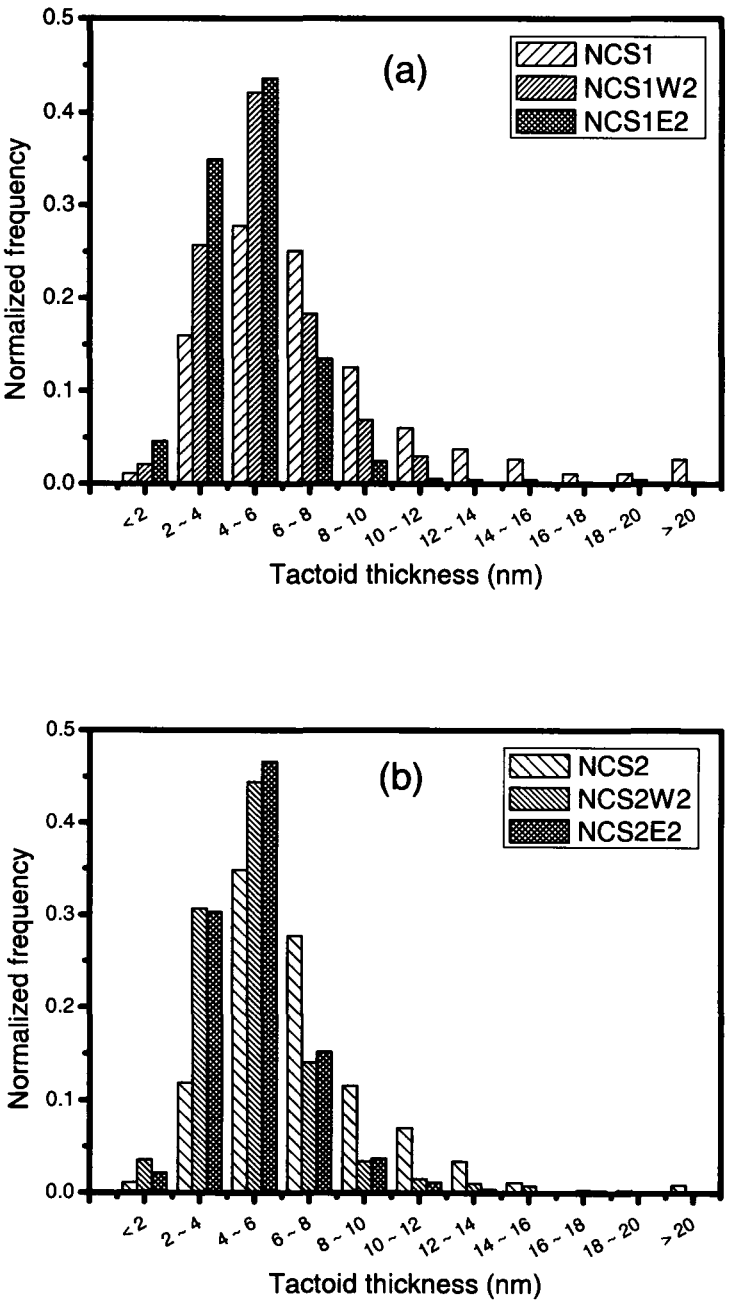

Figure 6.6 Histograms of normalized frequency of tactoid thickness present in TEM images in Figure B5 based on the gas used during annealing: (a) N_2 and (b) $scCO_2$

Table 6.3 Total number and average thickness of the particles in the TEM images *

Cosolvent	Tactoid number per unit area		Number average thickness, $t_{n, avg}$ (nm)		Weight average thickness, $t_{w, avg}$ (nm)	
	$scCO_2$	N_2	$scCO_2$	N_2	$scCO_2$	N_2
—	353	263	6.8	7.7	14.6	18.7
Water	675	432	5.0	5.5	14.4	14.5
Ethanol	789	1472	5.0	4.6	13.4	10.6

* Standard error in the values was 7.4%.

average thickness. Water was more effective when used as a cosolvent to $scCO_2$ than when it was added directly as a solvent but comparatively, in both gas cases water was a more effective exfoliating aid than $scCO_2$ (using the N_2, non-solvent cases as the baseline, representing conventional compounding practices). The ethanol cases were different from the above two. In Table 6.3, we can see that number average thickness values for the two gas cases are similar; however, the weight average number for NCS1E2 is much smaller than that of NCS2E2, showing that much fewer large particles existed in the N_2-based nanocomposite. Correspondingly, twice the numbers of particles were found with the nitrogen case for ethanol than for any other sample analyzed. The number indicated a higher extent of delamination and dispersion occurred for the nanofiller in TPO matrix for that condition.

Rheological analysis

Our previous studies have demonstrated that rheological properties of the TPO nanocomposite melt reflect morphology of the composite samples better than observations by XRD and even TEM [17-18, 21]. Efficiency of the measurement comes from the sensitivity of rheological properties to bulk nanoscale features of a nanocomposite. The interference of large-scale segmental motion for polymer chains by short-range filler-filler interactions can be readily observed especially at the lower oscillation frequencies. Therefore, it was expected that rheological properties of the TPO nanocomposites in this study could clarify the above observations by XRD and TEM. Figure 6.7 shows storage moduli of the ten composite melts over a frequency range of 0.1 – 100 rad/s, which was again classified by CO_2 and N_2 used for the annealing step. It can be seen from the figure that without the presence of $scCO_2$ (Figure 6.7a), addition of water or ethanol to the annealing process significantly increased the storage modulus of the TPO nanocomposite and that the higher amount of the solvent added the more increase in this property. At each concentration ethanol had better performance than water. These results showed that using water or ethanol as solvent during the annealing significantly encouraged formation of a percolating network by the silicate nanofiller within the polymer matrix, especially ethanol.

The storage modulus of the nanocomposite melt also increased significantly for the conditions when water or ethanol was used with $scCO_2$ (Figure 6.7b). However, extent of the improvement was not as large as when $scCO_2$ was absent and there was little difference between the two concentrations of these cosolvents. At low concentration, curves for the two cosolvent cases (with $scCO_2$) were overlapped whereas at the high

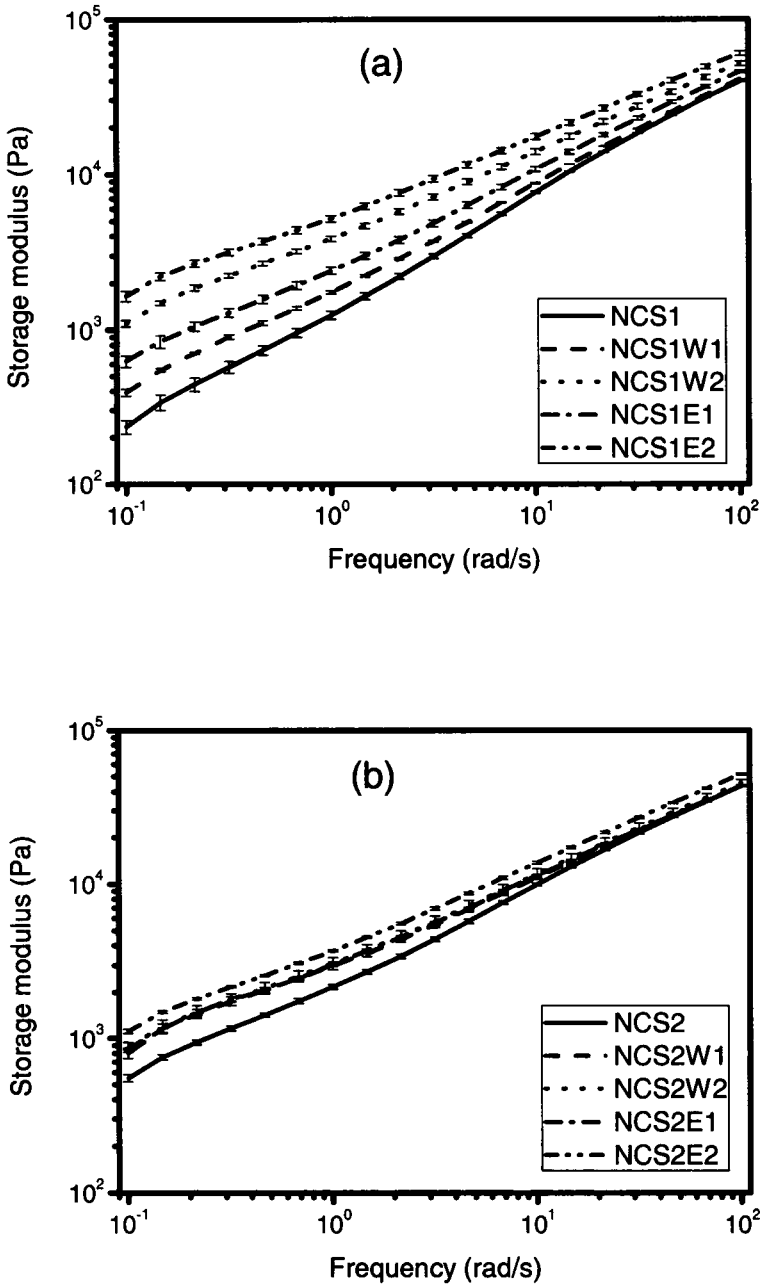

Figure 6.7 Storage moduli of TPO nanocomposites prepared using water or ethanol as solvent. (a) N_2 cases and (b) $scCO_2$ cases

concentration, the storage modulus for ethanol was higher than that of the water case. The highest storage modulus occurred to the sample when only ethanol was present in the annealing process, indicating that the best percolating network of silicate sheets was generated within TPO. In terms of the rheological property for the two non-cosolvent cases and four high-concentrated cosolvent samples, these rheological measurement results perfectly consisted with the TEM observations.

6.4 GENERAL DISCUSSION

Any circumstance which decreases the intercalation barriers and/or increases the driving forces to intercalation will positively affect the extent of the intercalation. Addition of water into the PB3200/C20A mixture during annealing increased not only chemical affinity of the two components through enhanced carboxylation but also the physical affinity through strengthened hydrogen bonding association between silicate surface and succinic groups. The presence of water led to a higher degree of succinic ring opening as well as hydrated the oxygen plane of silicate surface (Figure 6.2). Increasing the hydration radius of the residual metallic cations will reduce the van der Waals attractive forces between adjacent silicate sheets in the clay stacks [24]. The increased intercalation driving forces and reduced intercalation barrier could explain the apparently higher extent of intercalation noted by XRD (Figure 6.3) and NMR (Appendix 2) analyses for the compatibilizer chains. The smaller tactoids size dispersed in the final matrix and the larger storage modulus of the samples prepared by water can be attributed to the improved intercalation.

Ethanol showed similar influence on the clay as water because of its available hydroxyl groups. However, its capacity to terminate a free carboxylic acid from the opened anhydride group through esterification, seen by FTIR, was thought to be the reason for samples prepared with it having improved clay dispersion. The ethyl ester would mitigate any hydrogen bonding interactions with other platelets, reducing platelet-platelet coordination through the anhydride species of the compatibilizer so that the clay can swell more freely. Better swelled intercalated clay particles would explain the higher extent of delamination observed by TEM.

When water or ethanol is added to the bulk solvent, $scCO_2$, a dipole movement is introduced. The polar component of the environment reduces its solvation of alkyl chains of the surfactant and the MA-PP matrix (plasticization), but increases affinity between the MA groups and silicate surface, as well as interferes with the balanced associative forces between adjacent silicate planes. Reduction in the solvation and plasticization will negatively affect the MA-PP/C20A intercalation; however, the increased affinity will definitely improve the enthalpic interactions. On the other hand, presence of $scCO_2$ led to organic coverage on the silicate sheets increased [17, 22-23]. Thus, exposed silicate surface becomes limited, which reduced sites for its esterification and hydrogen bonding with succinic groups. Therefore, we saw that higher concentration of the cosolvent lost its effect (Figure 6.7b).

6.5 CONCLUSIONS

Ethanol and water were found to be effective additives to aid the preparation of a more highly exfoliated and well dispersed TPO nanocomposite. Ethanol showed improvements over water or $scCO_2$ alone, which was attributed to its ability to form ethyl esters during association of the maleated compatibilizer with the silicate sheets of our organoclay. Due to surfactant rearrangement occurring in the presence of $scCO_2$ which result in increased organic coverage over the silicate surface, the aiding effect of water or ethanol used as a cosolvent was offset partially. When used alone as solvents in the annealing, either water or ethanol achieved equivalent or even better results over $scCO_2$ or conventional practice in terms of exfoliation and dispersion of the TPO nanocomposite.

REFERENCES

1. Y. Zhao, H.-X. Huang. *Polymer Testing* 2008, 27, 129-134
2. M.A. Treece, J.P. Oberhauser, *J Appl. Polym. Sci.* 2007, 103, 884-892
3. J. Ma, E. Bilotti, T. Peijs, J. A. Darr. *European Polym. J.* 2007, 43, 4931-4939
4. S. Horsch, G. Serhatkulu, E. Gulari, R.M. Kannan, *Polymer* 2006, 47, 7485-7496
5. C. W. Manke, E. Gulari, D. F. Mielewski, E.C. Lee. US Patent 6,469,073 (2002)
6. Q. T. Nguyen, D. G. Baird. *Polymer* 2007, 48, 6923-6933
7. R. A. Ottaviani, W. R. Rodgers, P. D. Fasulo, D. A. Okonski. *US Patent* US 7,462,666 B2, Dec. 9, 2008
8. K.E. Strawhecker, E. Manias, *Chem. Mater.* 14 (2000), 2943

9. N. Hasegawa, H. Okamoto, M. Kato, A. Usuki, N. Sato, *Polymer* 44 (2003), 2933
10. P. Aranda, E. Ruiz-Hitzky. *Chem Mater* 4 (1992),1395–403
11. H.J. Choi, S.G. Kim, Y.H. Hyun, M.S. Jhon. *Macromol Rapid Commun* 22 (2001), 320-325
12. N. Ogata, G. Jimenez, H. Kawai, T. Ogihara. *J Polym Sci Part B: Polym Phys* 35 (1997), 389–396
13. M. Kawasumi, N. Hasegawa, A. Usuki, A. Okada. *Mater Sci Engng C* 6 (1998), 135–143
14. I. Dalmolin, E. Skovroinski, A. Biasi, M.L. Corazza, C. Dariva, J. Vladimir Oliveira. *Fluid Phase Equilibria* 245 (2006) 193–200
15. A. Bahadori, H.B. Vuthaluru, S. Mokhatab. *International Journal of Greenhouse Gas Control* 3 (2009) 474–480
16. T. Suzuki, N. Tsuge, K. Nagahama. *Fluid Phase Equilibria,* 67 (1991) 213-226
17. J. Liu, M. R. Thompson, W. R. Rodgers, P. D. Fasulo. Use of Supercritical CO2 as an Intercalation/Exfoliation Aid Agent in the Preparation of a Polymer Layered Silicate Nanocomposite, to be submitted.
18. M.R. Thompson, Z. Zhuang, J. Liu, P. D. Fasulo, W. R. Rodgers. Supercritical CO_2 as an Exfoliating Aid for Nanocomposite Preparation: Comparison of Different Processing Methodologies, to be submitted.
19. M.R. Thompson, W. R. Rodgers, P.D. Fasulo, J. Liu, Z. Zhuang, Method of Producing Nanocomposite Polymer Using Compatibilizer and Supercritical Fluid, *US Patent* 61/289614, filled, Dec. 23, 2009

20. J. Liu, M.R. Thompson, M.P. Balogh, R.L. Speer Jr., P.D. Fasulo, W. R. Rodgers. Influence of supercritical CO_2 on the interactions between maleated polypropylene and alkyl-ammonium organoclay. *J. Appl. Polym. Sci.* 2010, in press.

21. J. Liu, M.R. Thompson, P. D. Fasulo, W. R. Rodgers. Evaluating Compatibilizer Interactions with Different Alkyl Ammonium Modified Organoclays prepared under Supercritical CO_2, to be submitted

22. M.R. Thompson, J. Liu, H. Krump, L.K. Kostanski, P.D. Fasulo, W.R. Rodgers, J. *Colloid Interf. Sci.* 2008, 324, 177-184

23. M.R. Thompson, M.P. Balogh, R.L. Speer, Jr., P.D. Fasulo, W.R. Rodgers, *J. Chem. Phys* 2009, 130 (044705), 1-8

24. T. Suzuki, N. Tsuge, K. Nagahama. *Fluid Phare Equilibria,* 67 (1991), 213-226

Chapter 7

Mechanics of Supercritical CO_2 Aiding Dispersion of Organoclay in TPO Nanocomposites

In this chapter, the mechanism which $scCO_2$ aids the extent of exfoliation found in a TPO nanocomposite is proposed based on summarizing the results of this research. In order to build an understanding starting with the organoclay itself, some results from the previous Master`s study of the author were included.

7.1 INTRODUCTION

The focus of this work for the past few years has been to understand how dissolved CO_2 within a gas-laden molten nanocomposite interacts with the nanofiller in a manner that may lead to increased interlayer spacing of the clay platelets during the processing, and if that interaction can be exploited as a mechanism for creating a fully exfoliated structure. The first objective was to evaluate how the supercritical fluid interacted with the nanofiller, namely an organically modified montmorillonite. It was found that morphology of an organoclay can be altered when exposed to an environment of supercritical CO_2 ($scCO_2$). When $scCO_2$ was present the surfactant, an alkyl ammonium surfactant, was rearranged leading to the organic layers either swelling or collapse, dependent on its chemical structure and packing arrangement. The second task for the project was to evaluate complex interactions between the organoclay and a suitable compatibilizer such as maleic anhydride grafted polypropylene (MA-PP). It was found that $scCO_2$ was able to aid the polymer chains to diffuse into the interlayer space through plasticization. However, the aiding effect was dependent on grafted maleic anhydride (MA) content and molecular weight of MA-PP (which are correlated factors due to the manner which the polymer is maleated), as well as the basal spacing and organic loading of the original organoclay. The third step was to study the effect of supercritical fluid on dispersion of the clay particles in the TPO nanocomposite. Melt annealing the three components, matrix, compatibilizer and filler, before mixing under an environment of $scCO_2$ can improve exfoliation of the nanocomposite and concentrating

the supercritical gas at the compatibilizer/organoclay interface can generate a better aiding effect. The last work for the project was to examine if water or ethanol could be used as a cosolvent to $scCO_2$ to improve the aiding efficiency of the supercritical gas. Experiments showed that each cosolvent significantly improved exfoliation and dispersion of the TPO nanocomposite.

This chapter will be a summary for these researches and the focus will be on answering the central question for the project, 'how $scCO_2$ aids dispersion of organoclay particles in TPO nanocomposites?' Issues needing addressing included: How does the microstructure of an organoclay change?; How does an organoclay interact with selected compatibilizer?; and How is dispersion of the filler in the polymer matrix improved? Based on answers to these questions, an intercalation/exfoliation mechanism for TPO nanocomposite processing aided by $scCO_2$ will be put forward. In the end of the chapter, recommendations on strategy for industrial use of $scCO_2$ in the processing of TPO nanocomposites are given.

7.2 INTERACTIONS OF $scCO_2$ WITH INDIVIDUAL COMPONENTS

7.2.1 Organoclay

The discussion in this section pertains to the work of Jinling Liu during her Masters degree. It is included to help the reader understand the overall influence that $scCO_2$ has on the system.

Several morphologies of organically modified clays are shown in Figure 7.1. Organization of surfactants in the gallery areas of MMT can display lateral monolayer,

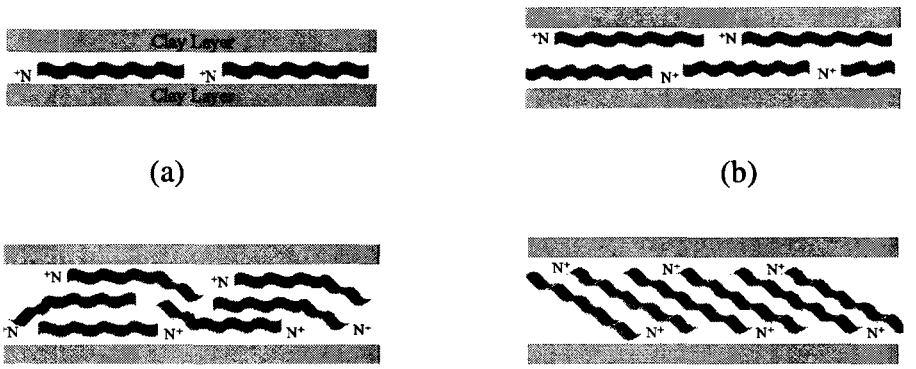

Figure 7.1 Alkyl chain conformations in layered silicates: (a) lateral monolayer, (b) lateral bilayer, (c) pseudo-trimolecular layer, (d) paraffin-type monolayer [1]

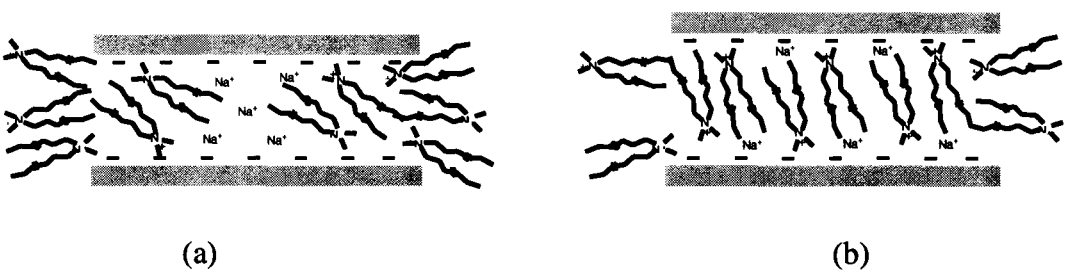

Figure 7.2 Schematic morphologies of pristine C20A (a) and after annealing in environment of $scCO_2$

lateral bilayer, pseudo-trimolecular layer or paraffin-type monolayer arrangements [1]. These are idealized spatial models based on observed basal spacing of modified MMT and calculations of the van der Waals radii of the surfactant structures. Actual prepared clays are thought to possess larger amounts of surfactant packed near the periphery of the gallery defined by two MMT platelets [2] (as shown in Figure 7.2a using a paraffin-type monolayer arrangement as an example) to explain observations by differential thermogravimetric analysis (DTGA) and the presence of residual inorganic cations. Chain entanglements and van der Waals associations of the alkyl groups on the surfactant hinder deep penetration into the galleries of a clay (this assumes of course that the exfoliated platelets of MMT dispersed in water during preparation of an organoclay rapidly reform into stacked structures at a point considerably before full replacement of all exchangeable cations at the oxygen plane).

Cloisite 20A (C20A), a commercial organoclay which was mainly used in this research due to its popularity in industry with polyolefinic materials, is believed to possess this morphology according to its mixed layered structure suggested by its X-ray diffraction (XRD) pattern. The majority of intercalated surfactant alkyl chains in the clay are considered to be tail-to-tail bound or end-tethered association [3, 4] and only a small amount is physically adsorbed to the exterior particle surface (<20%); this determination was made based on DTGA with recognition that surfactant in these different states exhibits different thermal stability. Inside the gallery space, surfactant molecules were assumed tilted with a certain angle off of the oxygen silicate plane to account for the recorded basal spacing by XRD and coverage area possible for the organic materials

based on its van der Waals radii. Negative charges on the uncovered silicate surface remained balanced by the un-exchanged metallic cations (primarily sodium). Atomic absorption spectrometric (AAS) analysis confirmed existence of the residual sodium cations, while the amount of moisture content in the organoclay and its hydration ability provided further evidence for the uncovered silicate surface and residual metallic cations. Four other organoclay materials, prepared by Southern Clay Products for this study, were analyzed in the same manner and each showed evidence of incomplete cation exchange with the surfactant. The chemical structure of surfactant and properties of C20A along with the other four organoclays used in this study are listed in Table 7.1. An unmodified MMT, Cloisite Na^+ (CNa^+) is included in the table for reference.

After annealing under $scCO_2$ above the melting point of the surfactant (i.e. greater than 45°C for C20A), the basal spacing of C20A increased from 25.8 Å to 27.8 Å. The swelling was attributed to rearrangement of the surfactant molecules. Significant amounts of the tail-to-tail bounded alkyl chains were turned into the more thermal stable end-tethered connection with the silicate surface, according to DTGA analysis. Being a hydrocarbon solvent, CO_2 can increase the mobility of long alkyl chains via plasticization, which provided more opportunities for surfactant species to migrate from the edges to being closer to the centre of the interlayer (if conceptually viewing the silicate platelets as circular disks). Denser packing of the alkyl chains would increase their tilt angle to explain their increased basal spacing as well as the noted drop in hydratable sites based on moisture analysis. Figure 7.2 schematically shows the considered changes to the morphology of the organoclay. The greater coverage by the organic material produced

Table 7.1 Properties of the quaternary ammonium modified montmorillonite

	C20A	ODTA	THMA	DDDA	C30B	CNa^+
Surfactant structure*	$(CH_3)_2(HT)_2$ N^+Cl^-	$(CH_3)_3(C_{18}H_{37})$ N^+Cl^-	$(CH_3)(C_{16}H_{33})_3$ N^+Cl^-	$(CH_3)_2(CC)_2$ N^+Cl^-	$(CH_3)(C_2H_4OH)_2$ $(HT)N^+Cl^-$	N/A
CEC content (meq/100g)	100	95	100	95	90	N/A
Surfactant content (wt %)	38.5 ± 0.2	26.8 ± 0.2	44.2 ± 0.3	30.6 ± 0.3	29.5 ± 0.1	N/A
Surfactant melting range (°C)	25-60	55-135	25-55	—	20-110	N/A
Na^+ content (wt%)	0.25	0.27	0.23	0.46	—	2.84
Moisture content (wt%)	1.90	2.83	1.04	2.16	—	5.77
Surface energy (mN/m)	38.1	39.9	37.9	39.3	42.4	—
***d*-spacing (Å)**	25.8	17.3	33.5	20.6	18.6	12.1

*HT= hydrogenated tallow (C_{18} ~65%; C_{16} ~30%; C_{14} ~5%); CC = coco (C_{12} ~56%; C_{14} ~18%; C_{18} ~7%; C_{16} ~7%; C_{10} ~7%; C_8 ~5%)

appeared to negatively impact the capacity to disperse the separated fragments of the clay once in a polymer, as discussed in a following section. Comparatively, the crystalline structure of HTMA was changed very little by the supercritical fluid and the other three organoclays exhibited a collapse in gallery spacing. HTMA being paraffin-type with intense packing and tilt angle of ~90° in its interlayer areas offered little opportunities for surfactant arrangement by the supercritical fluid. The surfactants in the other three organoclays are primarily packed in the lateral bilayer manner (Figure 7.1b), where the surfactant chain lays flat along the silicate surface. Collapse of their ordered layers was believed to be a result of transformation from their bilayer structure to the later monolayer arrangement (Figure 7.1a) through reorganization while highly mobile due to heat and the presence of $scCO_2$.

7.2.2 MA-PP

It is well recognized that $scCO_2$ has substantial solubility with many polymers, especially those with functional groups. For instance, solubility of this fluid in polypropylene and polyethylene can reach up to 1.5 wt% and 1.3 wt%, respectively [5]. Weak interactions between the gas and the functional groups are responsible for the solubility and these interactions are believed due to Lewis acidity of CO_2. Evidence for the weak interaction between carbonyl groups on polymer chains and CO_2 was identified by other researchers using Fourier transform infrared spectroscopy (FTIR), which included shifts of carbonyl stretching vibrations for cellulose acetate and poly(methyl methacrylate) [6] and splitting of the bending mode for CO_2 [7, 8]. Interactions of maleic anhydride with $scCO_2$ can be found in a few studies looking at Diels-Alder reactions

conducted under supercritical conditions. An example is ref [9] where evidence of the weak interaction was limited to observations of an increase in the rate of reaction between maleic anhydride and isoprene when CO_2 was at supercritical conditions. The authors of that paper had no hypothesis for how the increase in reaction rate occurred. Interaction between MA-PP and $scCO_2$ was reported by Clark and Lee [10] and they found that maleic anhydride was extracted from prepared MA-PP under $scCO_2$. Again, the authors provided little analysis on the mechanism. In the work of Liu et al. [11], the authors attempted to prepare MA-PP by a solid-state free radical reaction aided by $scCO_2$. They found a maximum in the grafted maleic anhydride content in relation to CO_2 pressure, which was attributed to the partitioning of MA between different phases within the mixture.

Our examination on the $scCO_2$/MA-PP interaction (not its relative interactions in the presence of the organoclay as well) was performed through melt annealing an MA-PP at the environment of $scCO_2$. A nitrogen blanket was used as the reference gas to prepare a control sample for comparison. FTIR spectra of the two melt annealed samples, after normalized using a band of 841 cm^{-1} (wagging vibration of CH_3/CH_2 in the polypropylene), were completely overlapped over a frequency range of 4000 – 400 cm^{-1}, indicating that $scCO_2$ did not persistently alter the chemical structure of maleated polypropylene. Same absorbance for the grafted anhydride groups at 1900 – 1700 cm^{-1} for the two gas cases can be looked as an indication that no anhydride groups were lost due to presence of the supercritical fluid at least under the conditions used for material preparation, i.e. 200°C and 9.6 MPa for 1 hour.

From rheological analysis it was found that a decrease in the viscosity of MA-PP occurred when annealing time extended to 3 hours. FTIR analysis for the 3-hour annealed PB3200 shows that absorbance for grafted anhydride groups at 1900 – 1760 cm^{-1} increased, which was attributed to dehydration of carboxylic acid, i.e. open anhydride groups turned into close rings (absorbance for the acid at about 1715 cm^{-1} decreased significantly). On the other hand, absorbance at about 1465 cm^{-1} for δ_{CH}^{as} and that at about 1380 cm^{-1} for δ_{CH}^{s} increased in comparison with the shorter annealing time, indicating that methyl groups increased. Based on the FTIR information, we infer that the viscosity decrease simply resulted from thermal degradation of C-C chains and that the grafted anhydride groups remained stable at the annealing conditions. In the absence of instrumentation for conducting in-situ FTIR analysis, our theories related to the effect of CO_2 on the compatibilizer material (MA-PP) were derived from indirect observation once mixed with the organoclay.

7.2.3 TPO

Since there are no functional groups on the polymer chains of TPO's components, homopolymer PP and a polypropylene-polyethylene copolymer elastomer, much weaker interaction between the matrix material and the solvent was expected. The polymer/solvent interactions are left only based on van der Waals attractions. Solubility of $scCO_2$ in the apolar materials is less than that in MA-PP, but still can reach ~2 wt% [12]. Comparatively, NaMMT will absorb ~2 wt% CO_2 at our test conditions [13] and solubility of CO_2 in MA-PP is assumed to reach up to 10% [5]. There is no information

on the solubility of CO_2 in organically modified MMT in the literature. Since TPO forms 90% of the final nanocomposite material based on typical formulations, these values presented mean that we can estimate up to 75% of the CO_2 will be segregated to the TPO phase and will not be readily available to aid the interactions at the clay/compatibilizer interface (assuming no CO_2 is being consumed at the interface to create a mass transfer gradient).

7.3 INTERACTION OF MALEATED PP WITH ORGANOCLAY

In order to understand the role of $scCO_2$ in polymer chain intercalation or clay dispersion in the compatibilizer/organoclay system, first the interactions between these components without the presence of $scCO_2$ had to be understood. Therefore, a large part of this section will talk about intercalation mechanism when $scCO_2$ is not present. Then, it will be easier to understand how $scCO_2$ aided the intercalation or dispersion mechanisms.

7.3.1 Barrier and driving force for intercalation

As shown in Figure 7.3, for a polymer chain diffusing into the interlayer of an organoclay, there are two major barriers: one is cohesion between two adjacent platelets due to their electrostatic repulsion and van der Waals attraction, and the other is the large entropic penalty for intercalation due to the interlayer confinement. When shear stress is not present, in order to enter the gallery space of stacked layers a polymer chain has to be active enough to overcome these thermomdynamic barriers. The driving energy comes from the affinity between filler and polymer which can be both chemical and physical. For the MA-PP/organoclay system examined, chemical affinity was found by FTIR

analysis through covalent bonding via esterification between the grafted anhydride groups and hydroxyl groups of the broken plane for stacked silicate sheets, and carboxylation of the carboxylic acid with residual metallic cations existing in the clay interlayer. The two chemical reactions are expressed in Figure 7.4. Chemical affinity can also be reaction between the grafted MA groups with surfactant if the surfactant contains proper functional groups. Physical affinity can occur by interaction of the surfactant alkyl tails with chain segments of the polymer via van der Waals forces and non-chemical bond associations of the polar groups on MA-PP with the silicate surface via hydrogen bonding.

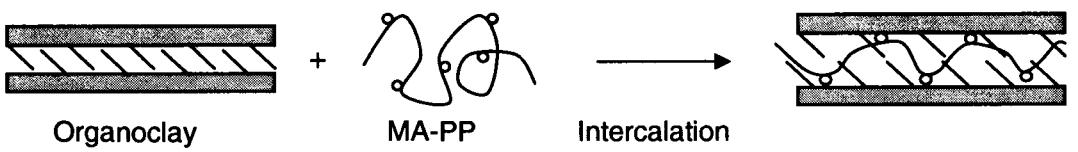

Figure 7.3 Schematic illustration of MA-PP intercalation. The small circles on the curves represent the grafted anhydride groups.

7.3.2 Factors affecting intercalation (WITHOUT $scCO_2$)

MA-PP

Any circumstance which increases the entropic barrier and/or decreases the driving forces will negatively affect the extent of intercalation. In our studies, three MA-

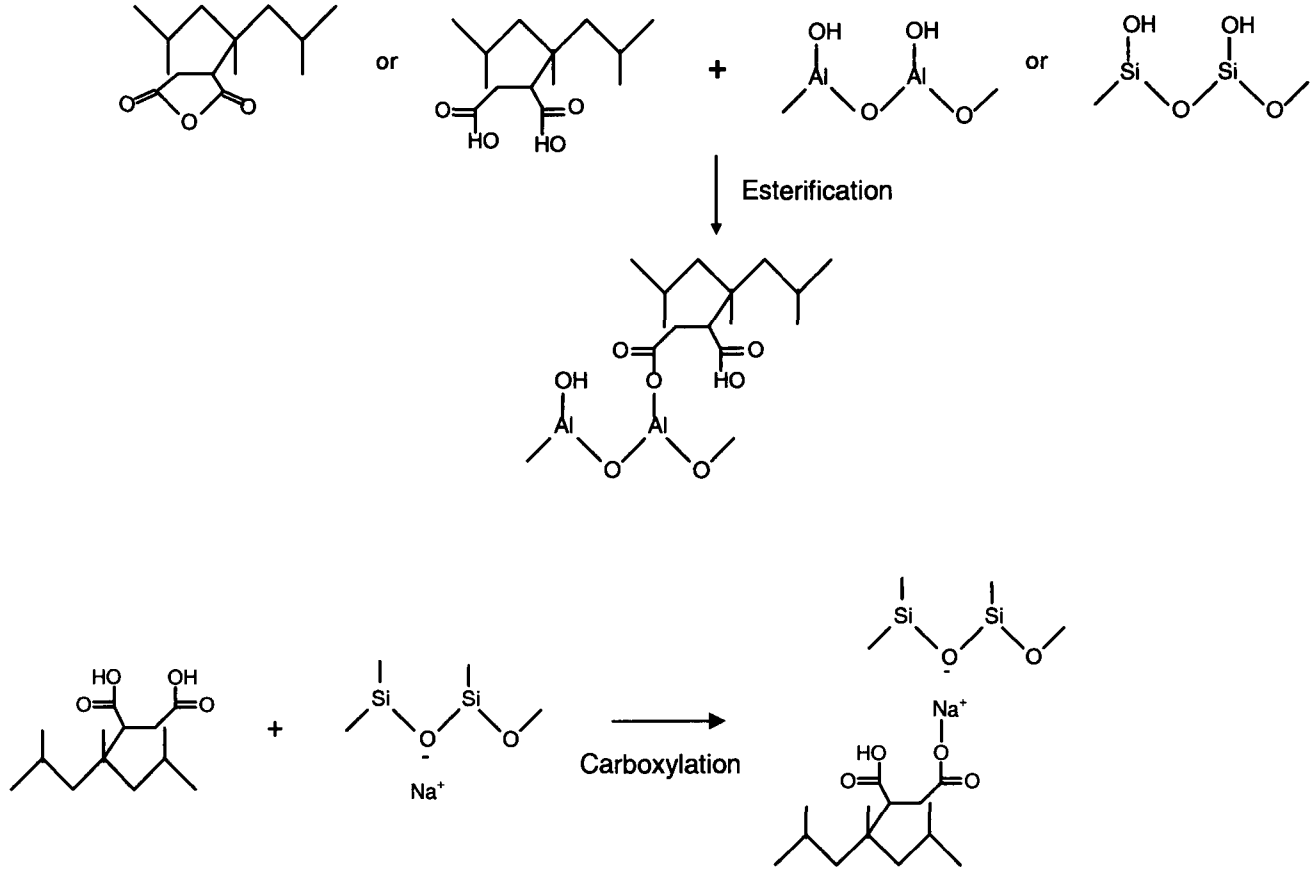

Figure 7.4 Chemical reactions occurred between C20A and PB3200. The upper relates to esterification and lower for carboxylation

PPs with different molecular weight and MA content, and five organoclays with different types of surfactants were examined. For the polymer intercalants, the greater the molecular weight, the larger radius of gyration for a polymer chain, and therefore the higher its entropic penalty for confinement in the clay galleries. On the other hand, the higher MA content, the more favorable enthalpic interactions for the intercalant with an organoclay, and therefore the more powerful the intercalation driving force. Almost complete intercalation or full exfoliation was found for Licocene 6252 (Li6252), a commercial MA-PP supplied by Clariant with $\overline{M}_w = 5{,}490$ g/mol and MA content of 4.7 wt %. At the other extreme, Polybond 3002 (PB3002) supplied by Chemtura with $\overline{M}_w = 254{,}350$ g/mol and MA content of 0.4 wt %, hardly diffused into gallery space of the organoclay examined (specifically C20A). Polybond 3200 (PB3200) also supplied by Chemtura had a moderate molecular weight ($\overline{M}_w = 87{,}670$ g/mol) and MA content (1.0 wt %) was found to readily diffuse but still left quite amount of layer-stacked organoclay particles (tactoids). Apparently, the lowest entropic barrier and highest driving force were responsible for high level of exfoliation of Li6252 while the reverse situation produced the worst intercalation using PB3002. PB3200 was balanced between these two extremes. Recall that these results do not include the presence of $scCO_2$ as a factor. This matter will be discussed later in Section 7.3.3. Since molecular weight and MA content were always correlates together being commercial MA-PPs produced by free-radical methods, we were not able to differentiate their roles individually.

Organoclays

Five selected organoclays varied in their organic modifiers, quaternary alkyl ammonium salts were studied, as mentioned earlier. These surfactants differed in their number of long alkyl chains, length of the alkyl chain and whether or not a polar group was present. However, these organoclays, based on their basal spacings, can basically be categorized into two groups, lateral bilayer and paraffin-type structures, as mentioned earlier in Section 7.2.1. From the point of view of entropic barrier, the way of surfactant arrangement may be the primary factor that affects the interaction occurred in the melt-annealed MA-PP/C20A composite.

Three organoclays, ODTA, DDDA and C30B, were defined as lateral bilayer structure and two, C20A and THMA, as paraffin-type. Properties of these organoclays have been listed in Table 7.1. For the lateral bilayer arranged species, after annealing with PB3200 basal spacing of all the three organoclays decreased, indicating that their layered structures collapsed and that no polymer chain intercalated into their interlayer areas. The collapse was attributed to transformation from the bilayer to monolayer arrangement occurred during the melt annealing. The transformation led to increased confinement exerted on the polymer chains and increased organic coverage on the silicate surface (more surfactant coverage on the silicate surface for monolayer arrangement is expected than bilayer). Facing the increased entropic barrier and decreased driving force, the polymer chains were considered to be restricted from diffusing into gallery areas of these organoclays. C30B included two hydroxyl groups per surfactant molecule which were chosen in the hopes to increase the intercalation driving force. However, the possible esterification of the hydroxyl groups with MA-PP was not able to compensate the driving

force loss due to the increased organic coverage and the entropic penalty due to the decreased interlayer distance. Therefore, for the lateral bilayer structure, properties of surfactant appeared little effect on the intercalation.

For paraffin-type arrangements which exhibit larger basal spacing than the lateral bilayer, the intercalation barrier was less. On the other hand, for similar CEC values the organic coverage over a silicate surface for lateral arrangement is larger than that for the paraffinic, i.e. paraffin-type organoclay can provide larger silicate surface to interact with the MA-PP intercalant. Therefore, the intercalation was expected more readily to occur with organoclays having paraffinic structure. The aforementioned C20A is a paraffin-type organoclay that proves to be able to be intercalated by Li6252 and PB3200. THMA is also of paraffin-type structure and has larger basal spacing than C20A. However, large interlayer distance of the clay did not result in better intercalation, as the basal spacing of the clay changed little after the annealing with PB3200 melt based on XRD analysis. The situation was ascribed to its bulky surfactant molecule (three alkyl chains in one molecule). CEC values of THMA and C20A were identical; thus, the bulky surfactant molecule meant more organic loading (Table 7.1) and more dense packing resulting in higher organic coverage of the silicate surface decreased favorable enthalpic interactions with the compatibilizer, the major intercalation driving force.

XRD analysis on the five organoclay masterbatches seems to point to a fact that organic coverage of the silicate surface is the major factor that influences the intercalation. It is true that in comparison with the paraffin-type arrangement, lateral structures (mono- or bi-layer) are of smaller basal spacing, offering more entropic penalty for the

intercalation. However, the lateral arrangement also means more organic coverage over the silicate surface than the paraffin-type when their CEC values are identical. Common feature of the four organoclays which did not exhibit intercalation by PB3200 based on XRD analysis was that they had higher surfactant coverage on the silicate surface. In order to add more evidence to the fact, a commercial unmodified MMT, Cloisite Na^+ (CNa^+), a sodium MMT (see Table 7.1), was annealed with PB3200 at the same conditions as those organoclays. Though its basal spacing was only 12.1 Å, much smaller than those organoclays, XRD analysis of the masterbatch shows that (001) plane diffraction peak disappeared, indicating that the clay in the masterbatch lost its ordered structure. Therefore, we may make a conclusion that exposed silicate surface plays a key role in the compatibilizer/clay intercalation. The more silicate surface exposed, the more powerful the intercalation driving force, and therefore the more possible for the intercalation.

7.3.3 Role of $scCO_2$ in the intercalation process

As discussed in Section 7.2, $scCO_2$ can cause surfactant in an organoclay rearranged and dissolve in MA-PP and TPO melts. Therefore, it is expected that the nanofiller/compatibilizer intercalation or dispersion of the nanofiller in the compatibilized TPO matrix would be influenced when the nanocomposite processing is performed under an environment of $scCO_2$. Positive effect has been observed by our group and other researchers [16-20]. However, details of the $scCO_2$-aid mechanism have not been revealed previously. After a series of studies, we basically understand how the supercritical fluid works in aiding dispersion of organoclay in a polymer matrix. We also

know from a series of studies that pre-treatment of clays with $scCO_2$ can have a negative outcome on final material properties, which may further aid us in understanding the mechanism. Our discussions on role of $scCO_2$ here in this section are limited to the compatibilizer/organoclay interactions.

When a mixture of compatibilizer and organoclay is exposed to an environment of $scCO_2$, the supercritical fluid interacts with surfactant, silicate surface and compatibilizer simultaneously. The surfactant of the organoclay starts to rearrange while the polymer compatibilizer is plasticized and starts to access the silicate galleries. A competition arises since surfactant rearrangement will result in more of the silicate surface being organically covered which shields it from other chemical interactions such as with the MA-PP (i.e. reduced enthalpic driving force for intercalation), while the surfactant rearrangement also impacts basal spacing. For instance, FTIR analysis showed that ester absorbance at ~ 1740 cm^{-1} for THMA did not change, but the absorption intensities for C20A, ODTA and DDDA decreased due to presence of $scCO_2$ during the melt annealing. The dissolved gas will also increase the free volume of the polymer melt, increasing chain mobility and decreasing the entropic penalty of intercalation as an extended chain state becomes more permissible [21]. In the case of C20A, the rearrangement leads to an increase in basal spacing which is beneficial to reducing the entropic barrier against intercalation. In terms of the broken plane at the edge of the silicate stacks where esterification with MA-PP predominantly occurs, with migrating of the surfactant from the periphery area into the galleries there is less surfactant to impede access of the polymer chains onto the silicate surface. We know this competition for C20A still favours intercalation when occurring

simultaneously, as the reduced enthalpic driving force on silicate layer surface is adequately compensated by the reduced entropy penalty against chain confinement and the increased chemical interaction occurred on edge area. Four points of evidence direct us to make this statement, 1) larger basal spacing or more disordered of the clay in the PB3200 masterbatch prepared under $scCO_2$ (XRD results), 2) smaller average tactoid thickness of the clay in the $scCO_2$-based masterbatch (TEM results), 3) the MA-PP to disorganize the surfactant structure from its all-trans state in C20A only when the $scCO_2$ was present meaning its chains deeply penetrated the silicate galleries only for this case (^{13}C NMR results), and 4) performance of s-C20A, C20A pretreated with $scCO_2$, that the compatibilizer did not adequately associate with the silicate surface, as noted by significant drop in mechanical and rheological properties of TPO nanocomposites prepared using the pretreated C20A (s-C20A). Therefore, a net aiding effect of $scCO_2$ to intercalation is exhibited. Figure 7.5 schematically shows the complicated intercalation process. We should stipulate here though, that this benefit only occurs for intercalation and not necessarily for exfoliation which will be discussed later. Essentially, we state that $scCO_2$ is an intercalation aid and not an exfoliation aid as originally thought.

In regard to the compatibilizer/organoclay masterbatch, the $scCO_2$ aiding effect described above only occurred to C20A. For the three lateral-arranged organoclays (ODTA, DDDA and C30B), surfactant mobility under $scCO_2$ allowed the surfactant to coordinate with the silicate plane, laying flat such that a transition from bilayer to monolayer arrangement occurred. That is, the presence of $scCO_2$ caused not only an increase in organic coverage of silicate surface but also decrease in the basal spacing of

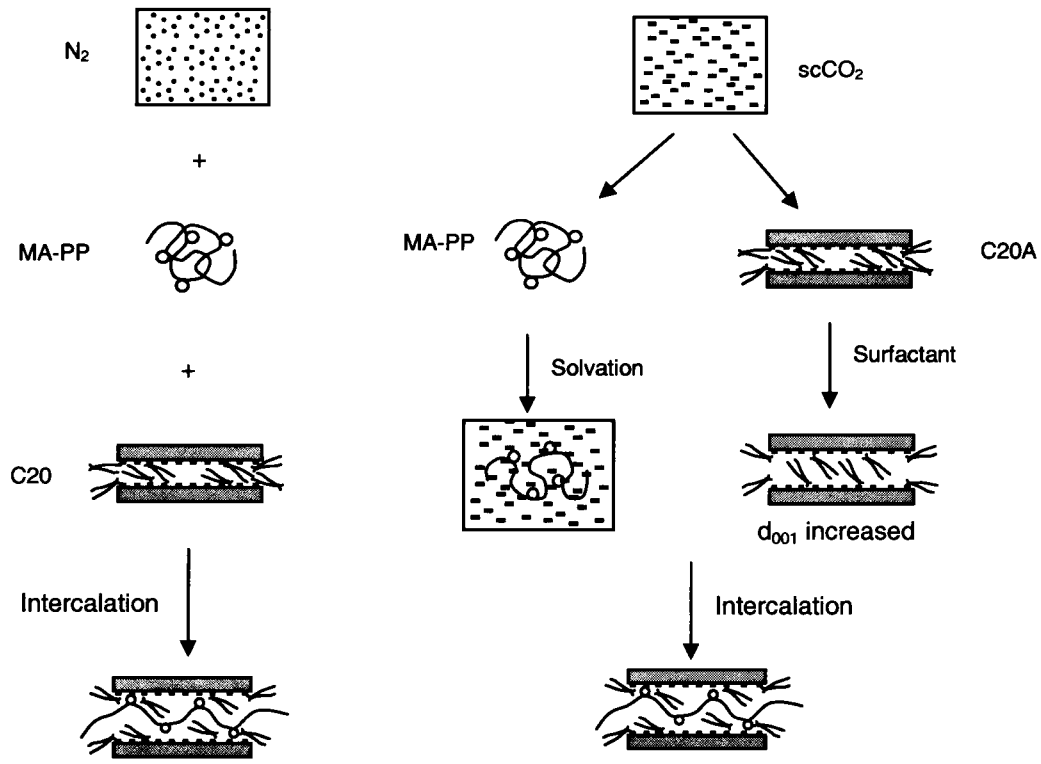

Figure 7.5 Schematic diagrams for interactions between C20A and PB3200 at environment of $scCO_2$ (right) and N_2 (left)

the silicate stack for these clays. Apparently, mobility gains and possible solvation of MA-PP chains under $scCO_2$ were not able to overcome the entropic barrier imposed by shrinking of the layer stacks as well as the driving force loss due to increased organic coverage over the silicate surface. The supercritical fluid in these cases was ineffective to improve intercalation. For the other paraffin-type organoclay, THMA, due to its highly packed surfactant the tilt angle of the alkyl tails was close to 90°. In spite of being under an environment of $scCO_2$, the clay structure changed little. The highly packed surfactant molecules were felt to sterically prevent polymer chains from accessing the silicate surface. With no occurrence of surfactant rearrangement due to its dense surfactant packing already and no change in basal spacing, the clay remained unaffected by the $scCO_2$ in this case and so intercalation remained limited to the broken plane where chain access was permitted. Intercalation and exfoliation of this clay proceeded as normal, unaffected by the use of the supercritical fluid but not deterred by it either.

Since one way of the $scCO_2$ intercalation-aiding effect is through plasticization or solvation of the MA-PP chains, intercalation for the MA-PP with high molecular weight and low MA content (PB3002) which was difficult when the supercritical gas was not present may become permissible. XRD analysis on the PB3002/C20A masterbatch showed that diffraction peak position of the clay in the N_2-based sample had no change (compared to its pristine state); however basal spacing of the clay in the $scCO_2$-based sample increased. Among the three MA-PPs studied, the most sensitive to the effects of $scCO_2$ was PB3200 for which a larger increase in basal spacing was found due to presence of the supercritical gas. Actually, for the $scCO_2$-based PB3200/C20A

masterbatch, the clay was not only intercalated but also partially exfoliated, i.e. part of the clay lost its ordered structure, as determined by XRD and TEM analyses. As for Li6252, since low molecular weight and high MA content already makes its chains active enough and the Li6252/C20A masterbatch exfoliated, apparently there would not be a difference between $scCO_2$ and N_2.

7.4 TPO NANOCOMPOSITES MADE FROM

7.4.1 Original materials

The interpretations of the mechanism in this section pertain to work done jointly with Mr. Zijin Zhuang. A paper based on this work is appended (ref to Appendix A). All analysis of the mechanism was specifically done by myself.

Effect of $scCO_2$ when preparing the complete formulation for a TPO nanocomposites was first examined by directly injecting the supercritical fluid into a mixing device (single screw extruder and/or twin a twin screw extruder) where the three components, matrix, compatibilizer and nanofiller, were melt compounded. There are reports stating that the injected supercritical fluid improved intercalation and exfoliation of the prepared nanocomposites [18, 22-23]. Unfortunately, our results could not confirm their conclusions. Our studies, compared to a reference environment of N_2, showed that injection of $scCO_2$ into the melt flow did not increase the storage modulus of the TPO nanocomposite melt; the storage modulus usually correlates well with the flexural modulus of a material. Rather this property in the low frequency range appeared to deteriorate. It is believed that viscosity of the polymer melt decreased due to addition of

the supercritical fluid. Shear stresses play a key role in the delamination of layer-stacked clay particles during melt compounding and generally speaking, a higher extent of exfoliation will be reflected by an increase in the storage modulus especially at low oscillatory shear frequencies. The introduction of $scCO_2$ to the TPO and MA-PP polymer phases would be expected to increase inter-chain distance and free volume, and reduce inter-chain interactions thus limiting shear transmission during the particle delamination. Supercritical CO_2 can also negatively impact the modulus of the final nanocomposite when initially given unfettered access to the clay before all other components are added (referred to as pre-treated clay) but that will be discussed in detail in the follow section. This issue was not in play for the present results since all components were added simultaneously.

7.4.2 Supercritical CO_2 pretreated orgnaoclay

Pre-treating the organoclay involves exposing it to a supercritical fluid environment without other polymer components, with the expectation of fracturing structure into individual platelets or at least swelling it by rapidly releasing the gas after a prolonged equilibrium time. The expanded clay species is then melt compounded into the matrix polymer of a nanocomposite. Reports show that exfoliation of nanocomposites prepared using this technique was improved [19-20]. The prepared clay maintained a structured, but swollen structure as indicated by XRD but its ordered crystalline pattern was lost upon compounding into our polyolefin matrix – lost more readily than pristine organoclay since it no longer required a compatibilizer to fracture under the shear stresses of the extrusion. However, the pre-treated organoclay did not result in better silicate

platelet dispersion within the final TPO nanocomposite than the organoclay used in its pristine state. XRD may have observed no (001) diffraction peak which indicates an absence of ordered structure; however, TEM studies found that the separated silicate platelets were agglomerated; and rheological analysis confirmed that the storage modulus of the nanocomposite significantly dropped in the low shear rate region – being closer in stiffness to a unreinforced TPO. The increased organic coverage of silicate surface arising from surfactant rearrangement under environment of $scCO_2$ is believed to be responsible for the decreased level of desired exfoliation (i.e. disordered exfoliation where individual platelets are well separated from one another). Reduced exposure to the oxygen plane meant fewer sites for interaction with compatibilizer. The importance of surfactant coverage is a new concept in the nanocomposite field and points to why only some organoclays are successful in commercialization of nanocomposites despite seemingly favourable oleophilic surfactants being used. The result of the reduced interactions with MA-PP was lost in compatibility at least partially, leading to phase separation of the silicate particles in the TPO nanocomposite. Additionally, in the phase separated composite, MA-PP would act as plasticizer when shear stress was applied to the composite. Therefore, pre-treatment of organoclay alone using $scCO_2$ has proven inefficient.

7.4.3 MA-PP/Organoclay Masterbatch

The idea of batch processing the mixture of MA-PP and organoclay in the presence of $scCO_2$ before melt compounding with TPO matrix was favoured by our group based on the evidence above. It was expected that batch processing would allow for

compatibilizer chains to diffuse into gallery areas of the stacked layers resulting in an intercalated or exfoliated morphology in a masterbatch material. Then in a shear stress flow field undiluted by the plasticizing effects of $scCO_2$, the intercalated silicate particles would delaminate readily into the TPO melt. Due to good compatibility of the compatibilizer with both organoclay and the matrix polymer, a thermodynamically stable TPO nanocomposite can be acquired. Our experimental results support this approach as being better than mixing all components together under $scCO_2$ or pre-treating the clay. Compared to the N_2 control environment, the level of exfoliation in nanocomposite prepared from $scCO_2$-based masterbatch was significantly improved. For instance, in comparison with the N_2-based nanocomposite the storage modulus of the $scCO_2$-based TPO nanocomposite at shear rate of 0.3 rad/s increased more than 75%. Of course, preparing a compatibilizer-clay masterbatch in the absence of shear presents problems in itself since the long time to melt and anneal the polymer can lead to thermo-degradation. The complicated issue in that regards is whether a more intercalated, thermodynamically stable masterbatch arises from the clay and compatibilizer first melting under the $scCO_2$ and then being mixed in the same environment, or first being melt mixed together and then further mixed under $scCO_2$.

7.4.4 MA-PP/organoclay masterbatch prepared using cosolvent

Water or ethanol has good affinity with the silicate surface of MMT as well as MA-PP and CO_2. Therefore, their addition to the $scCO_2$ aided mixing system is thought to increase the masterbatch intercalation and thereafter, bring about improved exfoliation and dispersion of TPO nanocomposite. Therefore, water and ethanol were tested as

cosolvents to the supercritical gas expecting that exfoliation of organoclay in the TPO nanocomposite could be improved. These two solvents were chosen as both are environmental benign and would be more acceptable to an industrial operation. Enhancement in chemical interactions between the organoclay and compatibilizer by the two cosolvents was confirmed with regards to changes in the FTIR spectra. XRD and solid state ^{13}C NMR analyses for the masterbatches prepared using the two cosolvents proved significant improvement occurred from their intercalation. TPO nanocomposites prepared from the highly intercalated masterbatches showed that both cosolvents were able to improve exfoliation and dispersion of the silicate tactoids or individual sheets in the TPO nanocomposite. Ethanol produced a higher extent of exfoliation compared to water or plain $scCO_2$ due to its reaction ability with the grafted anhydride groups on MA-PP. The ethyl esterification can swell the clay stacks further, reducing the intercalation barriers. On the other hand, the ester-connected ethyl groups increased the favourable enthalpy interaction between the compatibilizer and alkyl chains of the surfactant, which increased not only the intercalation driving force but also compatibility with the nanofiller in the TPO nanocomposite. Therefore, the ethanol-aided TPO nanocmposites exhibited the best exfoliation and percolating network of the clay platelets.

7.5 STRATEGY RECOMMENDED

Based on these understandings, now we are able to come up with suggestions for industrial use. Supercritical CO_2 is an efficient aiding agent in the processing of thermoplastic elastomer nanocomposites. However, the way of applying the solvent to the processing route is the key to retaining value for the added processing costs.

Concentrating the supercritical solvent at the compatibilizer/clay interface is an effective technique. Adding small amount of water or ethanol to the bulk $scCO_2$ environment can significantly improve dispersion of silicate sheets in the TPO nanocomposite. Considering the difficulty in maintaining a high pressure in the available mixing device in industry in order to keep CO_2 in supercritical state, water or ethanol, especially the latter, may be used as an alternative solvent instead of the supercritical gas. Their aiding effect as an independent solvent may be equivalent or even better than the plain $scCO_2$, especially ethanol.

REFERENCES

1. Bonczek JL, Harris WG, Nkedi-Kizza P, Monolayer to bilayer transitional arrangements of hexadecyltrimethylammonium cations on Na-montmorillonite, Clays Clay Miner., 50 (2002), 11-17
2. Deng Y, Dixon JB, White GN, Intercalation and surface modification of smectite by two non-ionic surfactants, Clays and Clay Materials 51 (2003), 150-161
3. He H, Frost RL, Bostrom T, Yuan P, Duong L, Yang D, Xi Y, Kloprogge JT, Changes in the morphology of organoclays with $HDTMA^+$ surfactant loading, Appli. Clay Sci. 31 (2006), 262-271
4. Thompson, M.R., Liu, J., Krump, H., Kostanski, L.K., Fasulo, P.D., Rodgers, W.R., 2008. Interaction of supercritical CO_2 with alkyl-ammonium organoclays: changes in morphology. J. Colloid Interf. Sci. 324, 177-184

5. Tomasko D.L., Li H., Liu D, Han X, Wingert M.J., Lee L.J., Koelling K.W. Ind. Eng. Chem. Res. 2003, 42, 6431 – 6456
6. Fried JR, Li WJ. High-pressure FT-IR studies of gas-polymer interactions. J. Appl. Polym. Sci. 1990;41:1123–31
7. Kazarian GS, Vincent MF, Bright FV, Liotta CV, Eckert CA. Specific intermolecular interaction of carbon dioxide with polymers. J Am Chem Soc 1996;118:1729–69
8. Kazarian SG, Brantley NH, West BL, Vincent MF, Eckert CA. In situ spectroscopy of polymers subjected to supercritical CO2: plasticization and dye Impregnation. Appl. Spectrosc. 1997;51:491–4
9. Glebov, E. M.; Krishtopa, L. G.; Stepanov, V.; Krasnoperov, L. N. J Phys Chem A 2001, 105, 9427
10. Clark, K.; Lee, S. Polym Eng Sci 2004, 44, 1636
11. Liu, T.; Hu, G.-H.; Tong, G.-S.; Zhao, L.; Cao, G.-P.; Yuan, W.-K. Ind Eng Chem Res 2005, 44, 4292
12. Sato, Y., Takikawa, T., Sorakubo, A, Takishima, S., Masuoka, H., Imaizumi, M. *Ind. Eng. Chem. Res.* 2000, *39,* 4813-4819
13. Pribylov, A.A., Muminov, S.Z., Kalinnikova, I.A., Shekhovtsova, L.G. Colloid J. 72(3), 2010, 417-422
14. Huang, W.-L., Bassett, W. A., Wu, T.-C. American Mineralogist, Volume 79, pages 683-691, 1994
15. Liu, J. Thesis for Masters degree, McMaster University, Aug. 2008

16. Liu, J., Thompson, M.R., Balogh, M.P., Speer Jr., R.L., Fasulo, P.D., Rodgers, W. R., Nov. 2010. Influence of supercritical CO_2 on the interactions between maleated polypropylene and alkyl-ammonium organoclay. J. Appl. Polym. Sci. (accepted)
17. J. Liu, W. R. Rodgers, P. D. Fasulo, and M. R. Thompson. Supercritical Carbon Dioxide as an Exfoliating Agent in the Preparation of a Layered Silicate Polymer Nanocomposite. 26th Annual Meeting of Polymer Processing Society, Banff, Canada, July 4-8, 2010
18. M.A. Treece, J.P. Oberhauser, J Appl. Polym. Sci. 2007, 103, 884-892
19. S. Horsch, G. Serhatkulu, E. Gulari, R.M. Kannan, Polymer 2006, 47, 7485-7496
20. Q. T. Nguyen, D. G. Baird. Polymer 2007, 48, 6923-6933
21. P. Vitoux, T. Tassaing, F. Cansell, S. Marre, C. Aymonier. *J. Phys. Chem. B* **2009,** *113,* 897–905
22. Y. Zhao, H.-X. Huang. Polymer Testing 2008, 27, 129-134
23. J. Ma, E. Bilotti, T. Peijs, J. A. Darr. European Polym. J. 2007, 43, 4931-4939

Chapter 8

Conclusions, Contributions and Recommendations

8.1 CONCLUSIONS

Major conclusions from this research are summarized as follows:

The plasticization hypothesis was proven valid for our TPO nanocomposites. Firstly, supercritical CO_2 can increase intercalation ability of a maleated polypropylene, though the aiding effect apparently depends on molecular sized and anhydride content. A maleated polypropylene with moderate molecular weight and anhydride content appeared most sensitive to the supercritical gas. Secondly, supercritical CO_2 demonstrates a significant improvement on the level of exfoliation for Cloisite 20A in a TPO nanocomposite, and concentrating CO_2 at the compatibilizer/clay interface can achieve more effective than when the polymer components are annealed separately from the clay before mixing or when all components of the nanocomposite formulation are heated together.

The fracturing hypothesis was shown only valid when the organoclay was processed alone and not for the compatibilizer/organoclay intercalation or exfoliation into the TPO nanocomposite. Rapid depressurization does lead to organoclay expansion; however, pre-swelling or separating silicate platelets of the organoclay using the supercritical gas does not readily improve dispersion of the clay in its TPO nanocomposite. Increased organic coverage on the silicate surface due to the $scCO_2$ pre-treatment notably increases agglomeration of the expanded or separated clay in the TPO matrix. The pre-treatment appears to diminish the interfacial stability of the dispersed filler when the compatibilizer has limited access by its functional group to interact with silicate surface.

Paraffinic arrangements for an alkyl surfactant can offer more effective access of the compatibilizer functionality to the silicate than lateral monolayer or bilayer arrangements due to their relatively larger basal spacing. However, organic coverage on silicate surface is a more important factor that influences intercalation. Higher organic coverage on silicate surface for an organoclay decreases the driving force for intercalation.

Plasticization of organic surfactant by supercritical CO_2 without simultaneous competition for sites by a compatibilizer results in increased organic coverage over the silicate surface of a modified clay.

Adding water or ethanol to the $scCO_2$-aided melt processing can significantly improve the driving forces leading to intercalation through increased chemical associations between the compatibilizer and organoclay. The result was a higher level of

the compatibilizer/organoclay intercalation and thereby better exfoliation and dispersion of the TPO nanocomposite. Water displayed an ability to enhance the carboxylation occurring between the compatibilizer and organoclay. Ethanol directly reacted with the compatibilizer generating ester bonding.

When used alone as solvents in the melt processing, either water or ethanol can achieve equivalent and in some cases, better results over $scCO_2$ or conventional melt intercalation practices in terms of exfoliation and dispersion within a TPO nanocomposite.

8.2 CONTRIBUTIONS TO KNOWLEDGE

The important contributions of this research are as follows:

- Systematically studied how supercritical CO_2 aids intercalation, exfoliation and dispersion of organically modified montmorillonite in a thermoplastic olefinic polymer matrix. The studies include how the supercritical fluid interacts with the silicate nanofiller (for Jinling Liu's Masters degree), how it influences interactions between silicate layers and maleated polypropylene that is used as compatibilizer in the TPO nanocomposite, and how it promotes exfoliation and dispersion of the nanofiller in the nanocomposite during the processing.

- Basically understood mechanism of supercritical CO_2 aiding dispersion of organoclays in TPO nanocomposites in the melt compounding process.

- Clarified that supercritical CO_2 is an intercalation aid rather than an exfoliating aid. The latter is a general view in literature about supercritical CO_2 in aiding exfoliation and dispersion of polymer layered silicate nanocomposites.

- Advanced a new concept of the importance of organic coverage on silicate layers in the field of polymer layered silicate nanocomposites. The new concept reasonably explains why only some organoclays are successful in commercialization of nanocomposites.

- Revealed that for analyzing microstructure of a polymer layered silicate nanocomposite rheological measurement is more effective than XRD and TEM, which are usually considered two traditional and complementary methods. Actually, rheology is more strongly affected by the clay-polymer interaction.

8.3 RECOMMENDATIONS FOR FUTURE WORK

Small scale experiments have shown that for TPO/layered silicate nanocomposites high level of exfoliation can be achieved using this two-step processing technique: melt annealing the compatibilizer/orgnaoclay mixture under environment of $scCO_2$ to make a masterbatch and then melt compounding the masterbatch with the TPO matrix without $scCO_2$. In order for industrial applications, larger scale experiments are recommended. The melt annealing can be performed in batch or continuously. For continuous melt annealing, a long residence time is necessary because it allows for sufficient time for the compatibilizer/clay intercalation. In compounding the masterbatch with TPO melt, $scCO_2$ is not necessary. More trials on adding water or ethanol as a cosolvent to $scCO_2$ in the

annealing step may be needed to confirm their aiding effects obtained from the small scale experiments performed by Jinling Liu.

Since in the small scale experiments water and ethanol, especially ethanol, when used as sole solvent, appeared equivalent and even better aiding effect than $scCO_2$, it is strongly recommended that further experiments on the two liquids. Use either of them as a sole solvent in the nanocomposite processing may generate surprising results. Importantly, substituting $scCO_2$ with water or ethanol in the nanocomposite processing is meaningful to the industry because high pressure processing condition that is necessary to maintain CO_2 at supercritical state can be avoided.

Appendix A

Supercritical CO_2 as an Exfoliating Aid for Nanocomposite Preparation: Comparison of Different Processing Methodologies

This is a paper based on the work done in collaboration with Mr. Zijin Zhuang (a Masters candidate in the group). Jinling Liu made about one third contribution to this work. The paper is to be submitted to a technical journal and is used to discuss the mechanism of $scCO_2$ in Chapter 7.

ABSTRACT

This paper examines the potential for several new methods using supercritical CO_2 as a processing aid to produce a more highly exfoliated polyolefin-layered silicate nanocomposite than the conventional melt intercalation technique. The methods varied the manner in which the plasticizing behavior of CO_2 influences the surfactant of an organoclay, a compatibilizer and the matrix during preparation of a polyolefin nanocomposite. The results have shown that targeting CO_2 to the organoclay-compatibilizer interface can benefit the extent of intercalation achievable but showed lower performance when introduced predominantly to the matrix or neat organoclay. Carbon dioxide exposure directly to the neat organoclay leads to a crystal structure more easily susceptible to fracture in a shear field yet this same pre-treated clay did not display the anticipated increase in modulus for being a highly exfoliated system. Conversely, CO_2 exposure predominantly to the matrix reduces the extent of clay dispersion, producing a material equivalent or worse (in terms of exfoliation) than if the gas was never present. In general, the different techniques for CO_2 did bring about greater structural changes to the organoclay, but the stiffness of the produced materials was lower than simply following a conventional melt intercalation approach.

A1 INTRODUCTION

The organic modification of natural (and synthetic) clay minerals has led to the development of a new field of polymer-matrix composites, referred to as polymer-layered

silicate (PLS) nanocomposites. Organic surfactant replaces the balancing inorganic cations naturally present within the interlayer spaces between the sheet-like layers making up aluminosilicate mineral like montmorillonite (MMT). As a result of the cation exchange, the swollen organoclay is made more compatible with polymers and experiences greater susceptibility to guest intercalation and exfoliation [1-4]. Dispersion of the nanoscale exfoliated silicate layers (sheets) within a polyolefin matrix is anticipated to generate a light-weight, strong material with lower thermal expansion and higher heat distortion properties compared to conventional composite materials.

There is great industrial potential for such a nanocomposite provided it can be economically prepared and maintain a stable dispersion through subsequent processing. However, compounding practices used for conventional composites based on addition of interfacial modifying additives and tailoring the specific mechanical energy of the process have not yet yielded satisfactory results for nanoscale organoclay dispersion in a polyolefin matrix [5]. It is common to see reported results in the literature [6-8] of dispersed nanoclay particles within polypropylene and thermoplastic polyolefins (TPO) retaining their well-ordered layered structure, albeit smaller in dimension after compounding. To reach the much coveted fully exfoliated morphology, researchers are now looking to unconventional approaches to overcome the thermodynamic barrier. Several new processes recently disclosed in the literature to aid disruption of the clay structure have included applying an electrical field [9, 10], use of high-energy ultrasound [11, 12], and injection of supercritical carbon dioxide ($scCO_2$) [13-23]. The latter has generated the most interest as it is readily adapted to the polymer industry.

Among the technologies using $scCO_2$ as an exfoliating aid, there are four unique approaches presently found in patent and published literature. In all cases, the focus of these methods is upon the supercritical fluid improving organoclay dispersion and not allowing the carbon dioxide to foam the extruded product. Each of the methods discussed here prepare the nanocomposite in bulk via melt intercalation, though with the solvent contributions of $scCO_2$ in the process it would seem more appropriate to refer to this as a hybid intercalation approach. The different methods are: i) *direct gas injection*, where $scCO_2$ is injected into the extruder at a downstream location after all components of the composite material have been compounded together [14, 20, 23]; ii) *pre-treated organoclay*, where the organoclay is batch processed offline as a suspension in the supercritical fluid and subsequently removed by rapid depressurization before being added to the compounding process in the same manner as a standard organoclay ($scCO_2$ gas may or may not be added to the extruder as well in the same manner as the direct gas injection method) [13, 16, 17]; iii) *continuously fed pretreated organoclay*, where the second method is performed continuously with the pre-treated clay experiencing rapid depressurization at the addition zone of the extruder [18]; and finally iv) *organoclay-$scCO_2$ suspension*, where organoclay enters the extrusion process in the supercritical fluid and is incorporated into the polymer melt stream while still at an elevated temperature and pressure corresponding to the critical state of the gas [19]. The first approach is most familiar to the polymer foams industry but here the gas is affecting all components in the composition equally without any control. The second approach targets the influence of the gas specifically to the organoclay but being batch in nature may not be conducive for

use in a compounding facility. The latter two approaches represent complex technologies involving the bulk conveying of cohesive solids (Geldart Group C class materials) under extremely high pressures (greater than 7.5 MPa) and elevated temperature (greater than 32°C) and could not be examined in our study. However, an alternative approach is proposed in this paper whereby the organoclay and compatibilizer are pre-conditioned together under supercritical conditions and injected continuously into the extruder as a molten fluid while being maintained above the critical state. The new approach avoids complications related to bulk solids conveying and is similar in its objectives to the approaches of Ottaviani [19] and Garcia-Leiner [22] but experiences its own difficulties related to thermo-degradation, as will be discussed. This final approach is referred to as *masterbatch-scCO$_2$ injection.*

This paper explores the benefits to the different approaches of using scCO$_2$ as an exfoliating aid in the preparation of polyolefin-layered silicate nanocomposites. The approaches of the direct injection method, pre-treated organoclay method, and masterbatch-scCO$_2$ injection method will be compared as each targets the gas influence to different components in the composition, and the resulting mechanical and rheological properties based on the developed clay dispersion in the final product will be measured. The work evaluates the capacity of these different technologies to delaminate the organoclay to a greater extent than the traditional route without use of CO$_2$, and determine whether more exfoliated materials necessarily translate to better properties in all cases.

A2 EXPERIMENTAL

Materials

A 13 MFR thermoplastic polyolefin (TPO) supplied by LyondellBasell (Lansing, MI) was selected for this study as the matrix. Pellets of the TPO material were used directly without any further treatment. A commercial maleated polypropylene (MA-PP) compatibilizer, Polybond® 3200 (PB3200) from Chemtura Corporation (West Lafayette, IN) was selected. This compatibilizer has sufficient molecular weight to minimize any losses in mechanical properties by its addition to the polymer matrix and demonstrates plasticization in the presence of supercritical CO_2 sufficient to aid intercalation [24]. For the *masterbatch-scCO$_2$ method*, pellets of the MA-PP were ground cryogenically by Ingenia Polymers (Brantford, ON) into powder to minimize segregation as it was mixed with the organoclay. Other properties of the MA-PP have been reported in a previous study [24]. Though some scCO$_2$ technologies propose that the addition of the compatibilizer is not necessary to prepare exfoliated clay nanocomposites, this work primarily compares materials with the same composition; the formulation of the prepared PLS nanocomposite was 90:5:5 (wt%) for the matrix, compatibilizer, and organoclay, respectively.

Cloisite 20A® (C20A) from Southern Clay Products (Gonzales, TX) was the selected organoclay for this study based on its high CO_2-philicity compared to other species tested in earlier work [25, 26]; the properties of C20A are well documented in those studies. The basal spacing of the as-supplied organoclay was 25.8 Å afforded by a

paraffin-type surface arrangement of its dialkyl ammonium surfactant. No further purification of the organoclay was done prior to use in the study. Table A1 provides a summary of select properties for the organoclay.

Table A1 Properties of the Organic Modified Montmorillonite

Surfactant structure	Surfactant content (wt %)	Surfactant melting range (°C)	*d*-spacing (Å)
$(CH_3)_2$ $(HT)_2N^+Cl^-$	38.5 ± 0.2	25-60	25.8

*HT= hydrogenated tallow (C_{18} ~65%; C_{16} ~30%; C_{14} ~5%).

The carbon dioxide and nitrogen gases used in the experiments were supplied by Air Liquide Canada Inc. (Burlington, ON) at 99.5% and 99.995% purity, respectively.

Preparation of the pre-treated organoclay

In accordance with the described method [16, 17], 15 g organoclay was placed in a 300 ml high pressure batch vessel which had been heated to 80°C (above the melting point of the surfactant). The sealed vessel was pressurized to 11.7 MPa with CO_2 (above its critical state) using a Teledyne-ISCO 260D syringe pump and the clay was allowed to equilibrate in that environment for 5 hours. The vessel was connected to a large 40 L polyethylene drum through a 12mm dia. ball valve (Swagelok). Upon conclusion of the experiment, the vessel was rapidly depressurized in less than 1 sec, and all material was allow to cool before being collected. The preparation was repeated till 1 kg of pre-treated

organoclay had been produced and then all material was stored in a dessicator till ready for the compounding step. This organoclay is designated as s-C20A in this paper.

Machinery

The compounding trials were predominantly conducted on a 40 L/D 27-mm ZSE HP co-rotating intermeshing twin screw extruder (TSE) from the American Leistritz Extruder Corporation. A pair of gravimetric feeders, a K-Tron F-1 and Brabender DDSR-2, were used for the addition of dry solids to the process. All samples extruded were strand cut using a Conair pelletizer. The screw design used in the machine is shown in Figure A1, comprised of both intensive shear kneading zones and more moderate shear distributive mixing zones.

Some trials under the *masterbatch-scCO$_2$ injection* method were done in a 28 L/D 50mm single screw extruder (SSE) from the Davis-Standard Corporation in place of the TSE for compounding. For this machine, a DSB-I moderate work barrier screw with spiral UCC mixer was used and a valved die adapter was attached to control pressure/output rate. Side addition of components was done at the end of the barrier zone of the screw (6 L/D before the breaker plate) under pressure.

The *direct injection* of gas into the twin screw extruder was done using an injection stem with a 1.5mm diameter outlet hole. High pressure tubing from High Pressure Equipment Co. connected the stem to a Teledyne-ISCO 260D syringe pump. The injection of organoclay and molten MA-PP under scCO$_2$ conditions for the *masterbatch-scCO$_2$* method was done using a specially constructed ram extruder. This

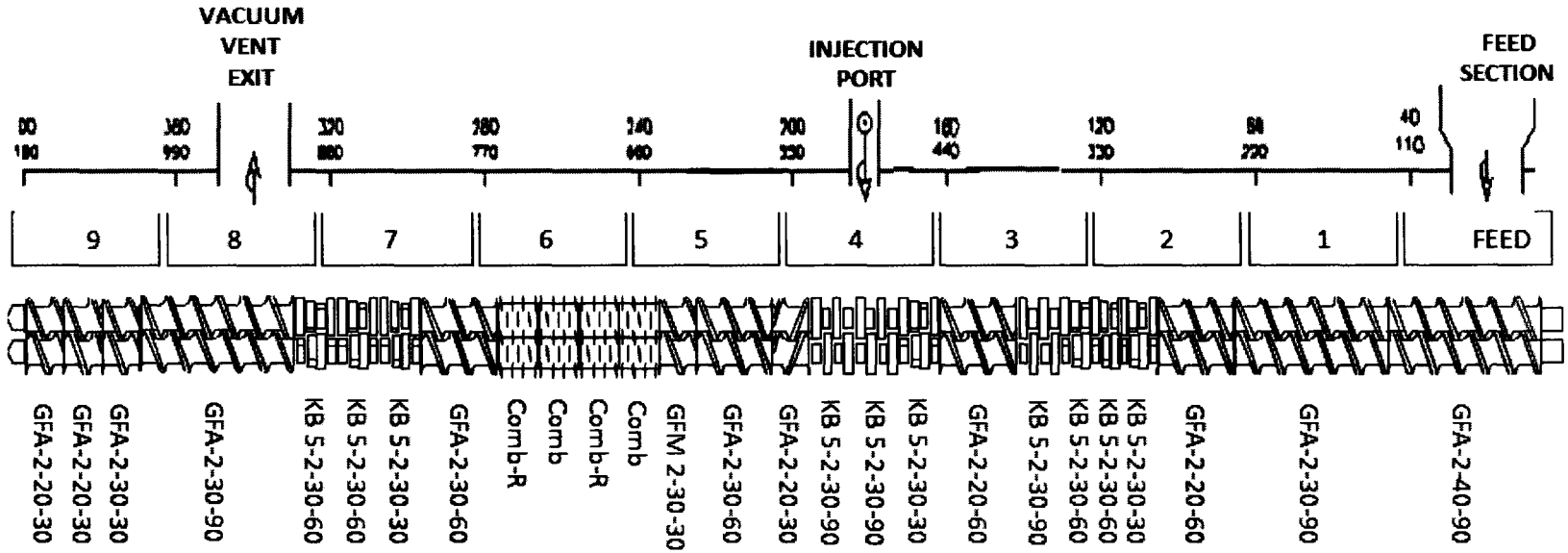

Figure A1. Layout of barrel and screw for all compounding trials in the twin screw extruder.

system was found suitable to meter the two components into the compounding process at high temperature and high pressure without excessive CO_2 being needed; addition of high gas content into an extruder diminishes output stability and leads to issues with polymer sputtering from the die. The apparatus, shown in Figure A2, had a heater band that was controlled by either the TSE or SSE drive panel and contains tapped holes to receive pressurized gas from the syringe pump and measure pressure (by a Dynisco PT462 melt pressure transducer). The ram assembly was mounted next to the designated extruder (TSE or SSE) and attached to the chosen barrel zone using a heated adapter pipe. Metering of the molten masterbatch under $scCO_2$ into the process was controlled by a screw-driven ram calibrated to meet the desired output rate.

Direct Organoclay Addition Processes

Three different methods fall under this procedure with minor differences in the steps of the synthesis. In all cases, a first pass through the TSE involved the TPO and an organoclay (either C20A or s-C20A) being mixed together after addition at the feed throat. The barrel temperature profile was 120-163-170-170-170-170-190-200-200°C and the die was set to 200°C. The screw speed was 120 RPM and the vent zone was open to atmosphere. In the absence of the compatibilizer the C20A was homogeneously dispersed without exfoliation, which was confirmed by XRD and TEM analysis; s-C20A demonstrated some exfoliation as will be discussed in the results. The first step was necessary to adequately disperse the organoclay since the second passes required much lower barrel temperatures to achieve pressures suitable to maintain CO_2 in its supercritical state.

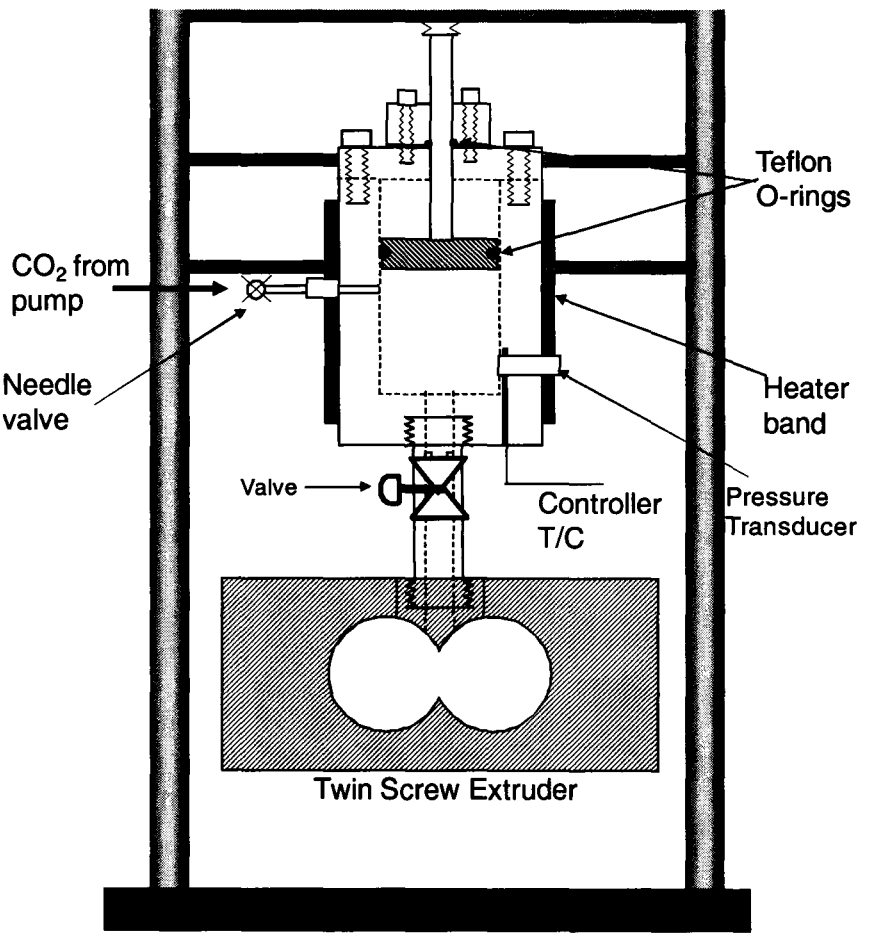

Figure A2 Constructed ram assembly for masterbatch injection with $scCO_2$.

The second pass differed to some degree based on the objective of the sample and method being tested. In all cases, pellets of the TPO/organoclay mixture were tumble blended with MA-PP pellets and added to the gravimetric feeder located at the feed opening. To reach a pressure of 8.4 MPa in the melt at the injection zone (Zone 4) over the mixing elements, the barrel profile was set to 120-130-105-105-105-145-190-200-200°C (and 200°C for the die temperature). A screw speed of 50 RPM was the maximum possible based on motor demand, as the barrel temperatures in the mixing region were 60°C below the DSC determined melting temperature of the matrix and compatibilizer. Maintaining a molten state for mixing was solely dependent upon the mechanical energy supplied by the motor (90% of full load amps under steady conditions). The samples collected by this procedure are listed in Table A2 along with their conditions for processing. The sample C20-C-TSE-0 is considered representative of conventional processing by melt intercalation (i.e. no CO_2 processing aid) and will be used as a control in our studies.

Table A2 Prepared materials by direct organoclay addition

Sample	Pass/Pass	C20A (wt%)	s-C20A (wt%)	CO_2 (w/w% formulation)
C20-C-TSE-0	TSE/TSE	5		0
C20-DG-TSE-4C8	TSE/TSE	5		4
sC20-C-TSE-0	TSE/TSE		5	0
sC20-DG-TSE-4C8	TSE/TSE		5	4

Organoclay Addition by Ram Extruder Assembly

In unpublished work by this research group it has been found that the TPO matrix should not be present to maximize the plasticizing benefit of the gas for intercalation of the compatibilizer into the galleries of our organoclay. The presence of the TPO matrix too early in the process would seem to reduce the concentration of the plasticizer at the clay interface with the compatibilizer, and the full intercalation of MA-PP chains into clay galleries found previously with $scCO_2$ [24] does not occur. It is expected that readers are familiar with the theorized steps leading to an exfoliated structure based on intercalation and delamination, which are well outlined by the research group of Paul [27].

For this processing method, a mixture of C20A and MA-PP powder was tumble blended for 5 minutes and then added into the ram extruder assembly. The system was pressurized with 8.4 MPa CO_2 while being heated for 80 minutes till the core temperature reached 180°C; the syringe pump controller maintained the desired pressure level throughout the heating procedure. The TSE injection site for the ram assembly was Zone 4 which was the same location as used for direct gas injection in the previous method. The difficulty in this approach was that the barrel zone could not be lowered in temperature as before to build up pressure else the injected molten MA-PP solidified. The barrel profile in this case was 120-130-105-170-105-120-190-200-200°C (same die temperature as earlier stated). Due to the high barrel temperature at Zone 4, the pressure at the site of injection only reached 5.86 MPa (sub-critical), but the pressure increased again for the melt in the later barrel zones 5-6 where mixing continued. The screw speed held the same as the direct addition trials, using 50 RPM. Two samples from this

procedure were collected, one under $scCO_2$ while the second was unaided by the CO_2 plasticizer but maintained under a lower pressure (4 MPa) of nitrogen to reduce the effects of thermal degradation during heating of the mass in the ram assembly. The samples and their preparation conditions are listed in Table A3.

Table A3 Samples prepared by masterbatch-$scCO_2$ method in TSE

Sample	Pass/Pass	Gas environment	Annealing pressure (MPa)	Injecting pressure (MPa)
C20-MSC-TSE-N4	TSE/ -	N_2	4.1	4.1
C20-MSC-TSE-C6	TSE/ -	CO_2	8.3	5.9

Due to difficulties in injecting the masterbatch-$scCO_2$ mixture into the molten TPO while maintaining conditions at the site of addition above the critical state in the TSE, a SSE was also tested in the study. The mixing in the SSE was considerably poorer compared to the TSE but it offered better pressurization capabilities to see whether the plasticizing effect of CO_2 needed to necessarily follow into the compounding machinery along with the masterbatch. A flat barrel profile of 170°C and screw speed of 20 RPM was used. As the material was injected the pressure in the ram assembly dropped to 6.9 MPa though the head pressure of the SSE was maintained at 8.4 MPa. Half of the samples from the SSE received a second pass through the TSE at 50 RPM and barrel profile of 120-163-170-170-170-170-190-200-200°C (with no gas present). The pass through the TSE offered the potential to address whether a higher extent of exfoliation could be

achieved if more shear was subsequently applied to the compounded materials. A list of the samples prepared is given in Table A4.

Table A4 Samples prepared by masterbatch-scCO$_2$ method in SSE/TSE

Sample	Pass/Pass	Gas environment	Annealing pressure (MPa)	Injecting pressure MPa
C20-MSC-SSE-N4	SSE/ -	N_2	4.1	4.1
C20-MSC-SSE-N4-TSE	SSE/TSE			
C20-MSC-SSE-C7	SSE/ -	CO_2	8.3	6.9
C20-MSC-SSE-C7-TSE	SSE/TSE			

Characterizations

The clay content in each sample was determined by measuring the ash content after burning off the organic material in muffle furnace at 600°C for 1 hour. These values were corrected for the original organic content of the organoclay. Standard error in the measurement was found to be 7% based on triplicate samples. The thermal characteristics of the organoclay given in Table A1 were evaluated by modulating differential scanning calorimetry (TA Instruments Q200). Two consecutive heating/cooling cycles with a ramp rate of 10°C/min were performed on a specimen over a temperature range from -20°C to 150°C under a nitrogen atmosphere. To improve peak resolution of the detected transition a modulated heating condition of ±1°C/60 s was selected.

The crystal structure of the modified clay, organoclay/compatibilizer masterbatch and prepared nanocomposite was characterized by powder X-ray diffraction (XRD) and transmission electron microscopy (TEM). XRD analyzes were performed using a Bruker D8 diffractometer with Cu K_α radiation (λ = 1.5407 Å). This analysis was carried out using an accelerating voltage of 40kV and a current of 20mA. TEM micrographs were collected from a JEOL 1200 EX TEMSCAN microscope operating at an accelerating voltage of 80kV and magnifications of 60,000x and 200,000x. Samples were microtomed with a diamond knife into thin sections approximately 70 nm thick and mounted on a carbon grid.

The rheological properties of the nanocomposite samples were evaluated using an ARES parallel plate rheometer (TA Instruments). A constant strain of 1.5% was chosen for the measurements based on the determined linear viscoelastic region from strain sweep testing. The tests were conducted at 200°C over a frequency range of ω = 0.1–100 rad/s.

A3 RESULTS AND DISCUSSIONS

Among the different methods of CO_2 injection tested in this work, the least complicated was the pretreated organoclay approach since there were no concerns regarding its addition to an on-going compounding process. The CO_2-treated clay (s-C20A) could be added just as a standard organoclay, by the gravimetric feeders. However, the approach required considerable preparation time, needing more than one month to generate sufficient filler for the small set of trials examined in this study. Direct

gas injection was readily implemented in the study with well established understanding already present in the polymer processing field from foaming technology. The issues with the approach, as with foaming, are controlling the environment within the extruder so that the gas dissolves into the melt but does not so significantly plasticize the system so that the resulting pressure drops below the solubility threshold. The most complicated process to manage within the study, largely due to the heat needed to keep the compatibilizer/clay mixture as a fluid, was the masterbatch-scCO_2 injection approach. It was unfortunate that the CO_2 could not be maintained in its supercritical state as the masterbatch entered the extruder, as was originally hoped. For the TSE the highest pressure achieved was 5.9 MPa (C20-MSC-TSE-C6) in the mixing zone under the point of injection while for the SSE a slightly higher condition of 6.9 MPa was achieved (C20-MSC-SSE-C7). While earlier studies by the group have shown that even at 5.5 MPa the plasticizing effect of carbon dioxide on the organoclay is significant [25], that same work noted the effect was greater with higher pressure. The greatest complication for the masterbatch approach was the long annealing times (80-100 minutes) at elevated temperature for the mixture in the ram assembly before injection. The time to conductively heat the entire mass of the mixture above the melting point of the compatibilizer took longer than desired, with some degradation of the compatibilizer species noted. Conversely, that annealing stage allowed substantial opportunity for guest intercalation by the compatibilizer into the organoclay and theoretically should provide the highest extent of exfoliation under adequate shear conditions. The following are

results on the microstructure and rheology properties for the produced samples by these different methods of preparation.

X-ray Diffraction

The diffraction patterns for neat C20A and s-C20A are shown in Figure A3. The as-supplied C20A organoclay exhibited an intense (001) peak at $2\theta = 3.4^{o}$ (26.0 Å) indicating an mixed-layer crystal structure. After annealing in $scCO_2$ and rapid depressurization the basal reflection from s-C20A indicated that minor disruption of the crystal structure was experienced, noted by the slightly broader d_{001} peak at $2\theta = 3.2^{o}$ (27.6 Å) compared to C20A. Horsch et al [13] similarly noted little change with Cloisite 15A (which has more of the surfactant present than C20A but is otherwise identical) in their XRD pattern after pre-treatment with $scCO_2$.

Included patterns in Figure A3 are for samples of s-C20A incorporated into TPO (with no compatibilizer) to show how readily the pretreated clay was disrupted by shear. For the sample prepared without direct gas addition, a potential shoulder peak was bearly distinguishable from the baseline at $2\theta = 3.4^{o}$, but otherwise the diffraction pattern indicated considerable loss of crystalline order in the clay structure. The addition of direct gas injection appeared to further aid clay dispersion for this pretreated clay with no notable diffraction pattern observed – though this could also be related to the fact that the material had now experienced a second pass through the extruder. The fragile structure of the pre-treated organoclay demonstrated ready exfoliation in the presence of shear, even in this case without the use of compatibilizer. Conversely, the pattern from the first

TSE pass a TPO sample with C20A (without compatibilizer) was not included in the figure since it was indistinguishable from the neat clay species, suggesting that no exfoliation occurred for that case. The subsequent discussion refers only to the nanocomposite materials which included PB3200.

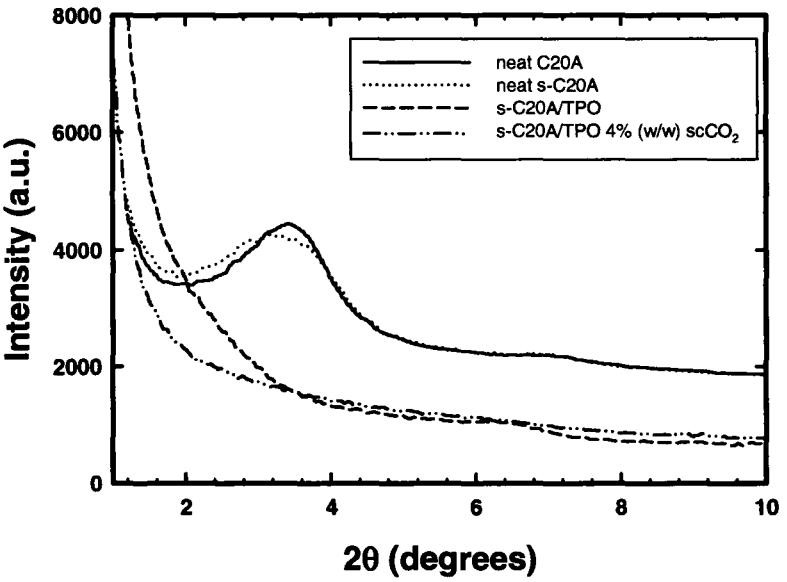

Figure A3 XRD patterns for the neat organoclay species

For the final samples produced after completing their second pass through the TSE as listed in Table A2, their corresponding diffraction patterns are shown in Figure A4. For the conventional nanocomposite produced in the absence of any CO_2 aid, the peak for C20A remained distinct but significantly broadened. The reflection at $2\theta = 3.4^{\circ}$ now appears as a shoulder in the diffractogram compared to the distinct peak for neat C20A due to the increased heterogeneity now in the crystal structure. With direct gas injection

of 4% (w/w) supercritical CO_2 there was little evidence that further exfoliation of C20A occurred. Hwang et al [14] reported a similar outcome after two passes of a PP nanocomposite through a TSE with direct gas injection, except in their case the CO_2 was used for the first pass and not the second. The nanocomposites based on the pre-treated method demonstrated well exfoliated structures but did not show distinguishable differences from the first pass sample without compatibilizer, shown in the previous figure. Furthermore, the analysis technique could demonstrate no effect of direct gas injection (4 w/w% $scCO_2$) in aiding exfoliation further with the use of pre-treated organoclay and compatibilizer now being present.

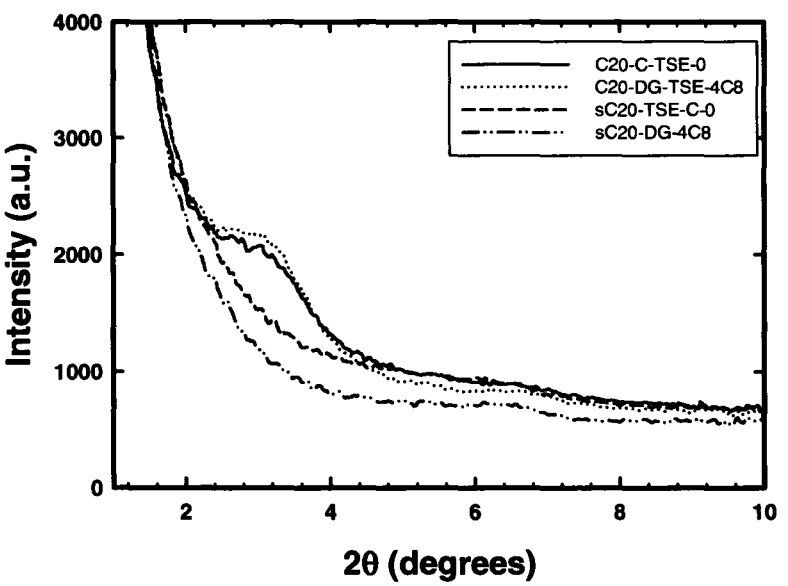

Figure A4 XRD patterns of nanocomposites filled with C20A and s-C20A by direct injection method.

For the samples prepared where the organoclay was injected by the ram assembly, Figure A5 shows the XRD patterns based on the different experiments. In Figure A5a, the diffractograms of the two samples from Table A3 prepared with the different gases by TSE appeared similar. The original d_{001} peak of C20A (referring to the region of $2\theta = 3\text{-}5^{o}$) was completely indiscernible from the baseline for these new nanocomposites. Due to its intensity the new peak at $2\theta = 6\text{-}7^{o}$ (14 Å) for both samples was not considered a (002) reflection, but rather thought to indicate a partial collapse of the remaining clay lamella. Possible reasons for the collapse stated in the literature include surfactant diffusion from the clay into the matrix and thermal degradation of the surfactant (via Hofmann elimination) [28], although these proposed causes have not been unanimous acceptance by some researchers as feasible for the processing temperature used [29]. Coalescence of thermodynamically unstable dispersed silicate sheets is equally considered as a potential cause by the present authors. Regardless of cause, the presence of the peak indicates that well organized regions of C20A persisted after processing, with no influence of gas type noted. The combination of high shear (provided by the TSE) and the lengthy masterbatch annealing time (80-100 minutes) while the ram assembly heated up would seem to not require the plasticizing effect of CO_2 – this was not similarly observed for the SSE trials in Figure A5b perhaps due to its poorer mixing capabilities.

In comparison to the samples prepared with only one pass by the TSE, the XRD patterns for nanocomposites prepared by the *masterbatch-scCO_2 injection* method first by the SSE and then by TSE (noted in Table A4) are shown in Figure A5b. A comparison

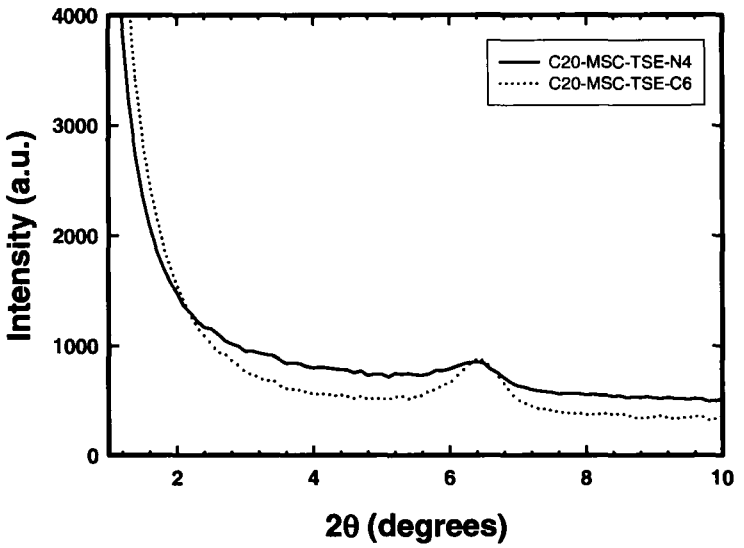

(a)

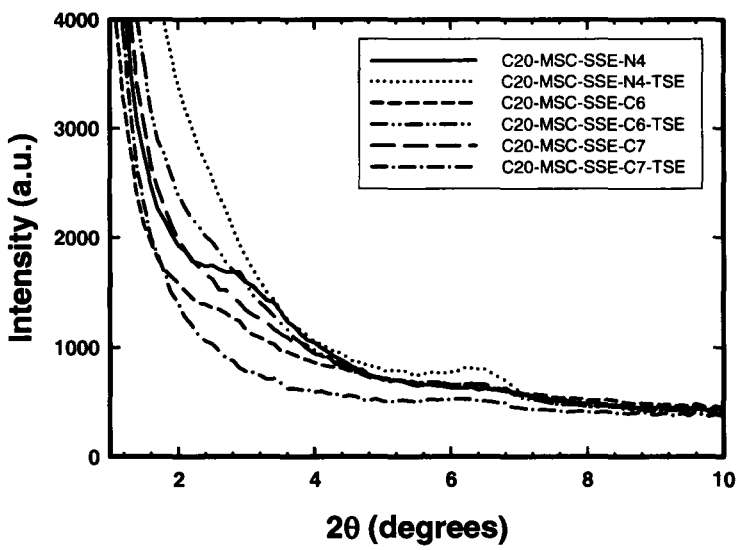

(b)

Figure A5 XRD patterns for nanocomposites prepared by masterbatch-scCO$_2$ injection method in TSE and SSE/TSE.

between diffraction patterns for CO_2 and nitrogen conditions of samples from the SSE indicate that there was an influence of CO_2 on the crystal structure of the clay. For the nanocomposites prepared under a nitrogen environment a shoulder peak was detected in the range of $2\theta \sim 3^{\circ}$ indicating that many galleries of the dispersed clay continued to exhibit interlamellar spacing similar to the original organoclay. After a second pass this time through the TSE the shoulder peak of the clay could no longer be distinguished from the baseline, but some collapsed clay lamella were once again noted by the weak peak at $2\theta \sim 6\text{-}7^{\circ}$. For the two CO_2 conditions (C20-MSC-SSE-C6 and C20-MSC-SSE-C7), the (001) diffraction peak of C20A in the samples could not be readily distinguished from the baseline, pointing to greater heterogeneity in the crystal structure being achieved. The diffraction patterns now bear close semblance to those found with the pretreated clay (s-C20A) earlier.

From Figure A5b, the effect of CO_2 pressure on the clay was not observable in the samples from the SSE but became better differentiated once the same two samples were subsequently processed through the twin screw extruder. The pass through the TSE in this case did not include any gas as already indicated and only provided extra shear mixing in the hope to observe effects that might be obscured by the poor mixing of the SSE. The nanocomposite sample (C20-MSC-SSE-C7-TSE) using the higher mixing pressure (6.9 MPa CO_2) showed a diffraction pattern devoid of structured clay while the lower pressure condition (C20-MSC-SSE-C6-TSE) showed a shoulder peak at $2\theta \sim 3^{\circ}$ as well as the weak reflections of collapsed lamella at $2\theta \sim 6\text{-}7^{\circ}$.

TEM Analysis

The morphologies observed by TEM for all of the samples prepared in this study can generally be split into two categories, clustered or exfoliated. The exfoliated morphology in this case refers the classical arrangement observed by researchers, where disrupted clay particles are dispersed as both individual platelets and dense tactoid stacks within the matrix – there was not implication of the extent of exfoliation being made by this classification. The clustered morphology was less expected and not well documented in the literature to the knowledge of the authors for the field of melt intercalation, where the silicate sheets appear to be locally confined and not well dispersed yet demonstrated internal disorder and substantial stack expansion due to the intercalating polymer. The disorder in the clay microstructure for the clustered morphology differentiates it from the ordered exfoliated structure often noted in nanocomposite literature.

Figure A6 shows the TEM micrographs for nanocomposite samples obtained under conventional and direct gas injection methods using s-C20A or C20A. The displayed morphologies in the micrographs are evident of an exfoliated morphology with delaminated silicate sheets and intercalated tactoids being present. The dark lines in the micrographs indicate tactoids with thicknesses ranging from 5 to 20 nm, and the grey silhouettes indicate individual platelets dispersed in the polymer matrix. Of these samples, the one prepared by the conventional method with C20A, i.e. C20-C-TSE-0, exhibited the densest tactoids. The clay dispersion for the nanocomposites prepared with pretreated clay (s-C20A) in Figure A6 showed an improvement compared to the control with thinner tactoids seen in the micrographs. Visually it would seem the absence of a (001) basal reflection noted by XRD would appear somewhat misleading as complete exfoliation was

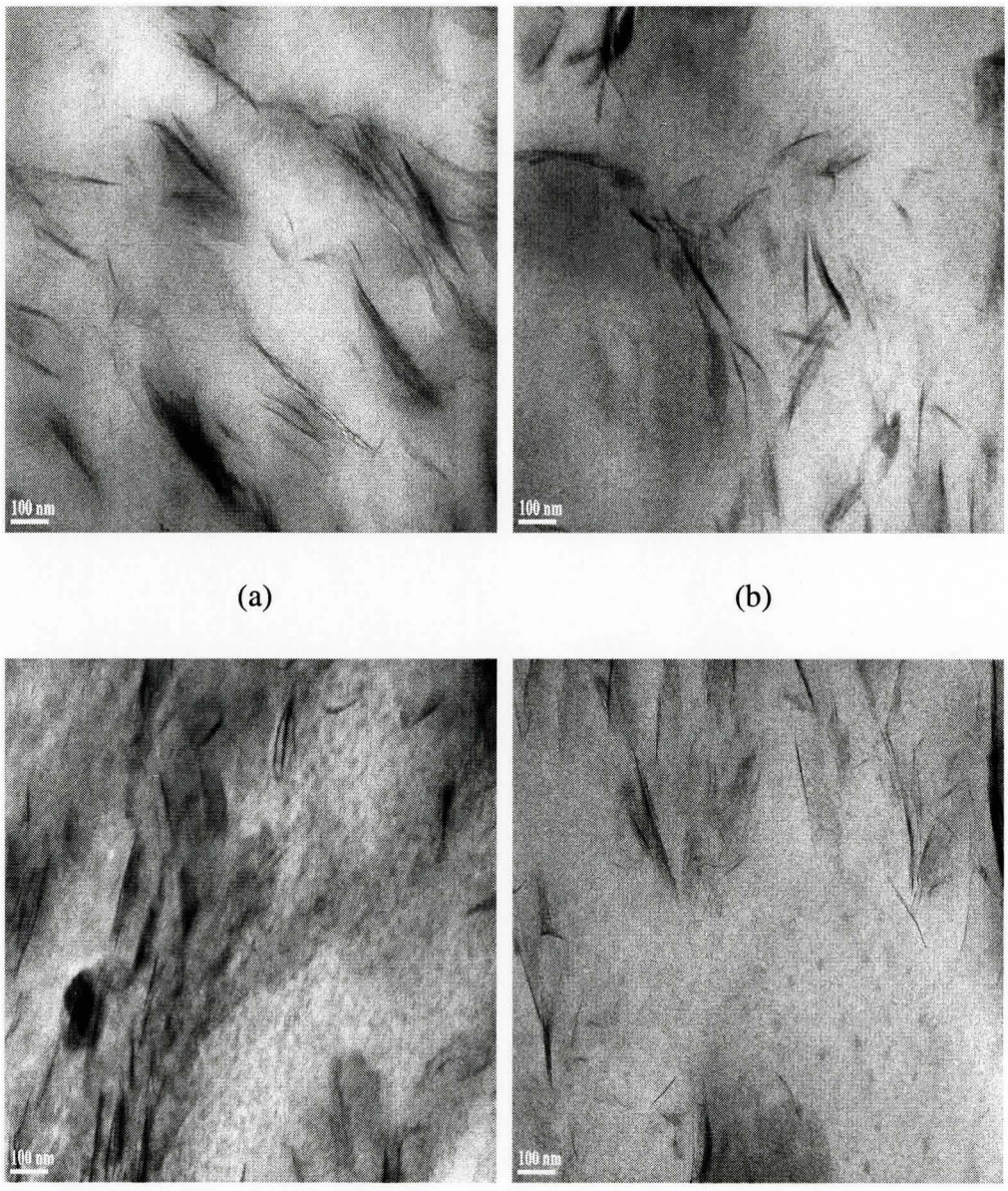

Figure A6 TEM micrographs for nanocomposites prepared by conventional (C) and direct gas injection (DG) methods, a) C20-C-TSE-0, b) sC20-C-TSE-0, c) C20-DG-4C8, and d) sC20-DG-4C8

not observed – this is not an unusual outcome in the analysis of exfoliation [30]. The addition of CO_2 by direct gas injection to the sample prepared with s-C20A showed no further improvement in exfoliation. Comparatively, the addition of direct CO_2 injection to the sample prepared with C20A had no detectable impact, in corroboration with the corresponding XRD results.

The top two micrographs in Figure A7 correspond to different selected nanocomposite samples displaying the clustered morphology. The morphology is similar in appearance to the micrographs reported by Treece [20] and by Nguyen and Baird [18] in the presence of $scCO_2$. Major portions of each observed organoclay particle in micrographs (a) and (b) can be seen experiencing substantial loss in its ordered stacking of silicate sheets, with many sheets no longer parallel. Meanwhile, other areas of the organoclay particles seen in the figure appeared to have remained densely packed. Based on the results by XRD corresponding to the displayed samples, those persisting tactoids do not exhibit the original interlamellar spacing of C20A but rather demonstrate basal spacing indicative of partially collapsed galleries. The samples displaying this clustered morphology corresponded to those runs from the first pass through either extruder (TSE or SSE) using the *masterbatch-$scCO_2$ injection* method.

The morphology is considered to be an indicator of poor dispersive forces being translated to the well intercalated silicate particles once in the compounding extruder. The effect was attributed to the plasticizing nature of CO_2 on the polymer matrix, lowering shear stresses on the clay particles during extrusion. For the two samples prepared by this injection method with the SSE, the average area of observed clusters calculated using

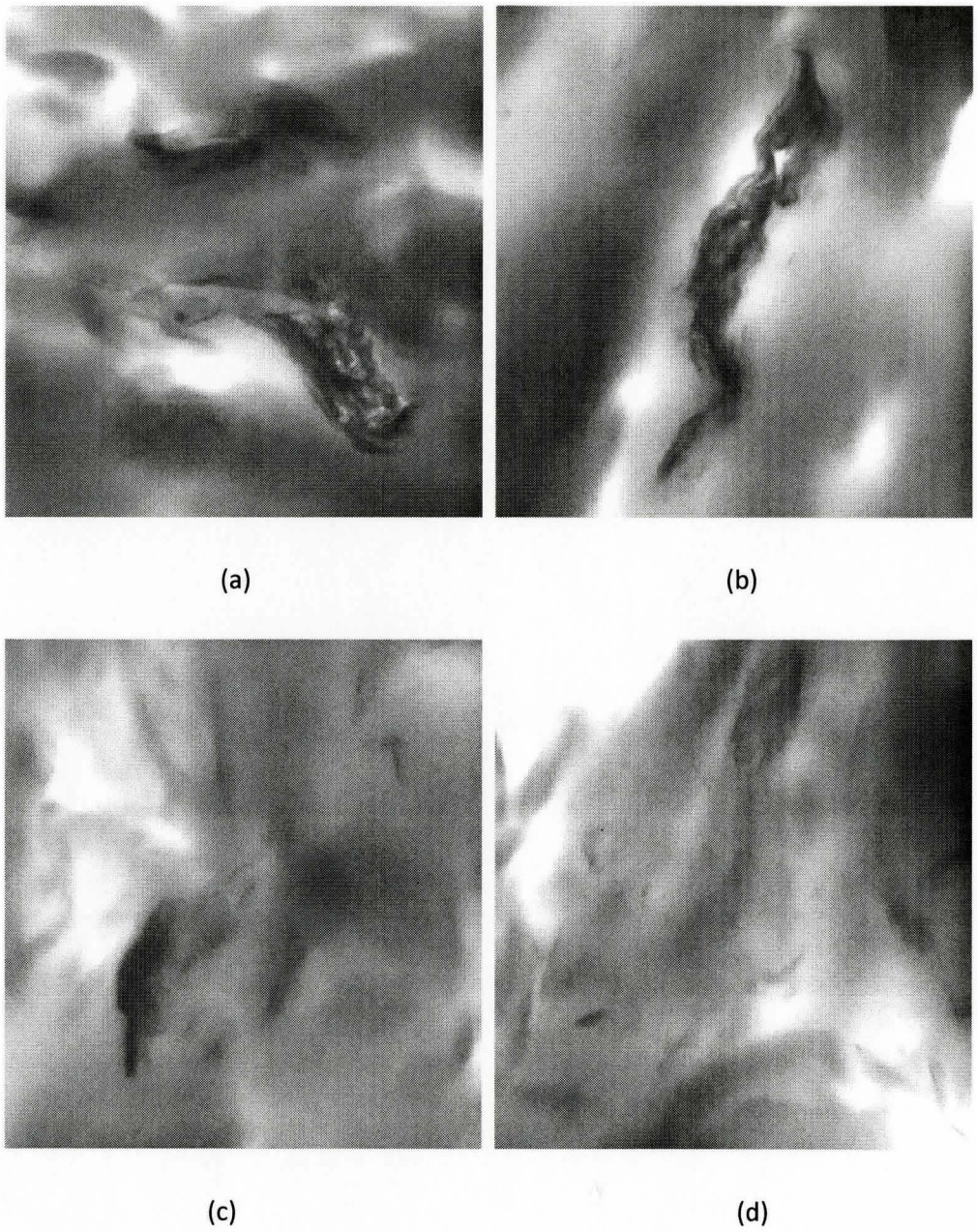

Figure A7 TEM micrographs for select nanocomposites displaying clustered clay morphology, (a) C20-MSC-TSE-6C and (b) C20-MSC-SSE-C7, versus exfoliated clay morphology (c) C20-MSC-TSE-N4 and (d) C20-MSC-SSE-N4

image analysis software (SigmaScan Pro5, SYSTAT) increased from $3.48x10^5$ nm^2 to $6.11x10^5$ nm^2 with increasing injection pressures from 5.5 MPa to 6.9 MPa, respectively. The trend is only qualitative but it supports our hypothesis that the cluster morphology may be persistent due to the ineffective capabilities of the highly plasticized matrix to translate shear stresses to the clay particles during mixing. It was interesting that the seemingly intensive mixing sections of the TSE could not adequately disperse the clay material in the presence of the high pressure gas, while the same outcome was not greatly unexpected for the less intensive Maddock mixer of the SSE.

The bottom two micrographs (c,d) in Figure A7 further highlight the interference of $scCO_2$ to mxing using the masterbatch-$scCO_2$ approach since these images corresponded to the control samples to those shown in micrographs (a,b) but being prepared with nitrogen instead. These two control samples showed only clay regions displaying an exfoliated morphology and none of the clustered morphology. The tactoids appear densest in micrograph (c) for the TSE-produced control with no visible differentiation of silicate layers, likely corresponding to the collapsed galleries noted by XRD. The control produced by SSE also included tactoid particles corresponding to incomplete delamination of the organoclay but the extent of exfoliation appeared greater than for all other cases shown in Figure A7 (if we consider the clustered regions as not demonstrations of exfoliation).

Since earlier work noted that annealing the organoclay with molten MA-PP under $scCO_2$ leads to clay galleries with fully intercalated polymer chains [24] it was expected that the reported cluster morphology could be readily lost once adequate shear was

applied. Our XRD results have already suggested this is the case. Figure A8 shows the micrographs corresponding to the SSE-prepared masterbatch/scCO_2 injected nanocomposite as well as its corresponding control (prepared with nitrogen in the SSE) after passing through the TSE. The second pass using the TSE (C20-MSC-SSE-C7-TSE) brought about comparable dispersion to the other sample showing the greatest degree of exfoliation in this study, namely the sample prepared with pre-treated organoclay (sC20-TSE-C-0). Layered stacks remained present in the sample but they were thinner and the field of view showed a higher occurrence of exfoliated silicate sheets than found in most other materials tested. Comparatively, the nitrogen-prepared control (C20-MSC-SSE-N4-TSE) showed no gain in exfoliation from its pass through the TSE, so it would appear that the shear of the SSE was sufficient for reaching the maximum extent of exfoliation possible when the matrix was not plasticized with CO_2 (though the rheology section will show that overall dispersion in the SSE was relatively poor).

Particle Size Determination

To quantify the analysis provided by TEM images, the normalized particle size distribution of the clay tactoids for selected samples are summarized in Figure A9. Among these samples, the one compounded within a nitrogen environment (C20-MSC-SSE-N4-TSE) demonstrated the broadest distribution, with considerably larger tactoids than found between the different CO_2 addition methods. Among the other three nanocomposites using CO_2, the largest tactoids were found for the nanocomposites filled with C20A and prepared by direct CO_2 injection. The other two samples shared similar

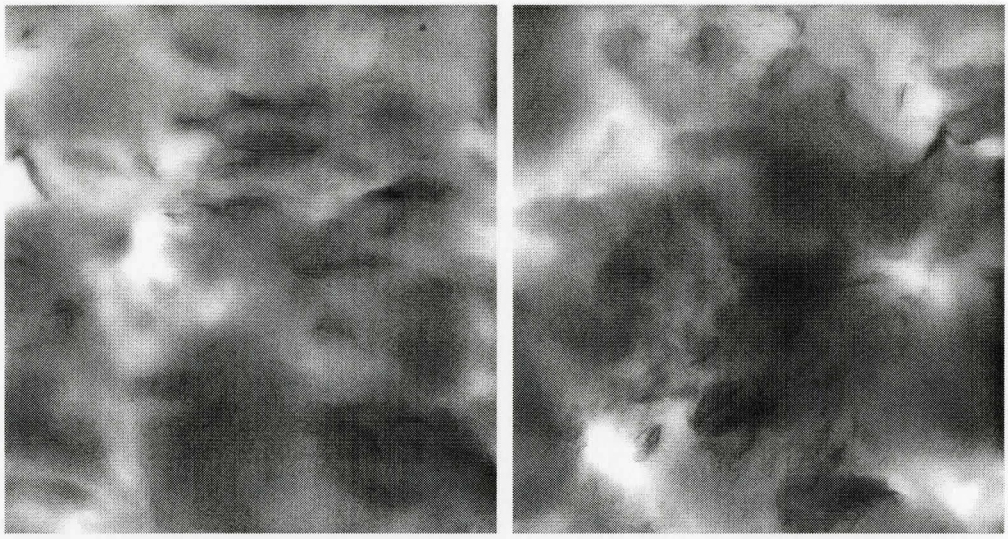

(a) (b)

Figure A8 TEM micrographs of nanocomposite samples showing increased dispersion by TSE compounding after first preparing by the masterbatch-scCO$_2$ method in the SSE, a) C20-MSC-SSE-C7-TSE and b) C20-MSC-SSE-N4-TSE

features of clay dispersion with the nanocomposite prepared by the masterbatch-scCO$_2$ method versus the pre-treated clay (direct CO$_2$ injection). These results seem correspond well with the XRD diffraction patterns.

Parallel Plate Rheology

Figure A10 compiles the storage modulus (G′) curves for nanocomposites prepared by conventional and direct gas injection method, using either C20A or s-C20A in their preparation. The error bars included in the plots indicate the standard error for three repeats and show excellent reproducibility of the measurements overall with the

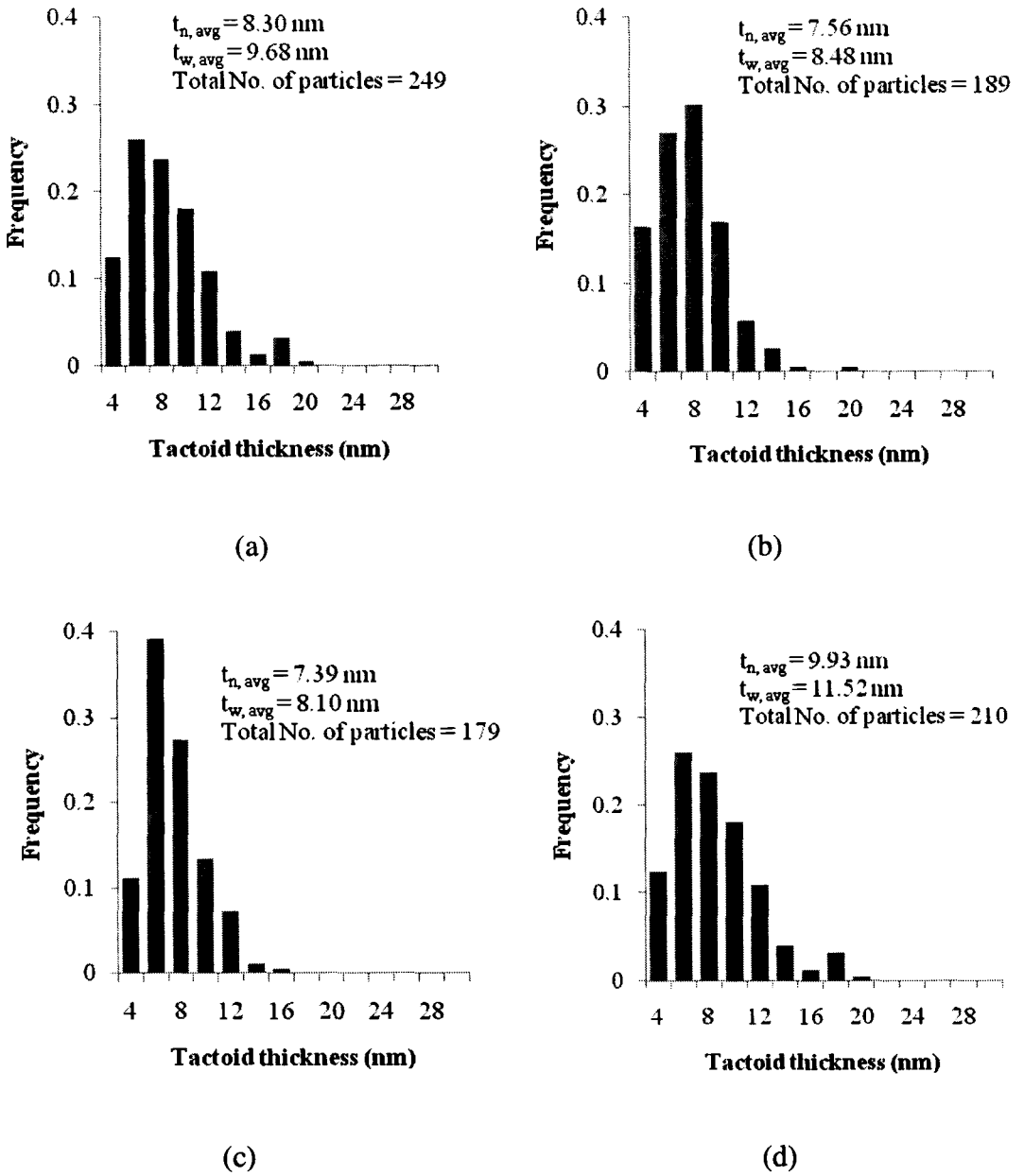

Figure A9 Particle size distribution of clay tactoids comparing the methods of (a) direct gas injection (C20-DG-TSE-4C8), (b) pre-treatment (sC20-DG-4C8) (c) masterbatch/$scCO_2$ injection method (C20-MSC-SSE-C7-TSE), and (d) masterbatch-$scCO_2$ control (C20-MSC-SSE-N4-TSE). Number average and weight average thickness are included.

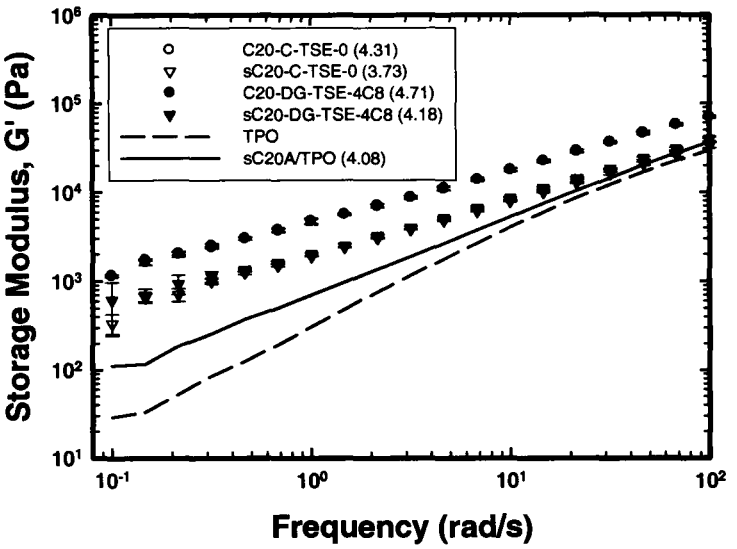

Figure A10 Storage modulus for TPO nanocomposites prepared by conventional (white symbols) and direct gas injection method (black symbols) using either C20A or s-C20A. Values in the brackets refer to the percent weight fraction of clay measured in the sample.

largest variance noted down at 0.1 rad/s. Focusing on the lower oscillatory frequency range, $\omega < 1$ rad/s where differences in large-scale segmental motion can best be detected, the samples prepared with C20A exhibited a solid-like terminal plateau indicative of a percolating network of silicate within the TPO matrix, similar to the findings of others [31-33]. The use of direct gas injection produced no improvement in the storage modulus of that material. The nanocomposites prepared with s-C20A exhibited a much lower G′ value than those using C20A but also showed greater solid-like behavior than neat TPO and once again there was no notable difference in properties when the mixing was aided with CO_2 by direct injection. The lower stiffness of s-C20A prepared samples was

unexpected in light of the earlier structural characterization results by XRD and TEM. The highly exfoliated clay microstructure reported by XRD and TEM provided the expectation that using s-C20A in the nanocomposite preparation should have led to greater reinforcement but that was not observed in the storage modulus data. The same behavior was noted for the pre-treated mixture prepared without compatibilizer (s-C20A/TPO) which showed stiffness values more closely matching the neat TPO despite the high level of exfoliation indicated by XRD.

Figure A11 shows the storage modulus curves for samples prepared by the ram assembly, either directly by TSE or first prepared by SSE then TSE. Plot (a) shows the samples prepared with CO_2 or nitrogen after a single pass through either the TSE or SSE. The stiffness behavior of these materials was closer to s-C20A/TPO or neat TPO than the conventional nanocomposite or the s-C20A based nanocomposite (with compatibilizer) reported in the previous figure. The cluster morphology of the organoclay could, in part, explain the low G′ for those materials prepared with CO_2 based on the improved G′ that arose from further mixing as will be shown in Plot (b), but that does not explain the results for the nitrogen controls. The low G′ values may also be attributed somewhat to reduced C20A interactions with compatibilizer as previously noted with s-C20A since, i) the organoclay particles were exposed to the CO_2 gas directly till the surrounding compatibilizer melted in the ram assembly, and ii) the temperature of the ram assembly was above the melting point of the surfactant allowing some changes to its coverage over the clay even when the CO_2 was not present [34]. While these causes can feasibly result

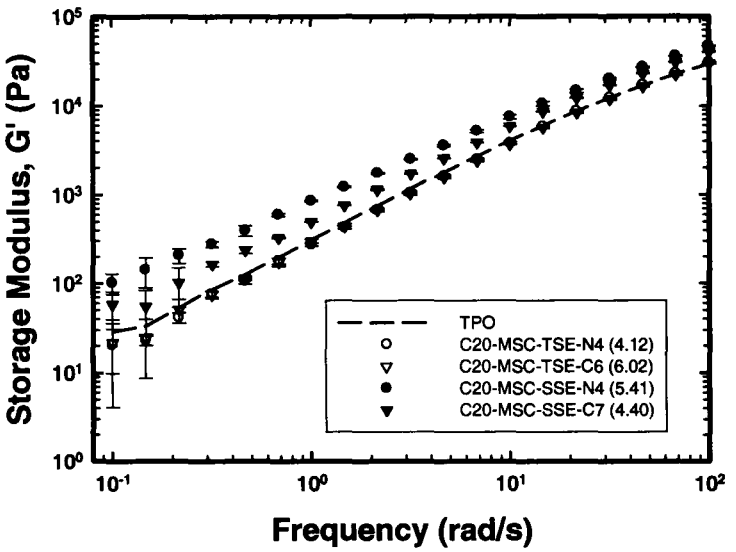

(a)

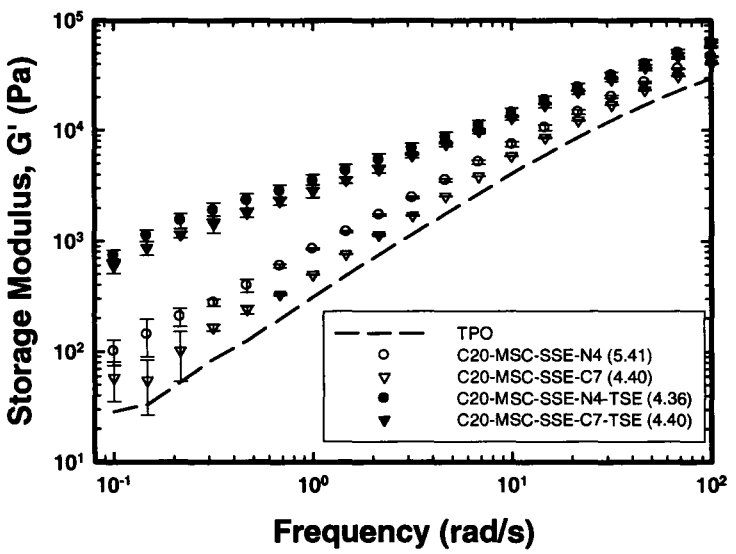

(b)

Figure A11 Storage modulus for nanocomposite samples comparing the masterbatch-$scCO_2$ injection method for, a) SSE versus TSE (both first pass), and b) SSE and TSE (second pass). Values in the brackets refer to the percent weight fraction of clay measured in the sample.

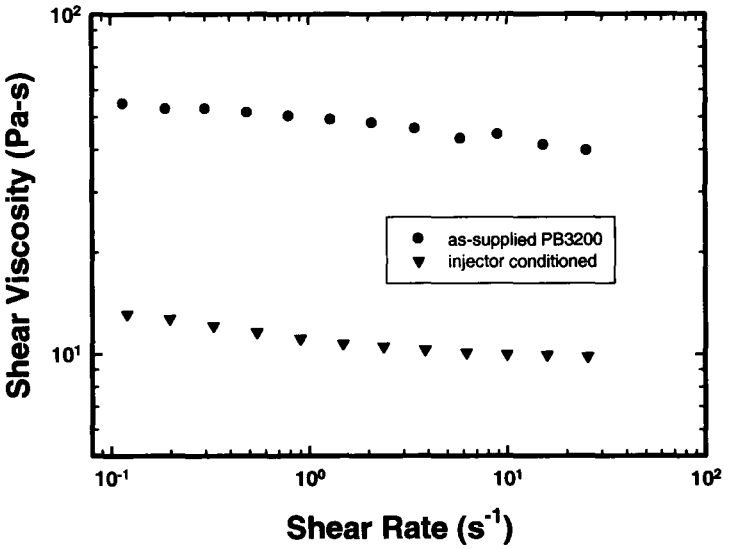

Figure A12 Viscosity for PB3200 before and after heating in the ram injector

in the low modulus, as already seen with the s-C20A materials, the greater likelihood in this case was that compatibilizer chain degradation occurred from the prolonged time at elevated temperature in the assembly's chamber before addition to the extruder, even if under an oxygen-depleted environment. This belief can be made clearer by rheological assessment of the neat compatibilizer compared to a sample of the same material which sat in the ram assembly under identical conditions to those used previously with the clay/compatibilizer mixture, as shown in Figure A12. An order of magnitude decrease in viscosity was seen in the data consistent with an outcome of thermal degradation.

Plot (b) in Figure A11 shows the increased stiffness of the SSE-prepared materials after that second pass through the TSE to improve mixing; the materials only prepared by TSE never did receive a second pass since it was felt at the time their potentially degraded

state would only be worsened by further processing. It seems unlikely that any other changes besides dispersion of the clustered clay particles could have resulted in this change in stiffness. With the improved state of dispersion both materials now displayed viscoelastic behavior comparable to the conventional melt intercalated nanocomposite from Figure A10 (even with the likelihood of more greatly degraded compatibilizer being in the formulation).

Understanding the Influence of Supercritical CO_2

Through a series of papers by the authors, understanding of how $scCO_2$ interacts with the different components making a polyolefin-layered silicate nanocomposite has evolved. All of those earlier mentioned studies were done completely in batch, in the absence of shear and so focused primarily upon the stage of intercalation since negligible forces were present to cause exfoliation. Initially, the focus of that work was on the organoclay alone, which concluded that the gas acted as a plasticizer of the modifying organic surfactant [25, 26]. The supercritical fluid allowed the residual unbound surfactant to more effectively penetrate the full depth of the clay galleries and as a result, the more uniform coating of organic matter would be present on the surface of the silicate. This use of $scCO_2$ targeted at the clay is best demonstrated by the process of Manke [16], which the present paper simply denotes as the *pretreated method.* The produced nanocomposites by this directed use of $scCO_2$ exhibited a high extent of exfoliation yet demonstrated storage modulus values lower than other samples with much poorer clay dispersion. The outcome was attributed to that higher surfactant coverage over the silicate surface mentioned due to the presence of CO_2. With less exposed polar sites at the

oxygen plane of the clay there would be less interactions with both compatibilizer and neighboring tactoids. Toth et al [35] showed in their simulations of an alkylammonium modified clay surrounded by MA-PP and PP that the coverage area and molecular volume of a surfactant could readily interfere with both polymer species as they attempted to develop associations with the silicate surface. Since the conventional melt intercalation technique does not normally allow exfoliation to occur without intercalation by the compatibilizer (for polyolefin nanocomposite species), these experimental results highlight a greater importance for compatibilizer interactions with the clay than had been previously possible to demonstrate, except by simulations.

Another study in our mentioned series examined the influence of $scCO_2$ on the diffusion (intercalation) of maleic anhydride grafted polypropylene compatibilizer (MA-PP) into the galleries of modified clay [24]. Once again the supercritical fluid demonstrated a plasticizing influence, which in this case allowed larger molecule sized compatibilizers into the internal structure of the clay than found under atmospheric conditions. By allowing longer chains to fully penetrate the stacked structure of montmorillonite it was felt that clay species prepared in this manner would be more susceptible to delamination once mixed in a shearing flow field. This use of $scCO_2$ targeted at the clay-compatibilizer interface was represented by the *masterbatch/$scCO_2$ injection* method using the ram assembly in the present paper. The produced nanocomposites could exhibited a high extent of exfoliation similar to the pretreated clay and had storage modulus values similar to conventional prepared nanocomposites, but stiffness values greater than by conventional melt intercalation methods in the present

study could not be obtained. The higher surfactant coverage experienced by an organoclay in the presence of $scCO_2$ was again considered a possible reason for the performance noted, though polymer degradation was likely the most significant contributor in this case.

Finally, during our series of studies there was unreported work by the authors finding that the changes brought about by $scCO_2$ for clay alone and the clay-compatibilizer mixture were no longer observed when both components were mixed into the polyolefin matrix (ex. TPO) before the batch annealing with the gas. The gas effect was diluted due to the diminished concentration of the plasticizing agent at the clay interface. This use of $scCO_2$ targeted at the matrix is best demonstrated by the *direct injection method* in the present paper, and was used with both as-supplied organoclay or pretreated organoclay species (as in the process of Mielewski [17]). The produced nanocomposites in the present study exhibited no change in the extent of exfoliation or storage modulus similar to our batch findings. The presence of the CO_2 offered no benefit if dissolved in the matrix polymer. Yang et al [23] made a similar note observing poorer clay dispersion when a supercritical fluid was used as a processing aid for the compounding of nanocomposites.

In general, the introduction of CO_2 to the TPO matrix phase would seem ill-conceived, based on both results from direct injection as well as the samples prepared by the single screw extruder which improved once mixed without the gas present. The increased inter-chain distance and free volume arising from the plasticizing gas limiting shear transmission during the delamination step. It is believed the results of this paper

show that this plasticizing influence negatively impacts the extent of dispersion achieved during compounding. The benefits of the gas appear to be better targeted to intercalation in order to develop a more highly exfoliated system.

A4 CONCLUSIONS

A comparison of several new methods for using supercritical CO_2 as processing aid leading to more highly exfoliated PLS nanocomposite was undertaken in this work. The methods varied the manner which the plasticizing behavior of CO_2 influences the surfactant of an organoclay, a compatibilizer and the matrix during preparation of a polyolefin nanocomposite. The results have shown that targeting CO_2 to the organoclay-compatibilizer interface can benefit the extent of intercalation achievable but showed negative performance when introduced predominantly to the matrix or neat organoclay. Carbon dioxide exposure directly to the neat organoclay leads to a crystal structure more easily susceptible to fracture in a shear field yet this same pretreated clay does not display the anticipated increase in modulus for a more highly exfoliated system. Conversely, CO_2 exposure predominantly to the matrix reduces the extent of clay dispersion, generally producing a material equivalent or worse (in terms of exfoliation) than if the gas was not present. Overall, the outcome of this work shows supercritical CO_2 must be added with great care in order to justify its use in the preparation of PLS nanocomposite material.

REFERENCES

1. S. Bin Bae, C.K. Kim, K. Kim, and I.J. Clung, *European Polymer Journal*, **44**, 3385 (2008)
2. Y. Kim and J.L. White, *Journal of Applied Polymer Science*, **96**, 1888 (2005)
3. D.R. Paul, Q.H. Zeng, A.B. Yu, and G.Q. Lu, *Journal of Colloid and Interface Science*, **292**, 462 (2005)
4. Y.F. Xi, R.L. Frost, and H.P. He, *Journal of Colloid and Interface Science*, **305**, 150 (2007)
5. M.T. Ton-That, F. Perrin-Sarazin, K.C. Cole, M.N. Bureau, and J. Denault, *Polymer Engineering and Science*, **44**, 1212 (2004)
6. D.H. Kim, P.D. Fasulo, W.R. Rodgers, and D.R. Paul, *Polymer*, **48**, 5960 (2007)
7. D.H. Kim, P.D. Fasulo, W.R. Rodgers, and D.R. Paul, *Polymer*, **49**, 2492 (2008)
8. Y. Wang, F.B. Chen, K.C. Wu, and J.C. Wang, *Composite Interfaces*, **13**, 831 (2006)
9. D.H. Kim, J.U. Park, K.S. Cho, K.H. Ahn, and S.J. Lee, *Macromolecular Materials and Engineering*, **291**, 1127 (2006)
10. J.U. Park, Y.S. Choi, K.S. Cho, D.H. Kim, K.H. Ahn, and S.J. Lee, *Polymer*, **47**, 5145 (2006)
11. E.C. Lee, D.F. Mielewski, and R.J. Baird, *Polymer Engineering and Science*, **44**, 1773 (2004)
12. J. Li, G.J. Jiang, S.Y. Guo, and L.J. Zhao, *Plastics Rubber and Composites*, **36**, 308 (2007)
13. S. Horsch, G. Serhatkulu, E. Gulari, and R.M. Kannan, *Polymer*, **47**, 7485 (2006)
14. T.Y. Hwang, S.M. Lee, Y. Ahn, and J.W. Lee, *Korea-Australia Rheology Journal*, **20**, 235 (2008)
15. J. Ma, E. Bilotti, T. Peijs, and J.A. Darr, *European Polymer Journal*, **43**, 4931 (2007)

16. C.W. Manke, E. Gulari, D.F. Mielewski, and E.C. Lee, System and Method of Delaminating a Layered Silicate Material by Supercritical Fluid Treatment, Ford Global Technologies Inc., Wayne State University, US6,469,073 2002).

17. D.F. Mielewski, E.C. Lee, C.W. Manke, and E. Gulari, System and Method of Preparing a Reinforced Polymer by Supercritical Fluid Treatment, Ford Global Technologies Inc., Wayne State University, US6,753,360 2004).

18. Q.T. Nguyen and D.G. Baird, *Polymer*, **48**, 6923 (2007)

19. R.A. Ottaviani, W.R. Rodgers, P.D. Fasulo, and D.A. Okonski, Method for Making Nanocomposite Materials, General Motors Corporation, US7,462,6662008).

20. M.A. Treece and J.P. Oberhauser, *Journal of Applied Polymer Science*, **103**, 884 (2007)

21. Y. Zhao and H.X. Huang, *Polymer Testing*, **27**, 129 (2008)

22. M. Garcia-Leiner and A.J. Lesser, *Journal of Applied Polymer Science*, **93**, 1501 (2004)

23. K. Yang and R. Ozisik, *Polymer*, **47**, 2849 (2006)

24. J. Liu, M.R. Thompson, M.P. Balogh, R.L. Speer, P.D. Fasulo, and W.R. Rodgers, *Polymer*, **submitted**, 2010)

25. M.R. Thompson, M.P. Balogh, R.L. Speer, P.D. Fasulo, and W.R. Rodgers, *Journal of Chemical Physics*, **130**, 2009)

26. M.R. Thompson, J. Liu, H. Krump, L.K. Kostanski, P.D. Fasulo, and W.R. Rodgers, *Journal of Colloid and Interface Science*, **324**, 177 (2008)

27. T.D. Fornes, D.L. Hunter, and D.R. Paul, *Macromolecules*, **37**, 1793 (2004)

28. R.K. Shah and D.R. Paul, *Polymer*, **47**, 4075 (2006)

29. S. Benali, S. Peeterbroeck, J. Larrieu, F. Laffineur, J.J. Pireaux, M. Alexandre, and P. Dubois, *Journal of Nanoscience and Nanotechnology*, **8**, 1707 (2008)

30. D.F. Eckel, M.P. Balogh, P.D. Fasulo, and W.R. Rodgers, *Journal of Applied Polymer Science*, **93**, 1110 (2004)

31. M.J. Solomon, A.S. Almusallam, K.F. Seefeldt, A. Somwangthanaroj, and P. Varadan, *Macromolecules*, **34**, 1864 (2001)

32. M.R. Thompson and K.K. Yeung, *Polymer Degradation and Stability*, **91**, 2396 (2006)

33. J.K. Mishra, K.J. Hwang, and C.S. Ha, *Polymer*, **46**, 1995 (2005)

34. H. Heinz, R.A. Vaia, R. Krishnamoorti, and B.L. Farmer, *Chemistry of Materials*, **19**, 59 (2007)

35. R. Toth, A. Coslanich, M. Ferrone, M. Fermeglia, S. Pricl, S. Miertus, and E. Chiellini, *Polymer*, **45**, 8075 (2004)

Appendix B

Results and Discussion of ^{13}C NMR Spectra for PB3200/C20A Masterbatches Prepared Using Ethanol as a Cosolvent to Supercritical CO_2

This work was done for Chapter 6. Due to funding limit, only the ethanaol related masterbatch samples were selected for the NMR analysis. NMR data for the samples with water as cosolvent was not available. In order to keep integrity of the paper, the available NMR data was not discussed in the main body of the thesis. Since the information provided by the NMR analysis is helpful for our looking at the intercalation and exfoliation occurring in the masterbatches, results and discussion of the experiment data were appended here.

In solid-state ^{13}C NMR spectra for the melt annealed mixture of PB3200 and C20A, appearance of the alkyl related resonance related to the surfactant was considered an indicator of intercalation [1]. Resonances corresponding to the all-trans conformation of the clay's surfactant did not change when annealing of the mixture was performed under N_2; however, for under $scCO_2$ annealing those resonances were no longer observed. The presence of the gauche conformation for the surfactant corresponded to significant gallery swelling noted by XRD and TEM analysis. This was interpreted as being related to the surfactant of the clay assuming a lateral bilayer arrangement to accommodate the inclusion of the intercalated compatibilizer species. The undisturbed galleries in the presence of N_2 suggest that under normal processing conditions the compatibilizer has difficulty accessing the interlayer of the clay, though likely this is somewhat overcome within a shear flow field.

In the work of cosolvents (Chapter 6), two ethanol-based masterbatches were selected for the NMR analysis to evaluate the influence of ethanol as a solvent alone (under nitrogen) or a cosolvent to $scCO_2$ during the annealing on the structural confirmation of the clay surfactant. The measurement was performed at 23°C and 50°C, respectively. The higher probe temperature used was above the melting point of the surfactant (i.e. 45oC) used in C20A, expecting different resonance response for surfactant at the two temperatures. Figure Ba shows the spectra measured at 23oC, with the baseline of the $scCO_2$ derived sample intentionally shifted above the others to clearly delineate differences between them. For that sample which did not include ethanol the three alkyl resonances at 22 ppm (CH_3), 26 ppm (CH) and 44 ppm (CH_2) for the backbone of the

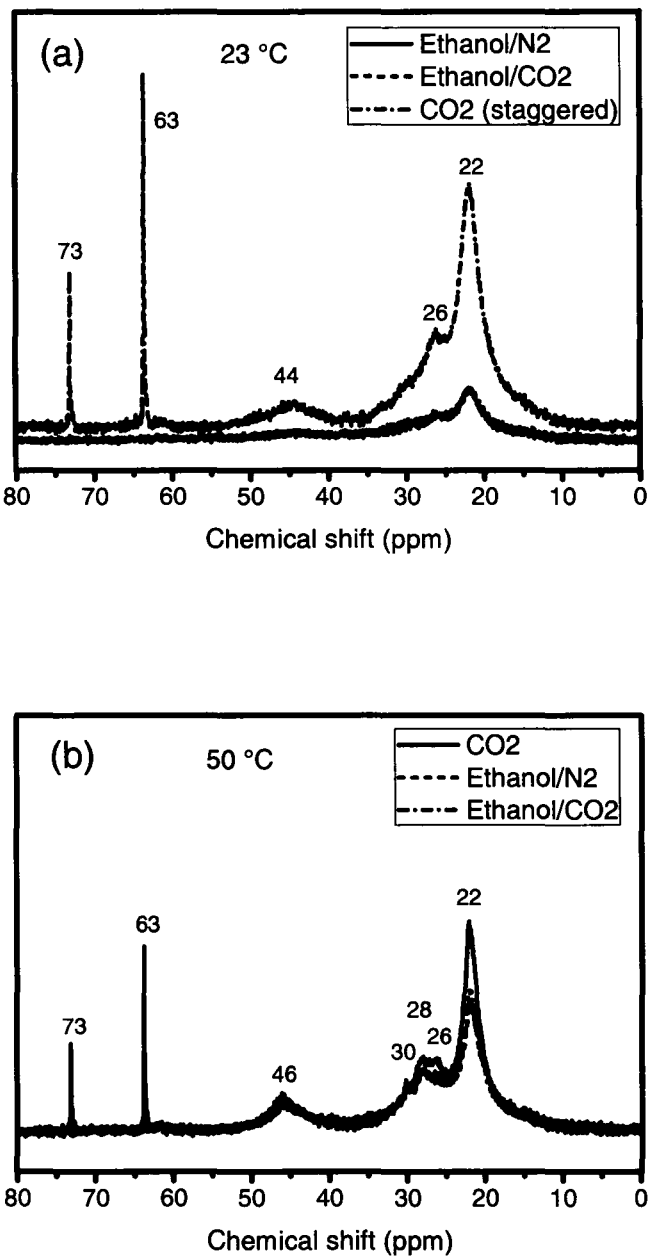

Figure B ^{13}C NMR spectra for the PB3200/C20A mixture processed under $scCO_2$ and ethanol used as solvent and cosolvent obtained at a probe temperature of 23°C (a) and 50°C (b)

maleated polypropylene (MA-PP) were clearly seen. The sharp peak at 63 ppm was assigned to the methyne group (CH) on an anhydride. For the surfactant, only the resonance at 73 ppm for its methylene attached to the nitrogen (CH_2-N) of the quaternary ammonium salt appeared clearly; all other resonances for the interior methylene groups and terminal methyl groups of its two alkyl chains as well as the methyl groups attached to the nitrogen were not distinguishable from the baseline. The absence of alkyl surfactant resonances for a sample annealed under $scCO_2$ was consistent with the results of our previous study [1]. When ethanol was used as a cosolvent to the $scCO_2$ during annealing, the resonance at 44 ppm of the polypropylene backbone methylenes, at 63 ppm for the methynes on the anhydride moiety, and at 73 ppm for the nitrogen-attached methylenes of the surfactant were also notably absent in the spectrum. The intensities of the methyne at 26 ppm and methyl at 22 ppm for the backbone of MA-PP dropped significantly. These changes for the cosolvent prepared sample indicated that both surfactant and polymer chains were being shielded, likely by close associations with the silicate sheets. The difference being that with only $scCO_2$ the polymer chain of the compatibilizer did not experience any shielding. When ethanol was used as a solvent in the nitrogen environment, the resonance spectrum of the sample was indistinguishable from the sample prepared with it being used as cosolvent. Association with $scCO_2$ was not apparently necessary for the ethanol to improve intercalation of the compatibilizer within the galleries of C20A.

In the spectra measured at 50°C shown in Figure Bb, new resonances were detected which had not been present at 23°C. A signal at 30 ppm for the interior

methylene (CH_2) groups on alkyl chains was now clearer. New signals detected at 28 ppm and at 46 ppm were assigned to methyne (CH) and methylene (CH_2) in the mixed compatibilizer and surfactant, indicating an increasingly liquid-like state for the mixture, consistent with our previous studies [1]. However, no new information on the ethanol was noted by these spectra.

REFERENCE

1. J. Liu, M.R. Thompson, M.P. Balogh, R.L. Speer Jr., P.D. Fasulo, W. R. Rodgers. Influence of supercritical CO_2 on the interactions between maleated polypropylene and alkyl-ammonium organoclay. *J. Appl. Polym. Sci.* 2010, in press